

**Quality Control of Oxidized RNA in *Saccharomyces Cerevisiae* and *Chlamydomonas*
*Reinhardtii***

James S. Dhaliwal

A Thesis
in The Department
of Biology

Presented in Partial Fulfilment of the Requirements
For the Degree of
Doctor of Philosophy (Biology) at Concordia University
Montreal, Quebec, Canada

September 2021

© James S. Dhaliwal

CONCORDIA UNIVERSITY
School of Graduate Studies

This is to certify that the thesis prepared

By: James S. Dhaliwal
Entitled: Quality control of oxidized RNA In *Saccharomyces cerevisiae* and
Chlamydomonas reinhardtii

and submitted in partial fulfillment of the requirements for the degree of

Doctor of Philosophy (Biology)

Complies with the regulations of the University and meets the accepted standards with respect to originality and quality.

Signed by the final Examining Committee:

_____	Chair
Dr. Selvadurai Dayanandan	
_____	External Examiner
Dr. Dr. Stephanie Weber	
_____	External to Program
Dr. Paul Joyce	
_____	Examiner
Dr. Christopher Brett	
_____	Examiner
Dr. Vladimir Titorenko	
_____	Thesis Supervisor
Dr. William Zerges	

Approved by

Dr. Robert Weladji – Graduate Program Director

November 8th, 2021

Dr. Pascale Sicotte – Dean, Faculty of Arts and Sciences

ABSTRACT

Quality Control of Oxidized RNA in *Saccharomyces cerevisiae* and *Chlamydomonas reinhardtii*

James S. Dhaliwal, Ph.D.

Concordia University, 2021

Reactive oxygen species can oxidize biological molecules, rendering them inactive or toxic. Oxidized RNA can stall ribosomes during translation, leading to the production of truncated, aggregation-prone nascent polypeptides. Cells have quality control systems that recognize and target oxidatively damaged molecules for repair or degradation. Ribosome collisions that occur due to stalled translation are recognized by a quality control pathway that results in the degradation of the defective mRNA, extraction and degradation of the truncated nascent polypeptide, and recycling of the ribosome subunits for additional rounds of translation. This thesis addresses the quality control of oxidized RNA. It uses two species, *Saccharomyces cerevisiae* and *Chlamydomonas reinhardtii* to examine how oxidized RNA is compartmentalized for quality control, and how a photosynthesis protein moonlights as an oxidized RNA quality control factor.

In Chapter 2, with results of immunofluorescence microscopy, genetic analyses, biochemical fractionation, and proteomics, I identify and characterize a previously undiscovered organelle, which we name “oxidized RNA bodies” or ORBs. I show that ORBs are membraneless phase-separated organelles that compartmentalize the translation quality control pathways which handle stalled ribosomes.

In Chapter 3, using immunofluorescence microscopy, genetic analyses, and biochemical fractionation, I present preliminary results on the moonlighting functions of RbcL, the large subunit of Rubisco, in handling oxidized RNA in chloroplasts. I show that a mutant unable to assemble the Rubisco holoenzyme has altered phenotypes related to the moonlighting functions of RbcL and explore the subcellular localization of the protein in various contexts associated with translation.

A powerful approach to understand the significance and management of RNA oxidation could be to find and characterize specialized intracellular compartments dedicated to it. The research contained herein advances the field of RNA quality control by providing a repertoire of candidate components, evidence for biochemical mechanisms that can be tested in future work, and a cytological context for these processes.

ACKNOWLEDGEMENTS

First and foremost, I would like to thank my supervisor, Dr. William Zerges. I am eternally grateful for the training, supervision, mentorship, and friendship that you have provided for over a decade of working together. You made your lab an ideal place for me to conduct research and grow as a scientist. Also, thanks for all the books you've loaned me! I would also like to thank my committee members; Dr. Christopher Brett and Dr. Vladimir Titorenko for their helpful advice and constructive criticism.

Thank you to the many collaborators and funding sources that allowed me to conduct my research: Lionel Benard, Cristina Panozzo, Rachid Mazroui, Pauline Adjibade, Robert Spreitzer, NSERC, and FRQNT.

All my lab mates, past and present, deserve a big thank you. Particularly; Shiva Bakhtiari, Matthew Peters, Oussama Rifai, Kristina Santilli, Marco Schottkowski, Madhav Soowamber, Yi Sun, Melissa Valente-Paterno, and especially, Yu Zhan. You've trained me, collaborated with me, and made life in the Zerges lab fun all these years!

Thanks to all the wonderful friends that I've made in the Biology Department all this time. To the friends I've met through the Martin and Walsh labs; Bjorn Bean, Alex Campbell, Karen Canales, David Colotriano, Meghan Davies, Nadine Exler, Benny Kacerovsky, Mindy Melgar, Shoham Mookerjee, Lauren Narcross, Mohammed Nasr, Arthi Ramachandran, Madhav Soowamber, Andrew Wieczorek, and Zach Wiltshire - thank you for keeping me sane – both on campus and off! To my friends in the SP-building; Noraldin Alderi, Daniel Beaudet, Stephanie Grimbert, Dilan Jaunky, Brandon Jaunky, Mahmoud Karim, Tom Kazmirchuk, Karina Mastronardi, and Samantha Sparapani - thank you for all the wonderful meals, trips to PJs, and

fantastic travels. To Chris Law, thank you for years of friendship, training, and a near-endless supply of things to nerd-out over.

To my friends outside the lab, Jordan Burgess and Tim Johnson, you've been my friends since the very beginning and are my friends for life. I look forward to finally have more time to spend with you both! Thank you to Marijosé Auclair, Eric Bellamy, Gordon Bradley, Chris Bushell, Chris Campbell, Darlene Francis, Chris McCusker, Pat McCusker, Ron Sullivan, and David White. I count myself very lucky to have found such amazing friends.

To my wonderful family: There are too many of you to list here, but you know who you are, and I thank you for your love and support throughout this entire process.

To my amazing husband, Wayne: I could never fully express my gratitude to you, although I suspect you have some idea. Thank you for years of unwavering encouragement and support, and for being my rock. I love you, and it's your turn to walk Buster.

I dedicate this thesis to my Mom (Dominique Vincent) and Dad (Michael Markowski). You've never stopped encouraging and inspiring us, and we all love you very, very much. RISE AND SHINE!

CONTRIBUTION OF AUTHORS

I am the principal author of this thesis and, except for the contributions described below, I was primarily responsible for the conception and design of experiments, data collection, data analysis, and the first draft of both manuscripts.

Chapter 2

Cristina Panozzo generated the *dom34Δ-rqc2Δ* strain used in figure 2.4. Cristina also generated the constructs used to detect stalled ribosome nascent chains in figure 2.3 and performed the northern blot shown in figure S2.4B. Christopher Law wrote ImageJ macros used to quantify ORB number and size in figures 2.1, 2.3, and 2.4. William Zerges and Lionel Benard contributed to the experimental design, and William Zerges edited the final draft of the manuscript.

Chapter 3

Yi Sun generated the *y1* light and dark sucrose gradients used in figure 3.3. Melissa Valente-Paterno provided the synchronized cells used in figure 3.1 and the *y1* greening cells used in figure 3.2. Mehrnaz Jamaat performed the survival assays and 8-oxoG measurements shown in figure 3.5F and G. Mehrnaz Jamaat and I performed the nitrogen starvation microscopy experiments shown in figures 3.8 and 3.9. Christopher Law wrote ImageJ macros used to quantify fluorescent signals in *Chlamydomonas* chloroplasts. William Zerges contributed to the experimental design and edited the final draft.

TABLE OF CONTENTS

LIST OF FIGURES	xii
LIST OF SUPPLEMENTAL DATA.....	xiii
LIST OF ABBREVIATIONS.....	xiv
CHAPTER 1. GENERAL INTRODUCTION	1
1.1 Oxidation of Biological Molecules	1
1.2 Quality Control of Oxidized RNA	2
1.3 RNA Granules.....	4
1.4 The Large Subunit of Rubisco, RbcL.....	6
1.5 Overview and Thesis Rationale.....	8
CHAPTER 2: AN RNA GRANULE COMPARTMENTALIZES TRANSLATION QUALITY CONTROL IN <i>SACCHAROMYCES CEREVISIAE</i>	10
2.1 INTRODUCTION.....	11
2.2 MATERIALS AND METHODS	12
2.2.1 Plasmids, yeast strains and growth conditions.....	12
2.2.2 Immunoblot analysis.....	13
2.2.3 Northern blot analysis.....	13
2.2.4 Indirect IF staining.....	14
2.2.5 Preparation of the ORB-enriched fraction	14

2.2.6	Microscopy and image analysis	15
2.2.7	Purification of ORBs.....	16
2.2.8	Mass spectrometry	16
2.2.9	Mass spectrometric data processing.....	17
2.2.10	Bioinformatic analysis of the ORB proteome.....	18
2.3	RESULTS.....	18
2.3.1	ORBs are cytoplasmic RNA granules in yeast.	18
2.3.2	TQC factors localize to ORBs	21
2.3.3	ORBs require translation.....	23
2.3.4	A stalled mRNA-ribosome-nascent chain complex localizes to ORBs.....	26
2.3.5	Genetic evidence for TQC compartmentalization by ORBs.....	27
2.3.6	Proteomic results further support ORBs as being an RNA granule for TQC.....	27
2.3.7	ORBs are distinct from P-bodies and stress granules but share proteins with each.	
	30	
2.4	DISCUSSION	31
2.4.1	ORBs are cytoplasmic RNA granules.....	31
2.4.2	ORBs compartmentalize steps in TQC.....	31
2.4.3	The position of ORBs among the cytoplasmic RNA granules in yeast.....	33
CHAPTER 3: CHARACTERIZATION OF NON-RUBISCO FUNCTIONS OF RBCL IN		
	<i>CHLAMYDOMONAS REINHARDTII</i>	36

3.1	INTRODUCTION.....	37
3.2	MATERIALS AND METHODS.....	41
3.2.1	Manipulation of Chlamydomonas.....	41
3.2.2	Determination of oxidative stress tolerance.....	41
3.2.3	Analysis of oxidatively damaged RNA	41
3.2.4	Chlamydomonas immunofluorescence and <i>in-situ</i> hybridization.....	42
3.2.5	Subcellular fractionation.....	42
3.2.6	Differential centrifugation	43
3.3	RESULTS.....	44
3.3.1	Investigation of a Role for RbcL in Chloroplast Translation	44
3.3.2	RbcL localizes to chloroplast translation membranes in the <i>yl</i> mutant.	49
3.3.3	RbcL localizes to chloroplast translation membranes during translation inhibition. ...	52
3.3.4	The moonlighting functions of RbcL are not affected by selected cysteine mutations.	52
3.3.5	The moonlighting functions of RbcL are altered in an <i>rbcL-G54D</i> mutant.	58
3.3.6	cpSGs are constitutively present in the <i>rbcL-G54D</i> mutant.	59
3.3.7	8-oxoG localization in the <i>rbcL-G54D</i> mutant.....	62
3.3.8	RbcL localizes to chloroplast translation membranes in the <i>rbcL-G54D</i> mutant.	63
3.3.9	RbcL functions during nutrient deprivation.....	63
3.4	DISCUSSION	66
	CHAPTER 4: CONCLUSIONS AND FUTURE DIRECTIONS	74

4.1 Summary of Major Findings/Overview	74
4.2 Outstanding Questions About ORBs.....	75
4.2.1 Identity and fate of the RNA in ORBs	75
4.2.2 Exploration of Novel TQC Factors	76
4.2.3 Context-Specific Studies of ORBs	77
4.3 Outstanding questions about RbcL and TQC in chloroplasts	78
4.3.1 A Molecular Dissection of RbcL.....	78
4.3.2 The RbcL Interactome	78
4.4 On Possible TQC Systems in Chloroplasts	78
REFERENCES	81
SUPPLEMENTARY INFORMATION	99

LIST OF FIGURES

Figure 2.1. ORBs are an RNA granule in <i>S. cerevisiae</i>	20
Figure 2.2. NGD and RQC factors localize to ORBs	22
Figure 2.3. Stalled ribosome-nascent chain complexes localize to ORBs.....	25
Figure 2.4. ORB phenotypes in NGD and RQC mutants	28
Figure 2.5. Features of the ORB proteome	29
Figure 2.6. Model showing the compartmentalization of translation quality control in ORBs...	34
Figure 3.1. Illustration of a <i>Chlamydomonas reinhardtii</i> cell.....	39
Figure 3.2. Localization of RbcL and 8-oxoG in the chloroplast across the diel cycle.....	46
Figure 3.3. Localization of RbcL and 8-oxoG in the chloroplast during <i>y1</i> greening	48
Figure 3.4. RbcL localizes to chloroplast translation membranes in the <i>y1</i> mutant.	51
Figure 3.5. RbcL localizes to chloroplast translation membranes during translation inhibition. 54	
Figure 3.6. Analysis of RbcL moonlighting functions in site-directed mutants.....	57
Figure 3.7. Localization of RbcL and 8-oxoG in the chloroplast in the <i>rbcL</i> -G54D mutant.	61
Figure 3.8. RbcL localizes to chloroplast translation membranes in the <i>rbcL</i> -G54D mutant.	65
Figure 3.9. Localization of RbcL during nutrient starvation	68
Figure 3.10. Localization of RbcL during nutrient starvation in pyrenoid-less mutants.....	70

LIST OF SUPPLEMENTAL DATA

Figure S2.1 Controls for immunofluorescence (IF) staining

Figure S2.2 ORBs are none of the known RNA-containing organelles

Figure S2.3 Foci form in response to hydrogen peroxide in live cells

Figure S2.4 The truncated HA-Ura3 nascent polypeptide accumulates in *dom34Δ* background to serve as a marker for the stalled mRNA-ribosome-nascent polypeptide complex

Table S2.1 .xlsx file containing the list of validated ORB proteins

Table S2.2 .xlsx file containing the list of candidate ORB proteins

Table S3.1 Strains used in Chapter 3

LIST OF ABBREVIATIONS

8-oxoguanine (8-oxoG)

immunofluorescence (IF)

hydrogen peroxide (H₂O₂)

no-go decay (NGD)

oxidized RNA bodies (ORBs)

processing bodies (P-bodies)

reactive oxygen species (ROS)

ribulose-1,5-bisphosphate carboxylase/oxygenase (Rubisco)

ribosome quality control (RQC)

rubisco large subunit (RbcL)

rubisco small subunit (RbcS)

translation quality control (TQC)

CHAPTER 1. GENERAL INTRODUCTION

1.1 Oxidation of Biological Molecules

Cellular homeostasis is dependent on proper RNA function which can be adversely affected during oxidative stress. This thesis examines the mechanisms by which RNA oxidation is managed by cells. Oxidative stress is a condition that results from the presence of reactive oxygen species (ROS) in excess of a cell's ability to eliminate them. As highly reactive intermediates with the ability to oxidize biological molecules, ROS can cause damage to the macromolecules of a cell (Gill and Tuteja, 2010). ROS can affect the cell by oxidizing lipids, proteins and DNA. ROS-induced peroxidation of lipids in membranes can lead to decreased membrane fluidity, leakage, and inactivation of membrane proteins, all of which compromise membrane function and integrity (Garg and Manchanda, 2009). Proteins can be oxidized in various ways. Some oxidative modifications are reversible and may serve roles in redox signalling, while others are irreversible and can lead to loss of function, degradation, misfolding, and aggregation (Ghezzi and Bonetto, 2003). DNA is also susceptible to oxidation. One of the most commonly identified forms of oxidative modification to DNA is the formation of 8-oxoguanine (8-oxoG). Oxidation of DNA can lead to genotoxic stress, resulting in errors in gene expression, DNA replication, and genome stability (Tuteja et al., 2009). Indeed, it has been hypothesized that organelle gene transfer and genomic compartmentalization in the nucleus may serve to distance DNA from potentially dangerous redox reactions occurring in energy-transducing organelles (Allen and Raven, 1996).

Like these other cellular components, RNA can also be oxidized. RNA is likely more susceptible to oxidation than DNA for several reasons: it is often single-stranded; it is less-associated with, and protected by, proteins than is DNA; and is more widely dispersed throughout the cell, potentially in proximity to areas of ROS generation (Li et al., 2006). Like in DNA, 8-oxoG is the most commonly identified oxidized base in RNA, and it is often used as a general marker of

RNA oxidation (Park et al., 1992). There are several adverse consequences of RNA oxidation. Oxidation of mRNA can lead to reduced protein expression or to the expression of truncated or misfolded proteins (Tanaka et al., 2007). Similarly, oxidation of rRNA can affect translation by impairment of ribosome function (Honda et al., 2005). There is also evidence that RNA oxidation is associated with disease in humans, particularly in neurodegenerative disorders, where 8-oxoG levels in brain tissue is elevated (Nunomura et al., 1999; Poulsen et al., 2012).

1.2 Quality Control of Oxidized RNA

In contrast to the known mechanisms for the prevention, repair, or degradation of oxidized DNA, little is known about the management of oxidized RNA. There is evidence of a mechanism for the turnover of oxidized RNA because it was shown that 8-oxoG levels decreased within a few hours during recovery from stress in cultured human lung epithelial cells (Hofer et al., 2005). Furthermore, it was shown that oxidized RNA can be targeted by a ribosome-based quality control pathway called No-Go decay (Simms et al., 2014) and some proteins are known to bind specifically to oxidized RNA. For example, the human RNA-binding protein, YB-1, is able to bind to 8-oxoG-containing mRNA and provide resistance to oxidative stress when overexpressed in *E. coli* (Hayakawa et al., 2002). PNPase, a 3'-5' exoribonuclease, also binds specifically to 8-oxoG-containing RNA (Hayakawa et al., 2001). It was found that PNPase-deficient *E. coli* cells are hypersensitive to oxidative stress and that overexpression of human PNPase in HeLa cells results in increased viability and reduced 8-oxoG RNA during oxidative stress (Wu and Li, 2008; Wu et al., 2009). Other proteins which have been also shown to bind oxidized RNA include HNRNPD/Auf1, SF3B4, HNRNPC, and DAZAP, however a specific function for them in this context has yet to be uncovered (Hayakawa et al., 2010).

Oxidized bases in mRNAs can stall translating ribosomes and translate to aggregation-prone polypeptides (Shan et al., 2003; Simms et al., 2014). mRNAs with oxidized bases and other

defects, such as unresolved mRNA secondary structures, stretches of poly(A) or CGA codons, or 3'-end truncations are recognized and cleared by the translation quality control (TQC) pathways, No-Go decay (NGD) and ribosome-associated quality control (RQC) (Inada, 2020). These TQC pathways are initiated through the detection of ribosome collisions that result from stalling on mRNAs (Ikeuchi et al., 2019; Juskiewicz et al., 2018; Simms et al., 2017a). Upon the recognition of colliding ribosomes on a mRNA by Hel2 in yeast (ZNF598 in humans), NGD separates their subunits and targets the aberrant mRNA for degradation (Inada, 2020; Yan and Zaher, 2019). RQC then catalyzes the addition of alanine-threonine residues to the C-terminus of the nascent chain, an event termed CAT-tailing. CAT-tailing events promote the extraction of the nascent polypeptide from the 60S ribosomal subunit, followed by its targeting for degradation by the ubiquitin-proteasome system (Bengtson and Joazeiro, 2010; Defenouillère et al., 2013; Dimitrova et al., 2009; Shen et al., 2015; Sitron and Brandman, 2019).

While evidence is only recently emerging for molecular quality control of oxidized RNAs, entire research fields are dedicated to quality control of oxidized DNA, proteins, and lipids. In these fields, a major theme is the localization of quality control processes to specialized intracellular compartments (Stoecklin and Bukau, 2013). The sequestration of damaged molecules to such compartments prevents them from interfering with the processes in which they normally function. Compartmentalization also prevents the degradation or attempted repair of undamaged substrates. Finally, compartmentalization could enhance local concentrations of substrate molecules and quality control factors. This can establish thermodynamic parameters that favor forward reactions, for example, in repair or degradation. Therefore, one approach to understand the significance and management of RNA oxidation could be to find and characterize a specialized intracellular compartment dedicated to it.

Our laboratory recently discovered that oxidized RNA is compartmentalized in two genetically distinct organisms, using immunofluorescence (IF) microscopy and an antibody against 8-oxoG (Zhan et al., 2015). We found that oxidized RNA localizes to the pyrenoid, a microcompartment in the chloroplast of the unicellular green alga, *Chlamydomonas reinhardtii*. Chloroplasts contain RNA as they are distant evolutionary cousins of photosynthetic bacteria that have retained a prokaryotic-like genetic system. We also discovered, in cultured human, HeLa, cells, the localization of oxidized RNA to cytoplasmic foci which we called *oxidized RNA bodies* (ORBs). In appearance these ORBs are reminiscent of RNA granules, a class of organelles that compartmentalize select RNA and proteins, described in the next section. The compartmentalization of oxidized RNA may be critical for its management. Given that we have identified ORBs as an example of this compartmentalization, an objective of this thesis was to characterize the properties and functions of ORBs.

1.3 RNA Granules

Cells are highly compartmentalized in order to control the location, specificity, and component concentrations of biological reactions or processes. Canonical examples of subcellular compartmentalization include organelles such as lysosomes, mitochondria, and chloroplasts. In these examples the biochemical activities that define the organelle are sequestered from the rest of the cell by enclosure within a membrane. More recently, attention has been paid to another type of subcellular compartmentalization which does not require membrane enclosure. RNA granules are membraneless ribonucleoprotein organelles with undefined component stoichiometries (Anderson and Kedersha, 2006; Buchan, 2014). They can assemble and disassemble dynamically, and their formation depends on multivalent weak interactions of component proteins and RNAs.

Most proteins found in RNA granules have two key features: many are RNA-binding proteins, and many contain low-complexity domains, regions with relatively little amino acid

diversity and structure (Calabretta and Richard, 2015). These regions share some similarity with prion-like domains and have the ability to drive protein-protein aggregation. Unlike pathological protein aggregation, RNA granules aggregate in a way that is controlled by the cell to serve specific functions. RNA granule formation can be seen as a localized phase-transition within the cellular environment, where RNA-binding and low-complexity domain-mediated protein aggregation drive component molecules towards a liquid droplet-like state (Weber and Brangwynne, 2012). These phase-transitioned liquid droplets are highly dynamic with the ability to grow or shrink, fuse or drip off from each other, or disassemble entirely (Hyman et al., 2014). Under certain conditions RNA-binding proteins can form more stable, pathological aggregates. An emerging model in the study of neurodegenerative diseases suggests that mutations in the low-complexity domains of specific RNA-binding proteins found in RNA granules favors stable aggregations that may contribute to the progression of those diseases (Aguzzi and Altmeyer, 2016; Shin and Brangwynne, 2017).

Many different classes of RNA granules have been characterized. Some examples of these include: nucleoli, germ granules, neuronal granules, processing bodies (P-bodies), and stress granules (Buchan, 2014). Nucleoli are RNA granules within the nucleus where ribosome biogenesis occurs. Germ granules are RNA granules found in all germ cells. Neuronal granules are RNA granules which allow for localized protein synthesis at synapses. P-bodies are RNA granules that specialize in mRNA turnover and miRNA-induced silencing. Finally, stress granules are RNA granules containing translationally silent mRNAs that form specifically under stress conditions (Anderson and Kedersha, 2008; Kedersha and Anderson, 2009).

RNA granules also form during stress in the chloroplast of *Chlamydomonas reinhardtii* (Uniacke and Zerges, 2008). These aggregates are called chloroplast stress granules (cpSGs) because they share many similarities with SGs found in the cytoplasm of mammalian cells and

other eukaryotes. The discovery of cpSGs in an organelle of bacterial ancestry suggests that the formation of stress-induced RNA granules is a conserved feature across evolution and that their functions may be particularly important for survival during stress. One unexpected feature that is unique to cpSGs is the presence of a photosynthesis protein, the large subunit of ribulose-1,5-bisphosphate carboxylase/oxygenase (Rubisco). This was unexpected because Rubisco is arguably the most extensively researched enzyme in photosynthesis and the presence of its large subunit in RNA granules, *viz.* cpSGs, suggests an alternate function for this protein.

1.4 The Large Subunit of Rubisco, RbcL

Rubisco is the enzyme responsible for CO₂ assimilation into ribulose-1,5-bisphosphate in chloroplasts during the Calvin-Benson cycle, and for the oxygenation of ribulose bisphosphate during photorespiration (Spreitzer and Salvucci, 2002). This soluble enzyme is located in the aqueous stroma of chloroplasts and comprises some 40-50% of the total protein content in photosynthetic tissue; as such, it is likely the most abundant protein on Earth (Ellis, 1979). The Rubisco holoenzyme is a multi-subunit protein complex that is composed of eight copies of a large subunit, RbcL, and eight copies of a small subunit, RbcS. RbcS is encoded for by a gene family located in the nucleus, while RbcL is encoded for by a single gene in the chloroplast genome (Miziorko and Lorimer, 1983). The finding that RbcL alone is recruited to cpSGs suggests that whatever function it has in that compartment, it is independent of its role in photosynthesis.

It was shown that during oxidative stress RbcL has several characteristics that are consistent with it being in cpSGs. *In vitro* biochemical analyses have shown that under oxidizing conditions RbcL is able to bind RNA in a sequence-independent manner (Yosef et al., 2004). The RNA binding activity of RbcL was predicted to lie within the N-terminal 150 amino acids of the protein because this region has structural similarity to an RNA-recognition motif found in certain RNA-binding proteins. The RNA-recognition motif and RNA binding activity of RbcL is conserved

throughout a broad range of photosynthetic organisms (Cohen et al., 2006). Furthermore, the Rubisco holoenzyme has been shown to disassemble during *in vivo* oxidative stress and *in vitro* oxidizing conditions, which results in the degradation of the RbcS subunit and the formation of high-molecular weight aggregates of RbcL (Knopf and Shapira, 2005). During oxidative stress Rubisco has also been observed to localize to an insoluble fraction of cell lysates (Marín-Navarro and Moreno, 2006; Mehta et al., 1992). These characteristics of RbcL that are observed during stress or oxidizing conditions (*viz.* holoenzyme disassembly, RNA binding activity, aggregation) are hypothesized to be regulated by the reversible oxidation of specific cysteine residues (Cohen et al., 2005; Marín-Navarro and Moreno, 2006; Moreno et al., 2008). Therefore, RbcL shares several characteristics with stress granule proteins in that it can bind to RNA and aggregate during oxidative stress.

In addition to being recruited to cpSGs, we recently demonstrated that a *non-Rubisco form of RbcL* is critical for controlling oxidized RNA levels in *C. reinhardtii*, while also being required for survival during oxidative stress (Zhan et al., 2015). RbcL is most well-known for its role in photosynthesis as a subunit of Rubisco. However, non-photosynthetic functions for this protein are supported by evidence indicating that RbcL accumulates several-fold above the equal stoichiometric amounts with RbcS that are required in the Rubisco holoenzyme (Recuenco-Muñoz et al., 2015). Intriguingly, the majority of RbcL in most algae and hornworts is localized to the pyrenoid, a phase-separated membraneless compartment within chloroplasts (Freeman Rosenzweig et al., 2017; McKay and Gibbs, 1991). Our discovery that oxidized RNA is also compartmentalized in the pyrenoid of *C. reinhardtii* suggests that RbcL is a key component in the localized control of oxidized RNA. Given this, characterizing the non-Rubisco functions of RbcL (in mitigating oxidized RNA levels, in promoting survival during stress, and as a cpSG protein) was the second objective of this thesis.

1.5 Overview and Thesis Rationale

Much regarding the effects of stress on cellular function remains unknown, including its effects on RNA. To further understand RNA metabolism during stress this thesis examines oxidized RNA and its handling. Novel mechanisms by which oxidized RNA is managed by cells were addressed using two parallel objectives: *objective 1* was to characterize the properties and possible function(s) of ORBs, novel intracellular compartments that contain oxidized RNA, in *Saccharomyces cerevisiae*; *objective 2* was to characterize non-Rubisco function(s) of RbcL, a protein that controls levels of oxidized RNA in chloroplasts, in *Chlamydomonas reinhardtii*.

The results of *objective 1* are presented here in Chapter 2: An RNA Granule Compartmentalizes Translation Quality Control in *Saccharomyces cerevisiae*. This chapter has been submitted for publication and represents the bulk of my contributions to original research. To achieve *objective 1*, several approaches were used. First, I characterized the basic properties of ORBs, which are hypothesized to be a novel type of RNA granule dedicated to the quality control of defective mRNAs. I found that ORBs do possess the known properties of phase-separated RNA granules, and that they contain defective mRNAs, stalled ribosomes, truncated and aberrant nascent chains, as well as several known quality control factors from the NGD and RQC pathways. The results contribute to our understanding of the functional significance of oxidized RNA compartmentalization. Next, I characterized the composition of ORBs, using mass spectrometry and proteomics. The results revealed a list of candidate proteins that may be involved in translation quality control and in the management of oxidized RNA. The ORB proteome will allow us to use the known or predicted functions of the proteins to reveal possible ORB function(s) at the molecular and cell physiological levels.

The results of *objective 2* are presented here in Chapter 3: Characterization of Non-Rubisco Functions of RbcL in *Chlamydomonas reinhardtii*. This chapter contains mostly preliminary

observations and is meant to serve as a reference for future researchers who study the moonlighting functions of RbcL. To achieve *objective 2*, I used several approaches. I hypothesized that RbcL controls oxidized RNA levels through an involvement with protein translation, with RbcL acting as a ribosome-based RNA quality control factor. I first dissected the structure of RbcL for amino acid residues that are required for its non-Rubisco functions. The results have revealed an RbcL mutant that is unable to form the Rubisco holoenzyme and has altered phenotypes related to the moonlighting RbcL functions. Next, I studied RbcL properties in several contexts related to chloroplast translation. The results of this approach were inconclusive. Lastly, I examined the subcellular localization of RbcL during conditions that induce autophagy, as stress granules have been reported to be degraded by this pathway. I found that RbcL re-localizes from the pyrenoid to distinct foci when autophagy is induced. Together, these preliminary data may provide insight into RNA quality control in chloroplasts.

CHAPTER 2: AN RNA GRANULE COMPARTMENTALIZES TRANSLATION
QUALITY CONTROL IN *SACCHAROMYCES CEREVISIAE*

Adapted from: Dhaliwal, J.S., Panozzo, C., Benard, L., and Zerges, W. (2020). Oxidized RNA Bodies compartmentalize translation quality control in *Saccharomyces cerevisiae*. *Biorxiv*. doi: 10.1101/2020.08.05.232983

ABSTRACT

Cytoplasmic RNA granules compartmentalize phases of the translation cycle in eukaryotes. We previously reported the localization of oxidized RNA to cytoplasmic foci called “oxidized RNA bodies” (ORBs) in human cells. Oxidized mRNAs are substrates of translation quality control, wherein defective mRNAs and nascent polypeptides are released from stalled ribosomes and degraded. Therefore, we asked whether ORBs compartmentalize the translation quality control pathways that handle oxidized mRNAs; no-go mRNA decay and ribosome-associated quality control. The results identify ORBs as RNA granules in *Saccharomyces cerevisiae*. Several lines of evidence support their role in the compartmentalization of translation quality control. Translation is required by these pathways and ORBs. Translation quality control factors localize to ORBs. A substrate of translation quality control, a stalled mRNA-ribosome-nascent chain complex, also localizes to ORBs. Translation quality control mutants have altered ORB numbers, sizes or both. Therefore, ORBs are RNA granules which serve as an intracellular hub of translational quality control in yeast. Finally, we identify 68 ORB proteins, by immunofluorescence staining directed by proteomics, which further support their role in translation quality control and reveal candidate new factors for these pathways.

2.1 INTRODUCTION

Ribosomes stall at oxidized bases and other lesions in defective mRNAs. Ribosome stalling is problematic because it generates truncated and aggregation-prone polypeptides, which can impair cellular homeostasis (Shan et al., 2003; Simms et al., 2014b). Consequently, defective mRNAs with stalled ribosomes and their truncated nascent polypeptides are recognized and cleared by the translation quality control (TQC) pathways, no-go decay (NGD) and ribosome-associated quality control (RQC). In TQC, collided ribosomes at a translation blockage on a defective mRNA are recognized, whereupon NGD separates their subunits and targets the aberrant mRNA for degradation (Doma and Parker, 2006; Ikeuchi et al., 2019; Juszkiwicz et al., 2018b; Shoemaker et al., 2010; Simms et al., 2017b). RQC extracts the nascent polypeptide from the 60S ribosomal subunit, and targets it for degradation by the ubiquitin-proteasome system (Bengtson and Joazeiro, 2010; Defenouillère et al., 2013; Dimitrova et al., 2009; Shen et al., 2015; Sitron and Brandman, 2019). These pathways are assumed to occur throughout the cytoplasm, based on intracellular distributions of fluorescent protein (FP)-tagged factors in genome-wide localization screens (Huh et al., 2003). However, any further compartmentalization has not yet been demonstrated, to our knowledge.

DNA and protein quality control pathways are localized to specialized intracellular compartments (Kaganovich et al., 2008; Paull et al., 2000; Rogakou et al., 1999). NGD has been proposed to occur in processing bodies (P-bodies), and RQC factors are involved in partitioning mRNAs from stalled ribosomes to stress granules (Cole et al., 2009; Moon et al., 2020). However, the proteomes of P-bodies and stress granules do not contain TQC proteins, with the exception of Rqc2 in yeast stress granules (Hubstenberger et al., 2017; Jain et al., 2016). Therefore, additional work is required to determine whether TQC is compartmentalized and, if so, the nature of the compartment(s) involved.

An avenue to explore RNA quality control was suggested by our identification of cytoplasmic bodies that contain oxidized RNA in human cells (Zhan et al., 2015). These “oxidized RNA bodies” (ORBs) were identified by immunofluorescence (IF) staining of HeLa cells using an antibody against an oxidized form of guanine, 8-oxoguanosine (8-oxoG). ORBs were shown to be distinct from P-bodies and stress granules, but their composition and function(s) remain unknown.

Here, we identify ORBs in *S. cerevisiae* and show that they are RNA granules. In addition, we provide the following evidence that ORBs compartmentalize NGD and RQC: 1) TQC factors localize to ORBs *in situ*; 2) two substrates of NGD and RQC localize to ORBs: oxidized RNA and a stalled mRNA-ribosome-nascent chain complex (RNC); 3) effects of pharmacological inhibitors reveal that translation is required for ORB formation; 4) certain mutants deficient for NGD, RQC or both have altered ORB numbers per cell. Finally, 68 ORB proteins were identified by IF microscopy, directed by proteomic analyses of affinity purified ORBs. These proteins include additional known factors of NGD and RQC and novel candidate factors for future analyses of ORBs and TQC.

2.2 MATERIALS AND METHODS

2.2.1 Plasmids, yeast strains and growth conditions

Yeast plasmids were constructed using standard molecular biology procedures starting from p415ADH1 (Mumberg et al., 1995) and were described previously (Navickas et al., 2020). Plasmid pLB138 expresses a truncated mRNA (Rz) from a 2HA-tagged-*URA3*-RZ (Ribozyme) construct. Plasmid pLB126 expresses a full length 2HA-*URA3* mRNA (FL). The wild-type strain was BY4741 (*MATa his3Δ1 leu2Δ0 met15Δ0 ura3Δ0*). All single mutant strains were obtained from the yeast knockout collection in the BY4741 background (Winzeler et al., 1999). All strains with GFP-tagged proteins were obtained from the GFP clone collection in the BY4741 background (Huh et al., 2003). The *dom34Δ-rqc2Δ* double mutant was generated by one-step gene replacement

using PCR fragment of the NatMX6 cassette amplified from plasmid pFA6a-natMX6 (Hentges et al., 2005).

Strains were grown at 30°C in YPD or SD (for live cell imaging) to mid-log phase (OD₆₀₀ of 0.5-0.8). Where indicated, cells were exposed to 100 µg/ml cycloheximide, 100 µg/ml puromycin, or 5% 1,6-hexanediol with 10 µg/ml digitonin for 30 min. For stress conditions, cells were exposed for 30 min to 5 mM H₂O₂. To induce autophagy, cells in mid-log phase were transferred to nitrogen starvation minimal medium (SD-N) for 2 hrs. Where indicated, cells were treated with 3.7% formaldehyde for 30 minutes.

2.2.2 Immunoblot analysis

Yeast cells from mid-log phase cultures were incubated on ice for 10 min in lysis buffer (0.2 M NaOH, 0.2% β-mercaptoethanol), whereupon 5% trichloroacetic acid was added followed by a 10-min incubation on ice. Precipitated proteins were pelleted by centrifugation at 12,000 x g for 5 min and resuspended in 35 µL of dissociation buffer (4% SDS, 0.1 M Tris-HCl, pH 6.8, 4 mM EDTA, 20% glycerol, 2% β-mercaptoethanol and 0.02% bromophenol blue). Tris-HCl, pH 6.8 was then added to a final concentration of 0.3 M and samples were incubated at 37 °C for 10 min. Total protein extracts were subjected to SDS-PAGE and immunoblot analysis. Membranes were reacted with 1:2000 mouse αHA primary antibody (Covance). Secondary staining used 1:10,000 goat anti-mouse-IgG antibody (KPL).

2.2.3 Northern blot analysis.

RNA Extracts and northern blots were performed as described previously (Navickas et al., 2020). Blots were exposed to PhosphorImager screens, scanned using a Typhoon FLA89500 (Fuji), and quantified with ImageJ software.

2.2.4 Indirect IF staining

Yeast cells from mid-log phase cultures were fixed in 3.7% formaldehyde for 15 min at room temperature, washed in phosphate buffer (0.1 M potassium phosphate, pH 6.5), and incubated with 10 mg/ml lyticase (in phosphate buffer containing 1.2 M sorbitol) for 30 min at 30°C. Spheroplasts were adhered to 0.1% poly-L-lysine-coated slides for 10 min. Slides were then submerged in ice-cold methanol for 5 min followed by room-temperature acetone for 30 seconds. Cells were blocked in 2% BSA, 1X PBS, 0.1% Tween-20 for 10 min and incubated with primary antibody (1:500 mouse α 8-oxoG, QED Bioscience; 1:5000 rabbit α GFP, ThermoFisher, 1:5000 mouse α HA, Covance) overnight at 4°C in a humidity chamber. Secondary antibodies were Alexa Fluor 647 donkey α goat IgG, Alexa Fluor 568 goat α mouse IgG, and Alexa Fluor 488 goat α rabbit IgG, each diluted 1:300 (ThermoFisher). The presence of RNA in ORBs was detected by staining with a 1:500 dilution of SYTO RNaselect™ (ThermoFisher) for 10 min prior to mounting. Where indicated, fixed and permeabilized cells were treated for 1 h at room temperature with 10 μ g/ml RNase A (Fermentas) prior to blocking.

The specificity of the α 8-oxoG antibody was confirmed by incubating with its antigen 8-hydroxy-2'-deoxyguanosine (10 μ g/ μ g of antibody) for 2 h before IF-staining; the α HA antibody is specific because the signal was not seen in a non-transformed strain or when the primary α HA antibody is omitted in IF of a pLB126 transformant, and it was significantly lower in the *dom34* Δ mutant; The GFP antibody is specific because no signal was seen in a non-transformed strain (Fig. S4).

2.2.5 Preparation of the ORB-enriched fraction

ORBs were prepared from BY4741 cells or the indicated strains from the GFP fusion library (Huh et al., 2003), as described previously for stress granule cores (Jain et al., 2016). Briefly, cell pellets from 50 mL cultures grown to mid-log phase were resuspended in 500 μ L lysis buffer (50

mM Tris-HCL (pH 7.5), 50 mM NaCl, 5 mM MgCl₂, 50 µg/mL heparin, 0.5 mM DTT, 0.5% Nonidet P-40, fungal protease inhibitor (BioShop), 1:5000 Antifoam B (Sigma) and lysed by vortexing with acid-washed glass beads for 2 min followed by 2 min on ice for three cycles. The initial lysate was cleared of unbroken material by centrifugation at 800 x g for 2 min at 4°C, and then centrifuged at 17,200 x g for 10 min at 4°C. This ORB-enriched pellet fraction was then resuspended in a final volume of 500 µL lysis buffer on ice. To test RNase A and Triton X-100 sensitivity of ORBs *ex vivo*, the final pellet was resuspended in lysis buffer containing either 10 µg/mL RNase A without heparin or 2% Triton X-100 and incubated for 30 min at room temperature on a nutator before a second centrifugation at 17,200 x g for 10 min at 4°C and resuspension in fresh lysis buffer. ORBs were detected by adhering the ORB-enriched fraction to poly-L-lysine-coated slides and probing for 8-oxoG as described above.

2.2.6 Microscopy and image analysis

IF microscopy images were acquired using a Leica DMI 6000 epifluorescence microscope (Leica Microsystems) with a 63X/1.4NA objective, a Hamamatsu OrcaR2 camera, and Volocity acquisition software (Perkin-Elmer). Z-stacks were taken by series capture at a thickness of 0.2 µm per section. Stacks were deconvoluted with AutoQuant X3 (Media Cybernetics Inc.). To quantify ORBs *in situ* we used a custom-written macro in ImageJ. Briefly, each cell was identified in a central z-slice, and its average 8-oxoG signal intensity determined. ORBs were defined as foci between 9 and 198 pixels² with a fluorescence intensity 1.5-fold higher than the cell average. The number of ORBs per cell, their size, and fluorescence intensity were then quantified by the macro. To quantify ORBs *ex vivo* we used the 3D objects counter plugin in ImageJ. ORB colocalization of stalled RNCs or GFP-tagged proteins *in situ* was determined using a custom-written ImageJ macro. Briefly, foci in each channel were determined as described above, and two foci from different channels were considered colocalized if at least 25% of the area of each foci in each

channel overlapped. For a candidate protein to be considered a validated ORB protein, three criteria were required: visual inspection of colocalization must be positive; at least 10% of identified ORBs must colocalize with a GFP foci; at least 18% of cells must have at least one colocalized foci. A minimum of three images were quantified for each biological replicate. One replicate from WT-FL in Figure 2.3F was considered an outlier because it was above 2 SEM and was not considered. Live cell images shown in Figure S2.3 were acquired using the Leica DMI 6000 epifluorescence microscope described above.

2.2.7 Purification of ORBs

ORBs were purified as described previously for stress granule cores (Wheeler et al., 2017). Protein A Dynabeads (Invitrogen) were added to ORB-enriched fractions from either untreated or cycloheximide-treated cultures for 1 hr at room temperature to pre-clear the fraction of non-specific interactions. Cleared lysates were then incubated with α 8-oxoG (QED Bioscience) at 4°C for 1 hr to capture ORBs, followed by a 1 hr incubation with Dynabeads to capture the ORB-antibody complexes. Purified ORBs were resuspended and boiled in SDS-loading buffer for 5 min, then loaded onto a 5% polyacrylamide gel for in-gel trypsin digestion.

2.2.8 Mass spectrometry

Purified ORB proteins were concentrated in a stacking gel using SDS-PAGE stained with Coomassie Brilliant Blue R-250 (Biorad). Proteins in the excised gel band were subjected to in-gel digestion as follows. Gel pieces were incubated for 30 min at room temperature in 50 mM NH_4HCO_3 (Sigma) + 10 mM dithiothreitol to reduce the proteins and then for 30 min at room temperature with 50 mM NH_4HCO_3 + 50 mM Iodoacetamide (SIGMA) in the dark to alkylate them. Gel dehydration was done with a series of acetonitrile (ACN, BDH) washes. Gel pieces were rehydrated in trypsin digestion solution containing 25 mM NH_4HCO_3 and 10 ng/ μL of trypsin (Sigma) followed by incubation overnight at 30°C. Tryptic peptides were extracted three times for

15 min at room temperature with extraction solution (60% acetonitrile + 0.5% formic acid (FA, Fisher), four volumes of the digestion solution). Peptides were dried using a Speedvac at 43°C and stored at -20°C until MS analysis. Liquid chromatography-tandem MS (LC-MS/MS) analyses were performed on a Thermo EASY nLC II LC system coupled to a Thermo LTQ Orbitrap Velos mass spectrometer equipped with a nanospray ion source. Tryptic peptides were resuspended in solubilization solution containing 97% of water, 2% of ACN and 1% of FA to give a peptide concentration of 100 ng/μL. 2 μL of each sample were injected into a 10 cm × 75 μm column that was in-house packed with Michrom Magic C18 stationary phase (5 μm particle diameter and 300 Å pore size). Peptides were eluted using a 90-min gradient at a flow rate of 400 nL/min with mobile phase A (96.9% water, 3% ACN and 0.1% FA) and B (97% ACN, 2.9% water and 0.1% FA). The gradient started at 2% of B, linear gradients of B were achieved to 8% at 16 min, 16% at 53 min, 24% at 69 min, 32% at 74 min, 54% at 81 min, 87% at 84 min followed by an isocratic step at 87% for 3 min and at 2% for 3 min. A full MS spectrum (m/z 400-1400) was acquired in the Orbitrap at a resolution of 60,000, then the ten most abundant multiple charged ions were selected for MS/MS sequencing in linear trap with the option of dynamic exclusion. Peptide fragmentation was performed using collision induced dissociation at normalized collision energy of 35% with activation time of 10 ms. Spectra were internally calibrated using polycyclodimethylsiloxane (m/z 445.12003 Da) as a lock mass.

2.2.9 Mass spectrometric data processing

The MS data were processed using Thermo Proteome Discoverer software (v2.2) with the SEQUEST search engine. The enzyme for database search was chosen as trypsin (full) and maximum missed cleavage sites were set at 2. Mass tolerances of the precursor ion and fragment ion were set at 10 ppm and 0.6 Da, respectively. Static modification on cysteine (carbamidomethyl, +57.021 Da) and dynamic modifications on methionine (oxidation, +15.995 Da) and N-terminus

(acetyl, +42.011 Da) were allowed. The initial list contained 1048 proteins identified with high confidence (false discovery rate <1%) and from combining three biological replicates. Of this list we retained 822 proteins according to criteria stated in the results section.

2.2.10 Bioinformatic analysis of the ORB proteome

The ORB proteome was classified according to GO Molecular Function and GO Biological Process information from the SGD database (yeastgenome.org). RNA binding activity was determined using GO analysis and published lists of yeast RNA binding proteins (Beckmann et al., 2015; Mitchell et al., 2013). Networks of physical and genetic interactions were generated and visualized using Cytoscape (version 3.7.2) with the GeneMania plugin (version 3.5.2) (Shannon et al., 2003; Warde-Farley et al., 2010). Proteins with intrinsically disordered regions or prion-like domains were predicted using the SLIDER and PLAAC tools, respectively (Lancaster et al., 2014; Peng et al., 2014).

2.3 RESULTS

2.3.1 ORBs are cytoplasmic RNA granules in yeast.

To determine whether ORBs exist in *S. cerevisiae*, we visualized the *in situ* distribution of 8-oxoG by IF-microscopy, the approach that revealed ORBs in human cells (Zhan et al., 2015). Cells from cultures in exponential growth phase showed the 8-oxoG IF signal in cytoplasmic foci that numbered 5.4 per cell and measured 450 nm in diameter (Figure 2.1A and B). While 8-oxoG can be in RNA, DNA and nucleotides (Wurtmann and Wolin, 2009), these foci contain oxidized RNA because they were eliminated by RNase A treatment of fixed and permeabilized cells, they stained positive for RNA with an RNA-specific fluorescent dye, and they did not stain for DNA with DAPI (Figure 2.1 C-E). The specificity of the antibody for 8-oxoG RNA was confirmed by the abovementioned RNase A sensitivity of ORBs and the loss of IF signal by preincubation of the

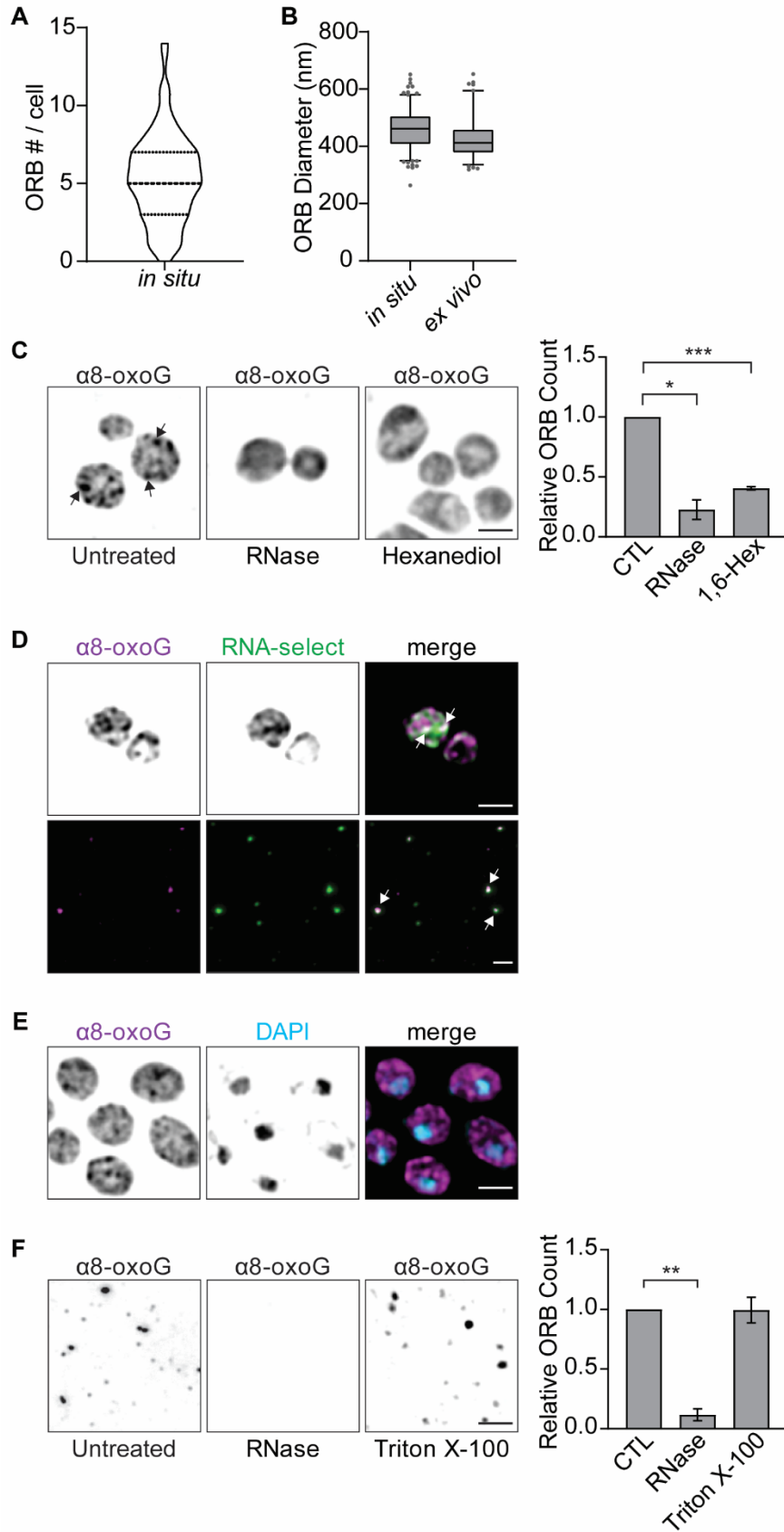


Figure 2.1. ORBs are an RNA granule in *S. cerevisiae*.

(A) Violin plot of the ORB number per cell. The median and interquartile ranges are indicated by thick and thin dashed lines, respectively (n=6). (B) Box plots of ORB diameter (nm) *in situ* and *ex vivo*. Box heights indicate the interquartile range, and whiskers indicate the 5th and 95th percentiles. (C) IF staining of exponentially growing unstressed cells revealed foci of 8-oxoG (black arrows). Cells were either untreated (CTL abbreviation) or treated with either RNase A, following fixation, or 1,6-hexanediol *in vivo*. Bar heights indicate ORB number per cell (relative to untreated cells) (n=3). Error bars = ± 1 SEM (D) Co-IF staining ORBs (α 8-oxoG) and RNA with SYTO RNASelect *in situ* (top) and *ex vivo* (bottom). Arrows indicate colocalized foci. (E) Co-IF staining for ORBs (α 8-oxoG) and DAPI. Scale bars = 2.0 μ m. N values refer to biological replicate experiments from independent cultures. (F) IF staining of ORBs (α 8-oxoG) *ex vivo*. Lysates were untreated or treated with either RNase A or Triton X-100. Bar heights indicate ORB count (relative to untreated lysates) (n=3). Error bars = ± 1 SEM. (C and F) Statistical significance was determined by one-sample t-tests. * = $p \leq 0.05$, ** = $p \leq 0.01$, *** = $p \leq 0.001$.

antibody with 8-oxoG (Figure S2.1; Park et al., 1992). Finally, ORBs are none of the membranous organelles that contain RNA and appear as foci in fluorescence microscopy (Figure S2.2).

ORBs are RNA granules, i.e., membraneless organelles that contain RNA and form by liquid-liquid phase separation (Shin and Brangwynne, 2017). ORB number per cell was reduced by treatment *in vivo* with 1,6-hexanediol, which dissolves RNA granules by disrupting the intermolecular interactions that underlie their formation by liquid-liquid phase-separation (Figure 2.1C; (Alberti et al., 2019; Kroschwald et al., 2017). Like the RNA granules P-bodies and stress granules, ORBs were stable in lysates, i.e., *ex vivo* (Figure 2.1D and F; Jain et al. 2016; Teixeira and Parker 2007). In addition, these foci were resistant to the non-ionic detergent Triton X-100 *ex vivo*, a property of RNA granules but not membranous organelles (Figure 2.1F; (Fujimura et al., 2009; Shelkovernikova et al., 2014). These *ex vivo* foci were ORBs because they were the same diameter, stained positive for RNA, and were eliminated by RNase A (Figure 2.1B, D, and F). These results reveal that ORBs exist in yeast and are RNA granules.

2.3.2 TQC factors localize to ORBs

Oxidized bases in mRNA stall ribosomes, which need to be resolved by the TQC pathways NGD and RQC (Inada, 2020; Yan and Zaher, 2019). Stalled ribosomes are recognized by Hel2, followed by the Dom34- and Hbs1-dependent splitting of their subunits, whereupon Rqc2 extracts the truncated nascent polypeptide from the 60S subunit. Moreover, TQC is required for the clearance of oxidized mRNA (Simms et al., 2014). To test whether ORBs compartmentalize these pathways, cells were IF-stained for GFP fused to each of the abovementioned TQC factors and co-IF stained for 8-oxoG to visualize ORBs. ORBs were seen to have each of these TQC proteins (Figure 2.2A). Quantification of the overlap with ORBs was 24% for Dom34-GFP, 25% for Hbs1-GFP, 24% for Hel2-GFP, and 32% for Rqc2-GFP (Figure 2.2, Table S1.1). Fortuitous overlap is

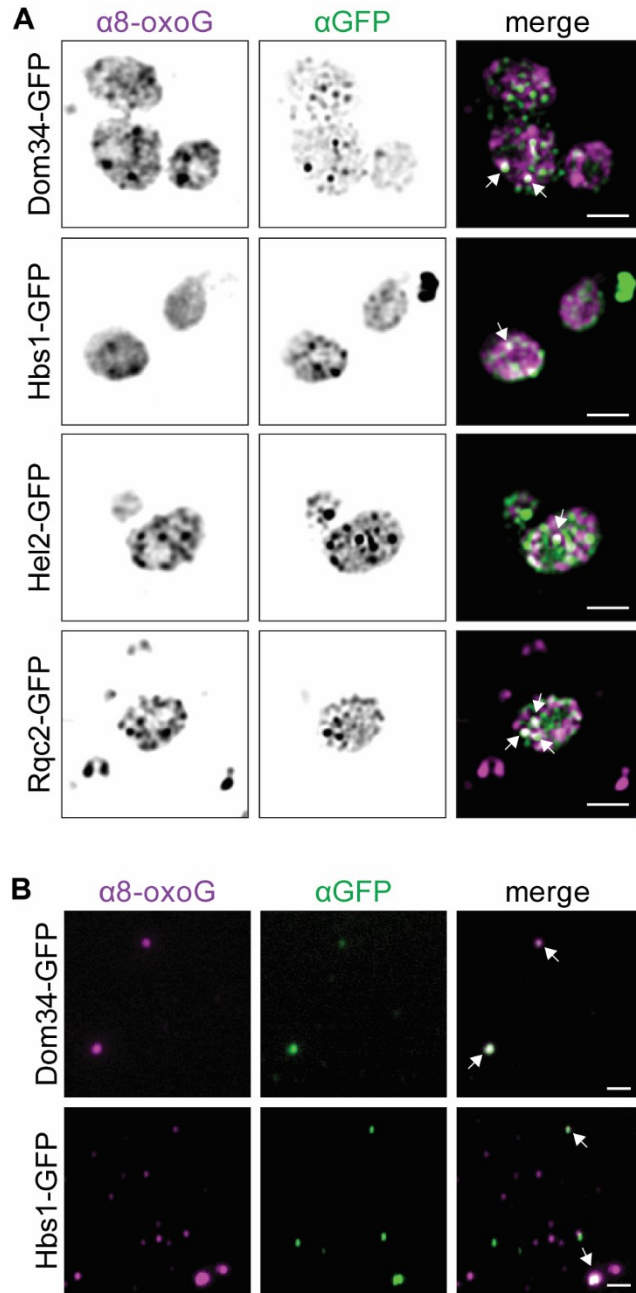


Figure 2.2. NGD and RQC factors localize to ORBs

(A) Co-IF staining of ORBs ($\alpha 8\text{-oxoG}$) and GFP-tagged TQC proteins (A) *in situ* and (B) *ex vivo*. Arrows indicate colocalized foci. Scale bars = 2.0 μm .

highly improbable because ORBs also co-IF-stained for Dom34-GFP or Hbs1-GFP *ex vivo*, i.e., after the dispersal of intracellular material (Figure 2.2B).

That only subpopulations of ORBs have these proteins is consistent with the heterogeneity of translation-related RNA granules (Anderson and Kedersha, 2006a; Buchan et al., 2011; Hoyle et al., 2007; Lui et al., 2014a). TQC factor localization to ORBs was surprising because the factors have not been reported to localize to foci, to our knowledge.

We attempted to determine whether these GFP-tagged TQC factors localize to ORBs in live cells. While most cells expressing either Dom34-GFP, Hbs1-GFP, Hel2-GFP, or Rqc2-GFP showed weak fluorescence from the cytoplasm, this signal was close to the background seen in the non-transformed strain (Figure S2.3). Moreover, wild-type cells that lack GFP formed multiple autofluorescent foci during exposure to hydrogen peroxide (Figure S2.3). Thus, the weak signals from the GFP-tagged proteins and the prominent autofluorescent foci, of unknown composition, prevented a determination of whether GFP-tagged factors form foci. These foci were not the ORBs detected by IF-microscopy because no autofluorescence was detected from fixed cells that were not reacted with primary antibody.

2.3.3 ORBs require translation.

If ORBs compartmentalize TQC, they would likely be affected by the inhibition of translation. Translational roles of P-bodies and stress granules were revealed, in part, by the effects of translation inhibition by cycloheximide and puromycin (Eulalio et al., 2007; Kedersha et al., 2000). We found that treatment of cells with either drug reduced the number of ORBs per cell by over 2-fold, supporting a connection between ORBs and translation (Figure 2.3A and B). The intensity of the 8-oxoG IF signal throughout cells increased by over 2-fold during translation inhibition (Figure 2.3B). This is consistent with the known role of translation in clearing oxidized

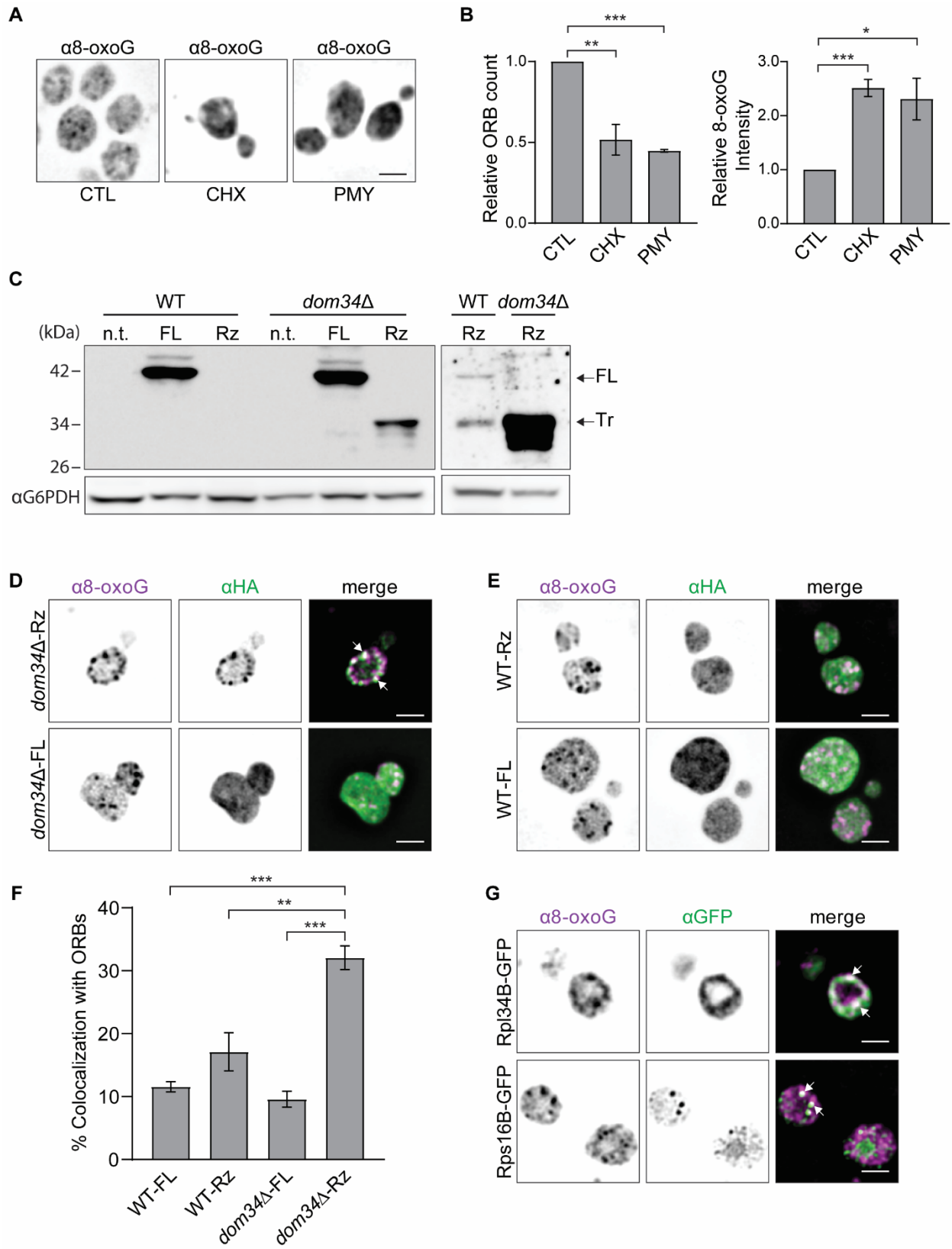


Figure 2.3. Stalled ribosome-nascent chain complexes localize to ORBs

(A) IF staining of ORBs (α 8-oxoG) in cells that were untreated (CTL) or treated with either cycloheximide (CHX) or puromycin (PMY). (B) Bar heights indicate relative ORB number per cell (left) or 8-oxoG IF signal intensity per cell (right) following treatment with CHX (n=5) or PMY (n=4). Error bars = \pm 1 SEM. Statistical significance was determined by one-sample t-tests. (C) Immunoblot analysis of HA-Ura3 in total protein from either WT or *dom34* Δ cells, transformed with the expression construct for the HA-*URA3* mRNA, either with the self-cleaving hammerhead ribozyme (Rz) or without it (FL). n.t.=non-transformed. The righthand blot shows that the truncated (Tr) band in WT accumulates to c.a. 2.4% of its level in *dom34* Δ cells. (D and E) Co-IF staining of ORBs (α 8-oxoG) and HA-Ura3, either as nascent polypeptides in the arrested RNC expressed from mRNA1Rz (Rz), or as the full-length protein (FL). Genetic backgrounds were (D) *dom34* Δ (to prevent the resolution of the arrested RNC) and (E) wild-type (WT, as the control). (F) Bar heights indicate the percentages of ORBs that colocalize with foci of HA-Ura3 (n =4 for WT-FL and WT-Rz, n=5 for *dom34* Δ -FL, and n=6 for *dom34* Δ -Rz). Error bars = \pm 1 SEM. Statistical significance was determined by unpaired two-sample t-tests. (G) Co-IF staining of 8-oxoG with Rpl34B-GFP (top) or Rps16B-GFP (bottom). Arrows in C, D, and F indicate colocalized foci. Scale bars = 2.0 μ m. N values refer to the number of independent biological replicate experiments. * = $p \leq 0.05$, ** = $p \leq 0.01$, *** = $p \leq 0.001$.

mRNAs through TQC pathways (Simms et al., 2014). These results support further a role of ORBs in the compartmentalization of TQC.

2.3.4 A stalled mRNA-ribosome-nascent chain complex localizes to ORBs

If ORBs compartmentalize TQC, they should be enriched in a translationally arrested RNC, a TQC-specific substrate (Brandman et al., 2012; Navickas et al., 2020). An arrested RNC was generated on a *URA3* mRNA with a self-cleaving hammerhead ribozyme inserted into its coding region (Figure S2.4A and B; Navickas et al., 2020). Ribozyme-catalyzed self-cleavage generates a 3' truncation, which arrests translating ribosomes. Our rationale was to determine whether the arrested RNC localizes to ORBs by IF-staining an HA-epitope tag at the N-terminus of the nascent Ura3 polypeptide. The truncated HA-Ura3 nascent polypeptide in a wild-type TQC background, although detected by immunoblot analysis, accumulated only to the levels of non-specific background bands, which would likely interfere with detection of the RNC *in situ* (Figure 2.3C). However, in a *dom34Δ* background, the defect in NGD enhanced the accumulation of the truncated nascent polypeptide by c.a. 40-fold, such that the HA-Ura3 truncated nascent polypeptide was the predominant species (Doma and Parker, 2006). Moreover, it was shown previously that mRNA1Rz in *dom34Δ* is bound by an array of colliding ribosomes (Navickas et al., 2020; Tsuboi et al., 2012). Therefore, the truncated HA-Ura3 nascent polypeptide in *dom34Δ* served as a marker for the arrested RNC *in situ*.

IF-microscopy images showed the HA signal from the arrested RNC localized to ORBs in *dom34Δ* cells (Figure 2.3D). Significantly less ORB localization was seen for the arrested RNC in the wild-type strain and for the full-length HA-Ura3 polypeptide in either background (Figure 2.3D, E, and F). These results are consistent with the levels of the truncated HA-URA nascent polypeptide in Figure 2.3C. Since ribosomes are present in arrested-RNCs, we also asked whether ORBs contain ribosomal subunits, by IF-staining GFP fused to ribosomal proteins. ORBs IF-

stained for both ribosomal proteins tested; one of each of the subunits (Figure 2.3G). Additional evidence of ribosomal protein localization to ORBs is presented below. Therefore, ORBs contain both ribosome subunits, as would be expected for a location of TQC. Together, these results demonstrate that a highly specific substrate for TQC localizes to ORBs.

2.3.5 Genetic evidence for TQC compartmentalization by ORBs.

As another test of a role of ORBs in the compartmentalization of TQC, we asked whether their size and number per cell are altered in TQC-deficient mutants (Figure 2.4A and B). Relative to in wild type, *hel2Δ* cells had 50% more ORBs; *hbs1Δ* cells had 18% fewer ORBs; *dom34Δ-rqc2Δ* double mutant cells had 46% fewer ORBs. The latter is a synthetic phenotype; it was not seen in *dom34Δ* or *rqc2Δ* single mutants. ORBs in *hbs1Δ* cells were 30% larger than those in the wild-type strain. That *hbs1Δ* cells had fewer but larger ORBs could be indicate that oxidized RNAs are not effectively degraded, but instead accumulate in ORBs in this mutant. Furthermore, the synthetic phenotype of the double mutant *dom34Δ-rqc2Δ* supports that there are two distinct but related pathways in ORBs (NGD and RQC). These phenotypes provide functional evidence that ORBs compartmentalize TQC.

2.3.6 Proteomic results further support ORBs as being an RNA granule for TQC.

We used proteomics to explore ORB composition and to further explore their functions. ORBs were immunoaffinity-purified by a procedure developed for stress granules, but using the antibody against 8-oxoG (Jain et al., 2016). Proteomic analyses identified 822 candidate proteins by at least two unique peptides, and which were not depleted by cycloheximide treatment (Figure 2.5, Table S2.2). By co-IF staining 109 of these GFP-tagged candidate proteins with 8-oxoG *in situ*, we identified 68 proteins that localize to ORBs (Figure 2.5, Table S2.1; Cdc42 was IF-stained with an antibody against it). These proteins tested positive for ORB-localization with a custom-written ImageJ macro (Table S2.1). To the list of validated ORB proteins, we added eight proteins

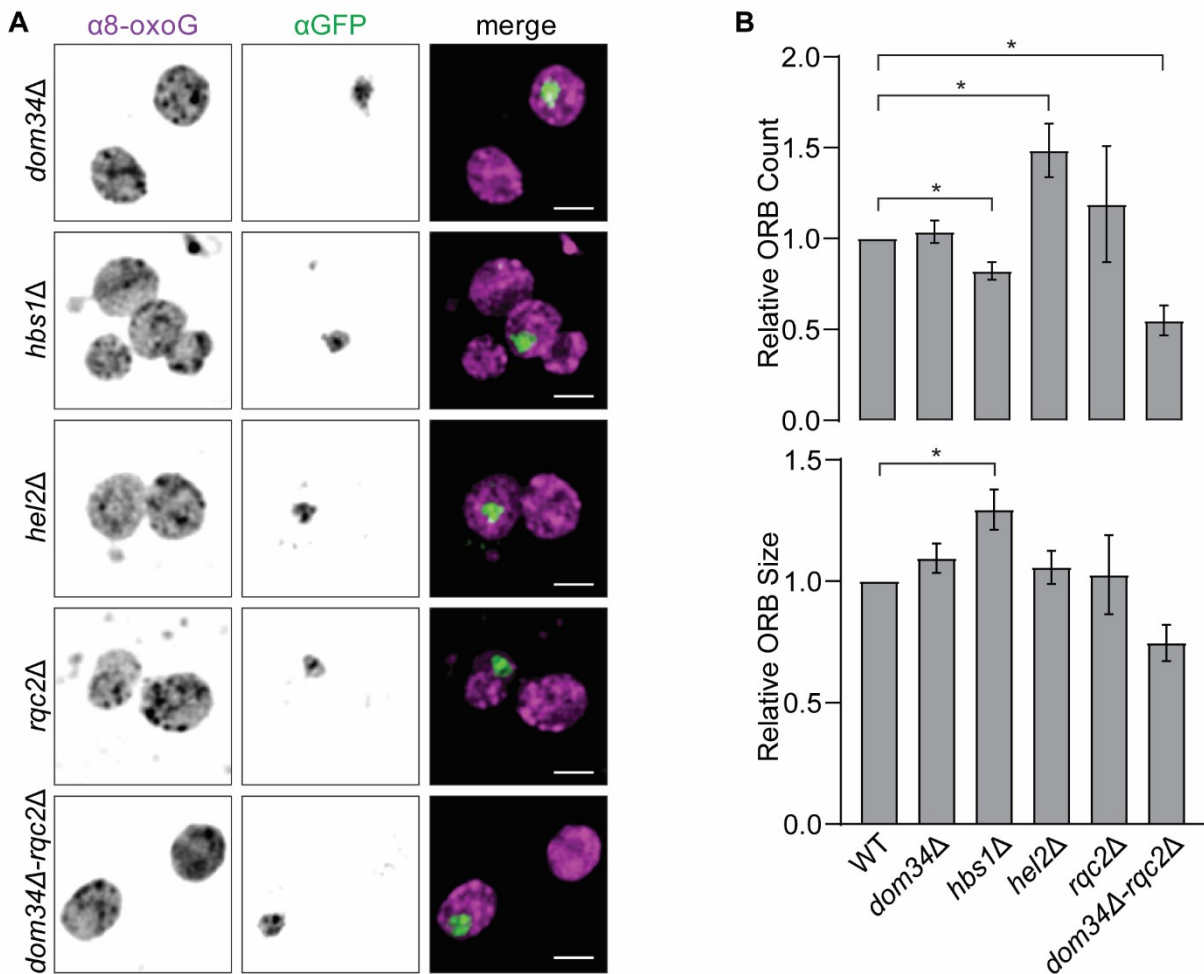


Figure 2.4. ORB phenotypes in NGD and RQC mutants

(A) ORBs were visualized by IF-staining $\alpha 8$ -oxoG in the mutants indicated, which were mixed with wild-type cells expressing Rpb2-GFP (a nuclear protein) as a marker for them. Scale bars = 2.0 μ m. (B) Bar heights indicate (top) ORB number per cell and (bottom) ORB size in the TQC mutants for *dom34* Δ , *hbs1* Δ , and *hel2* Δ (n= 4), *rqc2* Δ and *dom34* Δ -*rqc2* Δ (n=3), relative to in wild type. Error bars = \pm 1 SEM. Statistical significance was determined by unpaired two-sample t-tests. N values refer to the number of independent biological replicate experiments. * = $p \leq 0.05$.

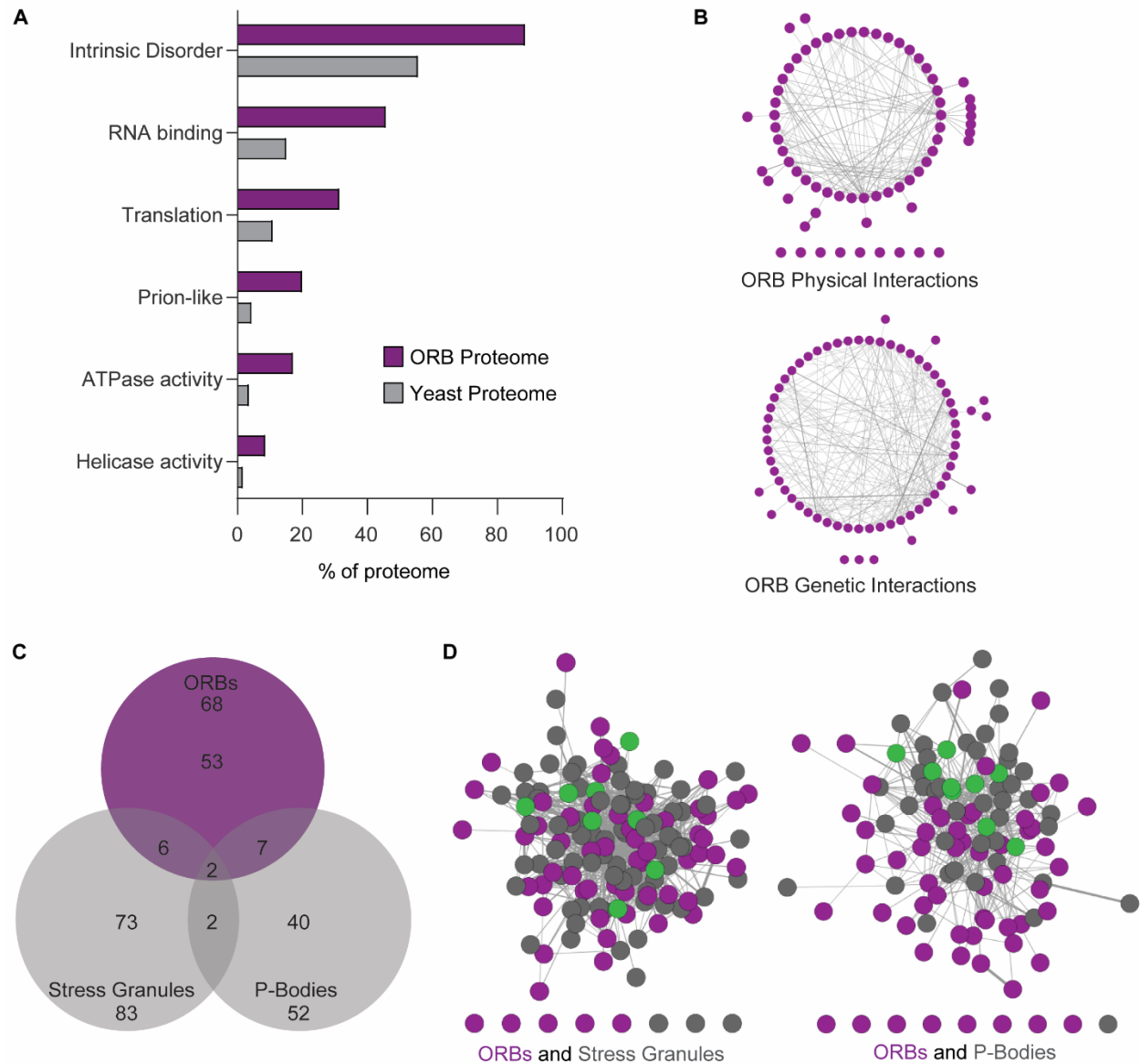


Figure 2.5. Features of the ORB proteome

(A) Enriched categories in the ORB proteome are presented as their percentage of the ORB proteome and, to show enrichment, the yeast proteome. (B) Known physical and genetic interaction networks within the ORB proteome. (C) The Venn diagram shows limited overlap between the ORB proteome and the proteomes of P-bodies and stress granules (Jain. et. al., 2016). (D) Known physical interactions between proteins in the ORB proteome and the stress granule proteome (left) or P-body proteome (right). Shared proteins are labelled green.

that were found to localize to ORBs prior to the proteomic analysis but, nonetheless, were supported by one unique peptide and non-depletion in the cycloheximide control. The resulting partial ORB proteome contains 68 proteins, all of which were validated *in situ* (Table S2.1).

This proteome supports further ORBs as being RNA granules with functions in RNA metabolism. Results of GO analysis revealed that, relative to the yeast proteome, the ORB proteome is enriched in protein classes found in cytoplasmic RNA granules: e.g. ATPases, RNA-binding proteins, and RNA-helicases, (Figure 2.5A; Hubstenberger et al., 2017; Jain et al., 2016). We identified additional RNA-binding proteins by comparison to published databases (Table S2.1; (Beckmann et al., 2015; Mitchell et al., 2013). Like other RNA granule proteomes, the ORB proteome is enriched in proteins with intrinsically disordered regions and prion-like domains (Figure 2.5A). ORB proteins form networks of physical and genetic interactions which are denser than would occur at random; 4.7 physical interactions per protein ($p = 3.83 \times 10^{-9}$) and 6.1 genetic interactions ($p = 1.76 \times 10^{-6}$) (Figure 2.5B). Finally, ORBs have several members of the Ccr4-Not complex, which contributes to most aspects of RNA metabolism (Table S2.1; Collart, 2016). The compartmentalization of TQC in ORBs is supported further by the proteome. These analyses also identified four additional TQC factors in ORBs: Not4, Cdc48, Cue3, and Rtt101 (Fujii et al., 2009; Yan and Zaher, 2019). Additionally, a total of six ribosomal proteins of both subunits were identified, as expected for a TQC compartment (see above). In summary, the validated proteome reveals that ORBs contain proteins that have concerted biochemical activities which would be expected in an RNA granule that compartmentalizes TQC.

2.3.7 ORBs are distinct from P-bodies and stress granules but share proteins with each.

This proteome allowed us to compare and contrast ORBs with P-bodies and stress granules, whose proteomes have been reported (Hubstenberger et al., 2017; Jain et al., 2016).

Most proteins in the ORB proteome are in neither P-bodies nor stress granules (Figure 2.5C). During validation of the proteome, ORBs did not IF-stain positive for two additional P-body proteins (Ccr4, Xrn1) and six additional stress granule proteins (Hrp1, Pab1, Rbg1, Rio2, Rpo21, Rvb1) (Table S2.1). Therefore, ORBs are distinct from stress granules and P-bodies.

The ORB proteome shares a minority of proteins with P-bodies and stress granules (Figure 2.5C). The ORB proteome has eight stress granule proteins, nine P-body proteins, and two proteins that are common to both (Dhh1 and Scd6; Figure 2.6C, Table S2.1). Finally, analyses of the ORB proteome combined with either the stress granule proteome or the P-body proteome revealed dense physical interaction networks, which involve many inter-proteome interactions (Figure 2.5D). Therefore, ORBs appear to be functionally related to stress granules and P-bodies, consistent with our evidence for ORB roles in mRNA metabolism and translation.

2.4 DISCUSSION

2.4.1 ORBs are cytoplasmic RNA granules.

We show that ORBs are RNA granules, i.e., membraneless cytoplasmic bodies that contain RNA and form by liquid-liquid phase separation. ORBs share functional classes of proteins with P-bodies and stress granules, e.g., factors in RNA metabolism and the remodeling of RNP complexes, RNAs or proteins (Figure 2.5; Hubstenberger et al., 2017; Jain et al., 2016). ORBs are enriched in proteins with intrinsically disordered regions and prion-like domains, hallmarks of RNA granules. Finally, proteins in our ORB proteome form a dense network of physical interactions, consistent with their being components of an organelle.

2.4.2 ORBs compartmentalize steps in TQC

We show that a subpopulation of ORBs compartmentalizes steps in TQC during stress with four lines of evidence. First, translation is required for both TQC and ORBs (Figure 2.3A, and B). Second, two NGD substrates localize to ORBs; oxidized RNA and an arrested RNC (Figures 2.1,

2.3). Third, ORBs have factors of NGD, RQC, and both ribosome subunits (Figures 2.2, 2.3, 2.5). Fourth, certain TQC-deficient mutants have altered ORB numbers per cell or size (Figure 2.4).

The TQC factors in ORBs function in the recognition of the arrested RNC (Hel2 and Cue3), the separation of the stalled ribosome subunits (Dom34, Hbs1, Rli1), the extraction of the nascent polypeptide from the 60S subunit (by CAT-tailing) or its ubiquitination (Rqc2, Cdc48, Not4; (Inada, 2020; Yan and Zaher, 2019). Notably, we did not detect ORB proteins involved in the endonucleolytic cleavage of the aberrant mRNA (Cue2) or the exonucleolytic degradation of the products (Xrn1, most exosome subunits; Table S2.1; Doma and Parker, 2006; D’Orazio et al., 2019).

The additional possibility that aberrant rRNAs undergo quality control in ORBs is suggested by their having Rtt101 and ribosome subunits (Fujii et al., 2009). Additional work is required to address this possibility.

ORBs could facilitate TQC by maintaining elevated local concentrations of substrates and intermediates to favor forward reactions and by sequestering aberrant mRNAs and truncated nascent chains to prevent them from undergoing deleterious side-reactions. For example, sustained translation initiation on an oxidized mRNA would likely lead to the production of aggregation-prone polypeptides and toxicity (Defenouillère et al., 2016; Jamar et al., 2018; Shan et al., 2003; Yonashiro et al., 2016).

The ORB proteome reveals candidate TQC proteins. For example, it contains four ribosome nuclear export factors, which prevent association of unassembled ribosomal subunits until they are competent for translation (Woolford and Baserga, 2013). Subunit separation is required in TQC when the mRNA and nascent polypeptide are extracted from the disassembled ribosome (Brandman and Hegde, 2016). The ORB proteome includes four nuclear export factors; two for each ribosome subunit (40S, Nob1 and Tsr1; 60S, Lsg1 and Nmd3; Table S2.1). These could be

acting like Rqc2 by separating ribosome subunits during RQC (Lyumkis et al., 2014; Shao et al., 2015; Shen et al., 2015). Therefore, our results open avenues to further dissect TQC.

2.4.3 The position of ORBs among the cytoplasmic RNA granules in yeast.

ORBs are in a rapidly growing class of cytoplasmic RNA granules with functions related to translation (Decker and Parker, 2012; Lui et al., 2014b; Panasenko et al., 2019). Our results support a role of ORBs in TQC of non-translatable defective mRNAs with arrested ribosomes (Figure 2.6). By contrast, translation granules are sites of active translation, Not1-containing assemblies contain temporarily paused ribosomes, and P-bodies and stress granules handle translationally repressed mRNAs (Ivanov et al., 2018; Lui et al., 2014; Panasenko et al., 2019). Distinctions between ORBs and both P-bodies and stress granules are revealed by our results. This was particularly important because P-bodies are a proposed location of NGD and stress granules have a relationship with a non-canonical stress-activated RQC pathway (Cole et al., 2009; Moon et al., 2020). Only one TQC factor was identified in the proteome of stress granules (Rqc2) and none were identified in the P-body proteome (Hubstenberger et al., 2017; Jain et al., 2016). We show that ORBs lack at least three P-body proteins and seven stress granule proteins (Table S2.1). These include canonical proteins of P-bodies (Dcp2, Xrn1) and stress granules (Pab1, Pub1). In addition, large majorities of the proteins in the ORB proteome are absent from the proteomes of P-bodies and stress granules (Figure 2.5C). Ribosomal subunit localization also differs between these RNA granule types; P-bodies lack both subunits, stress granules have only the small subunit, and ORBs have both subunits (Figure 2.3G, Table S2.1; (Hubstenberger et al., 2017; Jain et al., 2016). Puromycin stabilizes P-bodies and stress granules but decreased the number of ORBs per cell (Figure 2.3A and B; (Eulalio et al., 2007; Kedersha et al., 2000). ORBs probably are not translation bodies because cycloheximide has opposite effects on their respective numbers per cell (Figure 2.3A and B; Lui et al., 2014). P-bodies and stress granules have roles in the dynamic handling of

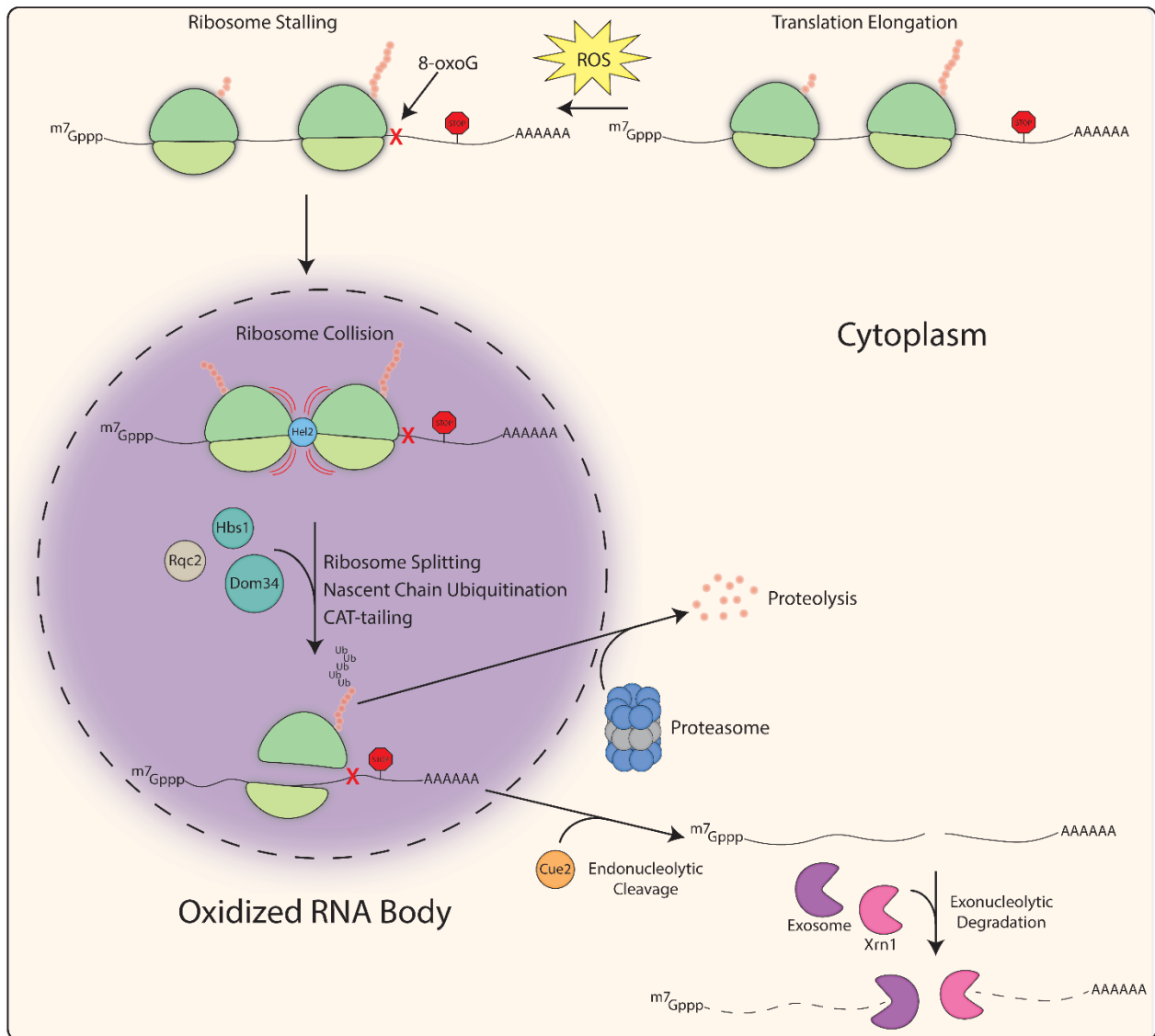


Figure 2.6. Model showing the compartmentalization of translation quality control in ORBs

Oxidized bases (red X) in mRNAs can cause ribosomes (green) to stall during translation, upstream of the stop codon (red stop sign). Collided ribosomes are detected by Hel2 (light blue) and localize to oxidized RNA bodies (purple) along with the translation quality control factors that separate ribosomal subunits (Hbs1 and Dom34, teal) and target the nascent chain for degradation (Rqc2, light brown). Aberrant nascent chains and defective mRNAs are degraded in the cytoplasm by the proteasome (dark blue) and nucleases, Cue2, Xrn1, and the exosome (orange, pink, and purple), respectively.

mRNAs cycling to and from the translated mRNA pool on polysomes. These roles were revealed, in part, by the opposite effects on their presence when the initiation or elongation phases of translation were inhibited, by puromycin or cycloheximide, respectively (Eulalio et al., 2007; Kedersha et al., 2000). By contrast, our findings that both cycloheximide and puromycin reduced ORB number per cell and increased 8-oxoG fluorescence intensity suggest that defective mRNAs do not exit ORBs and return to polysomes, consistent with their degradation by NGD, as expected.

Despite these differences, similarities between ORBs and both stress granules and P-bodies were revealed by partial overlaps of their proteomes. ORB localization was found for nine P-body proteins and eight stress granule proteins (Table S2.1, Figure 2.5C). Two proteins are common to P-bodies, stress granules, and ORBs: Dhh1 and Scd6. Analysis of the ORB proteome combined with the proteome of either P-bodies or stress granules revealed dense networks of physical interactions (11.8 average interactions between ORB and stress granule proteins, and 8.5 between ORB and P-body proteins), supporting further functional relationships between ORBs and these RNA granules (Figure 2.5D). The high density of interactions between the proteomes of ORB and stress granule is particularly interesting given that stress granules receive mRNAs released from stalled ribosomes, in a non-canonical stress-activated RQC pathway (Moon et al., 2020). Therefore, an intriguing possibility is that stress granules receive mRNAs released from TQC in ORBs, analogous to the exchange of components that occurs between stress granules and P-bodies (Buchan et al., 2008).

CHAPTER 3: CHARACTERIZATION OF NON-RUBISCO FUNCTIONS OF RBCL IN
CHLAMYDOMONAS REINHARDTII

ABSTRACT

RNA oxidation can detrimentally affect cells because it results in the production of misfolded or aggregation-prone proteins. We previously investigated the management of oxidized RNA in the chloroplast of the unicellular green alga *Chlamydomonas reinhardtii* and found that oxidized RNA is compartmentalized to the pyrenoid, a liquid-like microcompartment where the CO₂-fixing enzyme Rubisco is concentrated. We also reported a moonlighting function for the large subunit of Rubisco, RbcL, which localizes to chloroplast stress granules during oxidative stress, in mitigating the accumulation of oxidized RNA and promoting tolerance to hydrogen peroxide-induced oxidative stress. Here, I present preliminary findings that further explore the moonlighting functions of RbcL as an oxidized RNA quality control factor with a role in chloroplast translation. With results of immunofluorescence microscopy and biochemical fractionation I show that an RbcL mutant unable to assemble into the Rubisco holoenzyme has constitutively present chloroplast stress granules, increased survival to oxidative stress, and yet accumulates more oxidized RNA, relative to wild type. I show that RbcL associates with chloroplast translation membranes, which have previously been shown to house ribosomes and translation factors required for thylakoid membrane biogenesis. I also examine the subcellular localization of RbcL and oxidized RNA during conditions associated with chloroplast translation.

3.1 INTRODUCTION

Rubisco is the enzyme responsible for CO₂ assimilation into ribulose-1,5-bisphosphate in chloroplasts during the Calvin-Benson cycle (Spreitzer and Salvucci, 2002). Rubisco is a multi-subunit protein complex which is composed of eight copies of a large subunit, RbcL, encoded by the chloroplast genome, and eight copies of a small subunit, RbcS, encoded by two genes (*RBCS1* and *RBCS2*) in the nuclear genome (Knight et al., 1990). The majority of the Rubisco pool in most algae and hornworts is localized to a spherical body within the chloroplast called the pyrenoid, as part of a carbon-concentrating mechanism (Meyer et al., 2017). Rubisco is one of the most extensively studied enzymes, yet to date it has almost exclusively been studied in the context of its role in photosynthesis. This chapter describes evidence of alternative “moonlighting functions of RbcL.

Chloroplasts are the photosynthetic plastid in green tissues of plants and in algae. In chloroplasts, antioxidant systems and molecular quality control are particularly important because photosynthesis produces ROS as H₂O₂, singlet oxygen, superoxide and, indirectly, the hydroxyl radical (Foyer and Shigeoka, 2011). Moreover, chloroplasts have a genome and a gene expression system that have nucleic acid targets of oxidation and mutagenesis by ROS (Wurtmann and Wolin, 2009; Zheng et al., 2014). Oxidative damage of nucleic acids can be enhanced by inheritance of mutations in DNA or by the generation of aberrant proteins from oxidized RNA. Although chloroplasts have known quality control systems for oxidized DNA, proteins and lipids (Apel and Hirt, 2004), little is known about how they manage oxidized RNA.

An avenue to study RNA quality control and its localization in chloroplasts arose with the discovery of stress granule-like bodies that form during oxidative stress in the chloroplast of the unicellular green alga *Chlamydomonas reinhardtii* (Uniacke and Zerges, 2008). These chloroplast stress granules (cpSGs) are stress-induced foci containing mRNAs encoded by the chloroplast

genome, RNA binding proteins, and the small subunit of the chloroplast ribosome. cpSGs form at the inner perimeter of the pyrenoid and are enriched in RbcL, but not RbcS (Figure 3.1; Uniacke and Zerges, 2008). This finding and previous reports raised the possibility that cpSGs have a role in RNA metabolism during stress, analogous to cytoplasmic stress granules found throughout the eukaryotes (Decker and Parker, 2012). A specific function for RbcL in the context of cpSGs, i.e., in RNA metabolism during stress, remains to be determined.

Previous studies have shown that during oxidative stress, RbcL displays several characteristics that are consistent with a role as a cpSG assembly factor. *In vitro* biochemical analyses have shown that under oxidizing conditions, RbcL disassembles from the Rubisco holoenzyme, acquires the ability to bind RNA in a sequence-independent manner, and forms high molecular weight aggregates (Knopf and Shapira, 2005; Mehta et al., 1992; Yosef et al., 2004). The characteristics of RbcL that are observed during stress or oxidizing conditions (e.g., holoenzyme disassembly, RNA binding activity, aggregation) are thought to be regulated by the reversible oxidation of specific cysteine residues (Cohen et al., 2005; Marín-Navarro and Moreno, 2006; Moreno et al., 2008). Therefore, RbcL shares several characteristics with stress granule assembly factors in that it can bind non-specifically to mRNA and aggregate during oxidative stress. Taken together, these results, along with evidence indicating that RbcL accumulates several-fold above the equal stoichiometric amounts with RbcS that are required in the Rubisco holoenzyme, suggest that cpSGs, RbcL, and the pyrenoid have yet-to-be defined role(s) in chloroplast RNA metabolism during stress (Recuenco-Muñoz et al., 2015). This hypothesis and the previously reported role of RbcL in autoregulatory feedback translational repression are mutually compatible (Cohen et al., 2006; Wietrzynski et al., 2021).

The region around the pyrenoid is also dedicated to translation during thylakoid membrane biogenesis. Previous members of our lab have characterized this region, termed the “translation

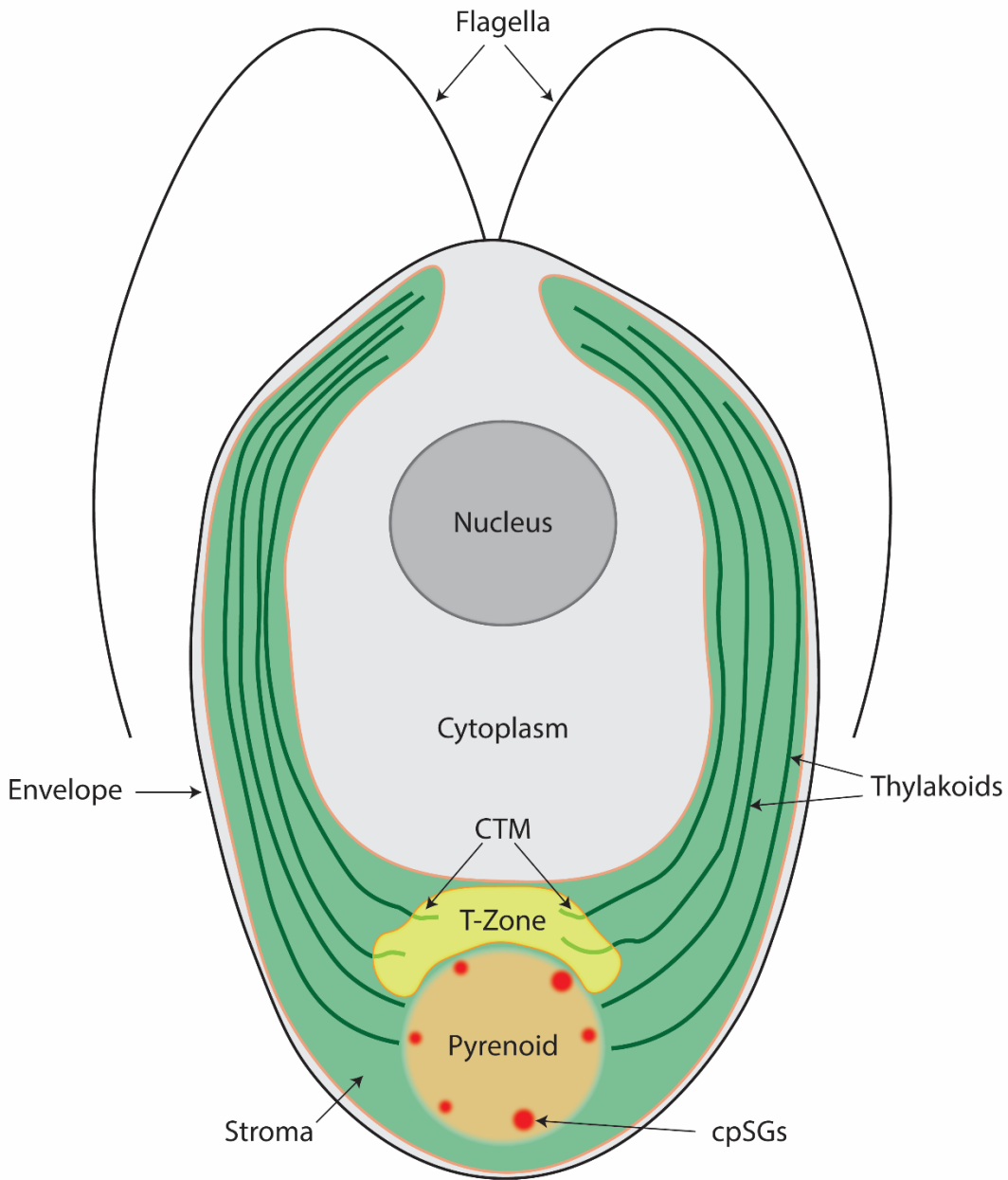


Figure 3.1. Illustration of a *Chlamydomonas reinhardtii* cell.

The chloroplast with cpSGs (red), the envelope (orange), the region with the aqueous stroma and thylakoid vesicles (green), the pyrenoid (brown), and the translation zone (yellow) with chloroplast translation membranes (CTM, light green). Also shown are the cytosolic compartments (gray), the nucleus, and the flagella.

zone” by fluorescence microscopy (Sun et al., 2019; Uniacke and Zerges, 2007). It was found that during conditions associated with thylakoid membrane biogenesis, chloroplast mRNAs and translation factors become enriched around the pyrenoid for the concerted synthesis and assembly of photosystem subunits. This region was also proposed to house extensions of the thylakoid membrane that are themselves dedicated to the synthesis and assembly of photosystem subunits, termed “chloroplast translation membranes” (Figure 3.1; Schottkowski et al., 2012).

We discovered a non-Rubisco requirement for RbcL in the control of oxidized RNA level and oxidative stress tolerance in *Chlamydomonas* (Zhan et al., 2015). We found that oxidized RNA localizes to the pyrenoid, that RbcL is required to control the accumulation of oxidized RNA in *Chlamydomonas*, and that RbcL is required for survival during oxidative stress induced by H₂O₂. Furthermore, we also identified an altered biochemical form of RbcL that could carry out such ‘moonlighting’ functions, which we refer to as the “alternate form of RbcL” (Zhan et al., 2015). We also found that RbcL is associated with chloroplast translation membranes independently of RbcS, indicative of a non-Rubisco function in chloroplast translation (Dhaliwal, Masters thesis, Concordia University, 2013).

Here we build on our previous findings that the large subunit of Rubisco has a moonlighting function as a stress-responsive protein with a role in translation. Using the results of biochemical analyses and fluorescence microscopy, we further characterize RbcL association with the chloroplast translation membranes and explore whether RbcL localizes to the translation zone. Furthermore, we use genetic analyses and immunofluorescence microscopy to examine whether certain amino acid residues are required for the moonlighting functions of RbcL. We characterize a site-directed mutant of RbcL, *rbcL-G54D*, which has phenotypes suggestive of an enhanced level of RbcL moonlighting functions. Finally, we explore RbcL localization during nitrogen starvation-

induced autophagy, which has been proposed as a pathway for stress granules clearance in yeast and mammalian systems.

3.2 MATERIALS AND METHODS

3.2.1 Manipulation of *Chlamydomonas*

All strains used are listed in table S1 and were obtained from the *Chlamydomonas* Resource Center (<https://www.chlamycollection.org/>). Unless otherwise indicated, cell cultures were grown to mid-logarithmic phase ($2-4 \times 10^6$ cells/ml) in a 24°C orbital shaker, in Tris-Acetate Phosphate (TAP) media (Harris, 1989). The *rbcL-G54D* mutant is non-photosynthetic, but fully viable under heterotrophic conditions, with acetate provided as an exogenous energy source (Satagopan and Spreitzer, 2004). The yellow-in-the-dark 1 (*y1*) mutant is “yellow-in-the-dark” because it lacks an enzyme in chlorophyll biosynthesis. It will green upon exposure to light because it has a light-dependent enzyme with the same enzymatic activity (Cahoon and Timko, 2000). Therefore, for all viability, biochemical, and microscopic analyses, cultures were grown and tested in the dark unless otherwise indicated. To induce nutrient starvation (-N, -P, -S), cultures in mid-log phase were pelleted, resuspended in TAP media lacking the indicated nutrient, and cultured for 24 hours prior to analysis.

3.2.2 Determination of oxidative stress tolerance

Cultures of each strain were exposed to exogenously added 4 mM H₂O₂, and cell survival was monitored at two-hour intervals for four hours. Survival was defined as the percentage of cells that exclude Trypan Blue, a dye that is selective for dead cells (Strober, 2001). Each test was performed a minimum of six times, and significance was determined using two sample t-tests ($p \leq 0.05$)

3.2.3 Analysis of oxidatively damaged RNA

Total RNA was extracted using TRI-reagent (Sigma-Aldrich) according to the manufacturer's protocol. Total RNA (5 µg) samples were transferred to a nitrocellulose membrane with a

Minifold-II slot blot system (Schleicher & Schuell). Membrane filters were reacted with the commercial antibody against 8-oxoG (1:500, QED Bioscience Inc., clone 15A3) overnight, at 4°C. A goat anti-mouse-IgG secondary antibody (KPL) was used and ECL detection was performed with a commercial kit (Millipore). Each test was performed a minimum of six times, and significance was determined using two sample t-tests ($p \leq 0.05$).

3.2.4 Chlamydomonas immunofluorescence and *in-situ* hybridization

Immunofluorescence and *in situ* hybridization were performed as previously reported (Uniacke et al., 2011; Zhan et al., 2015). 8-oxoG was detected using a monoclonal mouse antibody (clone 15A3, QED bioscience, dilution 1:500). RbcL was detected using a rabbit polyclonal antibody (provided by Dr. Robert Spreitzer, dilution 1:2,000). Primary antibodies were incubated for 2 hours at room temperature. Secondary antibodies were Alexa Fluor 568 goat α mouse IgG and Alexa Fluor 488 goat α rabbit IgG, each diluted 1:300 (ThermoFisher). Secondary antibodies were incubated for 1 hour at room temperature. The *psbA* mRNA FISH probe used here was described previously (Uniacke and Zerges, 2007). 18-20 ng of FISH probe per sample was hybridized overnight at 37°C in a slide hybridization oven.

Images were acquired using a Leica DMI 6000 epifluorescence microscope (Leica Microsystems) with a 63X/1.4NA objective, a Hamamatsu OrcaR2 camera, and Volocity acquisition software (Perkin-Elmer). Z-stacks were taken by series capture at a thickness of 0.2 μ m per section. Stacks were deconvoluted with AutoQuant X3 (Media Cybernetics Inc.). The average distribution of fluorescent signals in cells was determined as described previously, using a custom-built ImageJ macro (Sun et al., 2019).

3.2.5 Subcellular fractionation

Analytical subcellular fractionation was performed as described previously, with some modifications (Schottkowski et al., 2012). 300 ml of cell cultures were pelleted and resuspended

in ice cold MKT-buffer. The cells were broken by three passes through a chilled French Pressure Cell at 1,000 psi, and breakage was verified by light microscopy (400X and 1000X magnification). Cell lysates were centrifuged at 100,000 x g for 1 hour at 4°C. The supernatant was removed and stored at -80°C while the pellet was resuspended in 2 ml MKT buffer containing 2.5 M sucrose. A 750 µl 2.2 M sucrose cushion was added on top of the resuspension, followed by a 10 ml 0.5 M-2.0 M linear sucrose gradient. The gradient was centrifuged at 100,000 x g for 16 hours at 4°C, and then collected in 750 µl fractions. The pellet of the gradient was resuspended in 750 µl MKT and stored at -80°C along with the gradient fractions. Equal proportions of each fraction were analyzed by SDS-PAGE and western blotting. Antisera were: αRbcL (1:30,000, Dr. Robert Spreitzer); αRBP40 (1:1000; Dr. Jörg Nickelsen); αS-21 and αL-30 (30S and 50S r-protein, 1:4000 and 1:10,000, respectively, Randolph-Anderson et al., 1989). Goat anti rabbit secondary antibody (1:10,000) (KPL) was used for 1 h at room temperature.

3.2.6 Differential centrifugation

Cells from a 75 ml culture were pelleted by centrifugation at 5,000 x g for 5 minutes at room temperature and resuspended in 5 ml ice cold MKT buffer. The cells were broken by three passes through a chilled French Pressure cell at 1,000 psi, and breakage was verified by light microscopy (400× and 1,000× magnification). The lysate was centrifuged at 3,200 x g for 1 minute to remove unbroken cells and the supernatant was then centrifuged again at 17,000 x g for 20 minutes at 4°C. The resulting supernatant was removed and stored at -80°C (P16), while the pellet (P16) was resuspended in the same volume of MKT-buffer with 2.0% Triton X-100 (v/v) and incubated on a rocker for 15 minutes at room temp. The resuspended fraction P16 was then centrifuged again at 17,000 x g for 20 minutes, to generate supernatant (P16-TS) and pellet (P16-TI) fractions. P16-TS was removed and stored at -80°C, and P16-TI was resuspended in MKT-buffer and stored at -80°C. Prior to freezing, aliquots of each fraction were removed and prepared for SDS-PAGE and

immunoblot analysis. Antisera were: α RbcL (1:30,000, Dr. Robert Spreitzer); α RbcS (1:2000; Dr. Robert Spreitzer). Goat anti-rabbit secondary antibody (1:10,000) (KPL) was used for 1 h at room temperature. Replicate gels were stained using the ProteoSilver Silver Stain kit (Sigma), according to the manufacturer's instructions.

3.3 RESULTS

3.3.1 Investigation of a Role for RbcL in Chloroplast Translation

Our lab has previously established conditions during which thylakoid membrane biogenesis (and therefore active translation) are enhanced (Schottkowski et al., 2012; Sun et al., 2019; Uniacke and Zerges, 2007). To explore further the alternative role(s) of RbcL, unrelated to Rubisco, we first examined the subcellular localization patterns of RbcL and 8-oxoG using IF microscopy during biogenesis conditions.

The first context in which we examined the localization pattern of RbcL and 8-oxoG was in cells from cultures that were undergoing synchronous growth and division in the diel cycle. This allowed the analyses of uniform populations of cells at the same stage, for example, undergoing high rates of chloroplast biogenesis and photosynthesis. *Chlamydomonas* cells can be entrained to a diel cycle by using a 12/12-hour light/dark regime, during which >90% of cells will progress through the cell-cycle synchronously. The 24-hour diel cycle is measured in Zeitgeber time (ZT) where time points ZT0 and ZT12 represent the transitions from dark to light and light to dark, respectively. It was previously shown that translation factors are enriched in the translation zone during thylakoid membrane biogenesis between ZT2 and ZT4 (Sun et al., 2019).

At ZT23 and ZT24 (the last hour of dark and the first hour of light), we observed the RbcL and 8-oxoG IF signals primarily in the pyrenoid, at the basal region of the chloroplast, as was reported previously (Figure 3.2; Zhan et al., 2015). Four hours into the light phase of the diel cycle (ZT4), the IF signals are no longer enriched in the pyrenoid, but localized to the chloroplast lobes in a

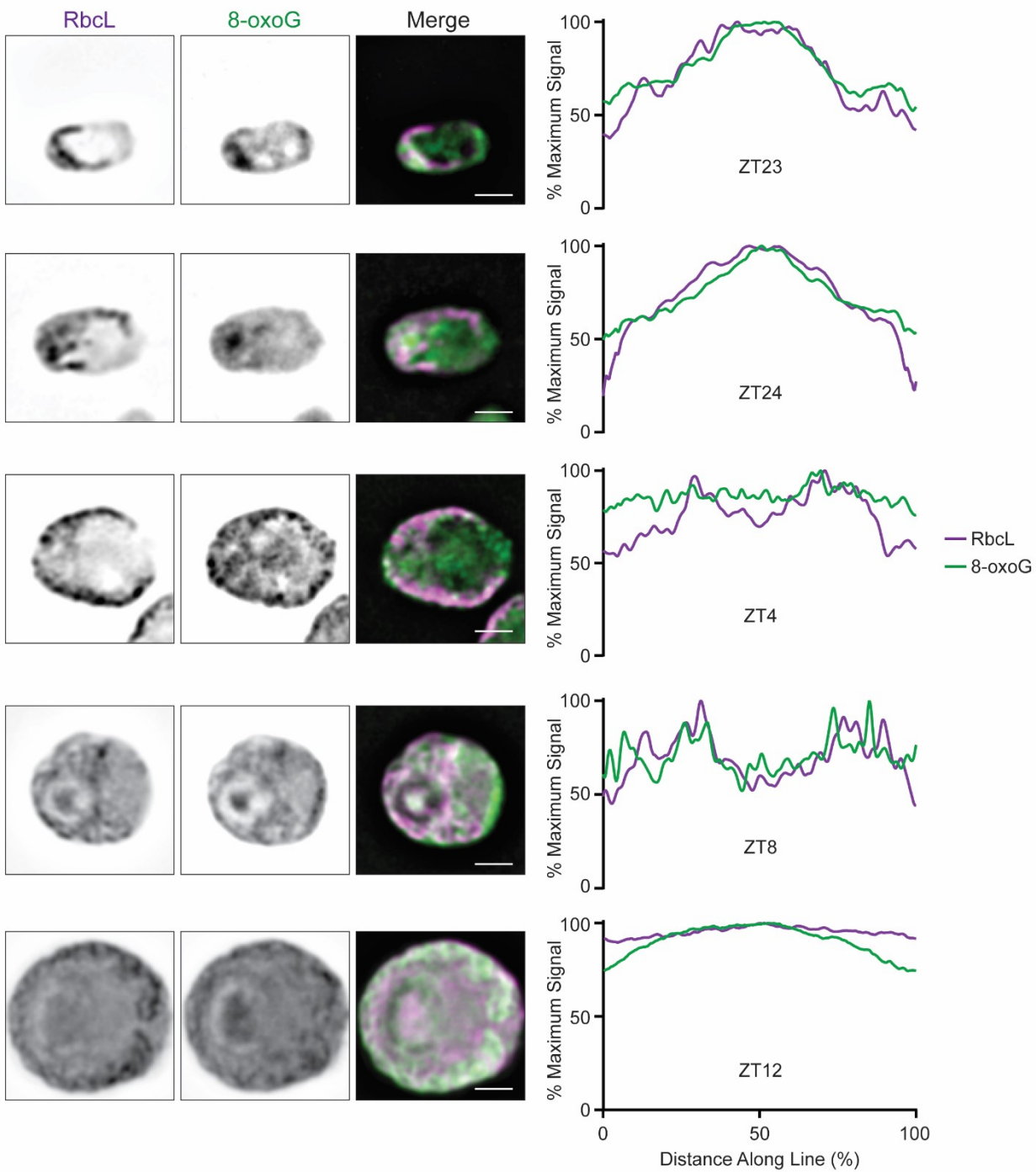
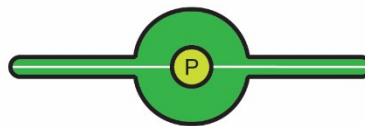
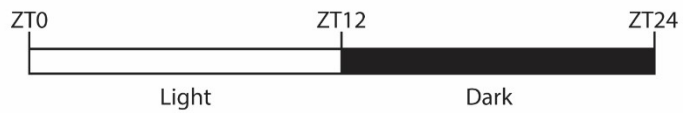


Figure 3.2. Localization of RbcL and 8-oxoG in the chloroplast across the diel cycle.

Immunofluorescence signals of RbcL (left columns) and 8-oxoG (middle columns). The diel cycle and ZT times are indicated by white and black bars. Chloroplasts are illustrated as their axis (white line) is presented on the horizontal axis of each graph. P indicates the pyrenoid. Plots show average signal intensity (as percentage of maximum signal from all cells in the data set across the chloroplast axis (as percentage of the total length)). ZT23, $n = 20$; ZT24, $n = 34$; ZT4, $n = 17$; ZT8, $n = 3$; ZT12, $n = 1$. Scale bars indicate 2 μm .

pattern that does not resemble that of the translation zone (Sun et al., 2019; Uniacke and Zerges, 2007). After 8 hours in the light (ZT8) and in the first hour of dark (ZT12), the IF signals appear more evenly distributed throughout the chloroplast with less enrichment in any particular area. These results suggest that RbcL and 8-oxoG do not localize to the translation zone during timepoints of the diel cycle previously associated with thylakoid membrane biogenesis.

The next context in which we examined the localization pattern of RbcL and 8-oxoG was during greening of the *y1* mutant. This *Chlamydomonas* mutant lacks the light-independent protochlorophyllide oxidoreductase, an enzyme required for chlorophyll biosynthesis, and can therefore only synthesize chlorophyll when exposed to light (Cahoon and Timko, 2000). In the dark, in the absence of chlorophyll production, thylakoid membrane biogenesis does not occur, and the *y1* mutant cells are yellow. Once exposed to light, chlorophyll synthesis is initiated via the light-dependent protochlorophyllide oxidoreductase enzyme, thylakoid membrane biogenesis occurs, and the mutant cells become green over the course of several hours.

We observed the localization pattern of RbcL and 8-oxoG IF signal in *y1* mutant cells during greening (Figure 3.3). In the dark, i.e., prior to greening, both the RbcL and 8-oxoG IF signals are primarily localized to the pyrenoid. After 2 and 4 hours of light the RbcL signal is still present in the pyrenoid, but also appears as foci surrounding the pyrenoid. These foci may be cpSGs because the dark-grown *y1* mutant accumulates intermediates in chlorophyll biosynthesis. These intermediates can potentiate the generation of ROS by light, and thereby photooxidative stress, a known inducer of cpSGs (Apel and Hirt, 2004; Uniacke and Zerges, 2008). Meanwhile, the 8-oxoG signal does not appear to change during greening in the *y1* mutant. In both cases, the IF signal does not accumulate on either side of the pyrenoid (in the translation zone) during greening, as was seen previously for translation factors during thylakoid membrane biogenesis and for these signals in synchronized cells at ZT4 (Sun et al., 2019; Uniacke and Zerges, 2007).

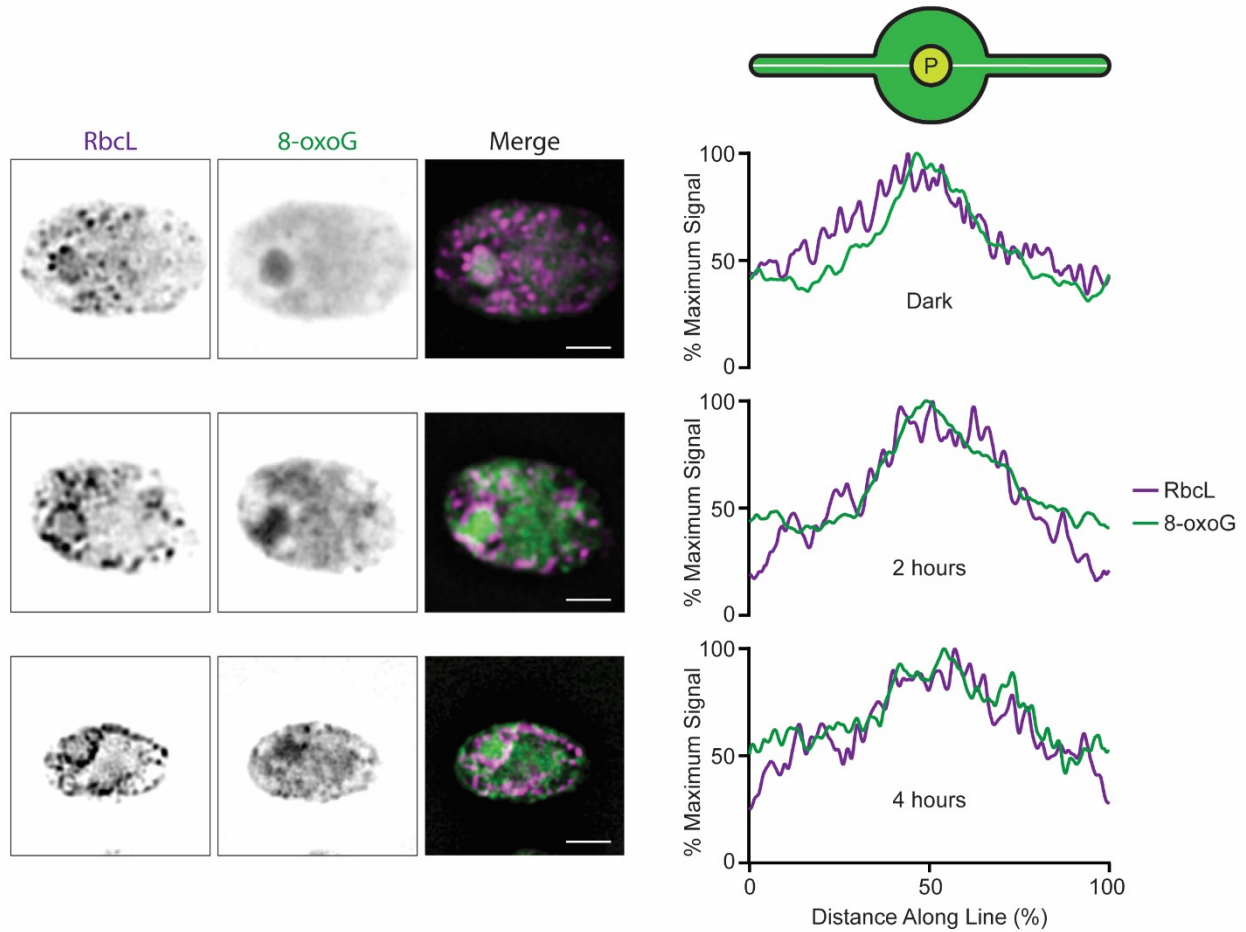


Figure 3.3. Localization of RbcL and 8-oxoG in the chloroplast during *y1* greening.

Immunofluorescence signals of RbcL (left columns) and 8-oxoG (middle columns). Chloroplasts are illustrated as their axis (white line) is presented on the horizontal axis of each graph. P indicates the pyrenoid. Plots show average signal intensity (as percentage of maximum signal from all cells in the data set across the chloroplast axis (as percentage of the total length). 0 hours, $n = 15$; 2 hours, $n = 20$; 4 hours, $n = 8$. Scale bars indicate $2 \mu\text{m}$.

3.3.2 RbcL localizes to chloroplast translation membranes in the *y1* mutant.

Our lab previously demonstrated the existence of chloroplast membranes dedicated to translation, called chloroplast translation membranes (Schottkowski et al., 2012). These membranes are characterized as fractions of a sucrose gradient that are denser than thylakoid membranes and enriched in biogenesis factors such as ribosomal proteins and translation factors. I previously found that RbcL also localizes to chloroplast translation membranes in the absence of RbcS, supportive of a moonlighting function of RbcL that is independent of Rubisco activity and involving chloroplast translation (Dhaliwal, 2013). Given the published evidence that RbcL can act as a translation factor (Cohen et al., 2006; Wostrikoff and Stern, 2007), we examined whether its localization to the chloroplast translation membrane is altered during conditions of thylakoid membrane biogenesis, such as greening in the *y1* mutant.

Using a French pressure cell, we generated cell lysates from *y1* mutant cultures that were grown in the dark and then exposed to light for 4 hours. Using ultracentrifugation, soluble material was separated from insoluble material. The insoluble pellets, which contain all membranes, were then separated by isopycnic density ultracentrifugation, where membranes float to and equilibrate at their native buoyant density. Fractions from these gradients were then collected for western blot analysis (Figure 3.4). As was the case for wild-type cells, RbcL in the *y1* mutant was found in dense membranes that are known to be enriched in thylakoid biogenesis factors (F5-F6 in dark, F6-F7 in light). The lack of RbcS in these fractions suggest that the RbcL found there is a non-Rubisco pool consistent with it carrying out an alternate function, either autoregulatory feedback repression, oxidized RNA quality control, or both. We did not observe a major change in the localization of RbcL to chloroplast translation membranes fractions upon exposure to light. This result suggests that RbcL localization to chloroplast translation membranes is independent of the increased biogenesis conditions that occur during *y1* greening.

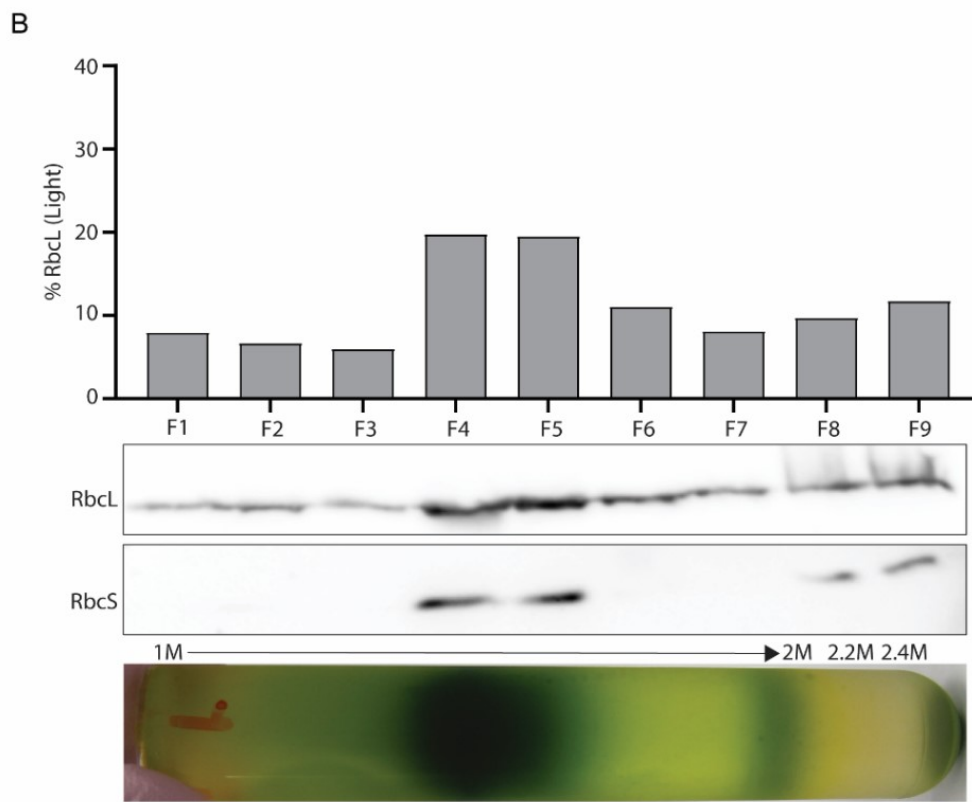
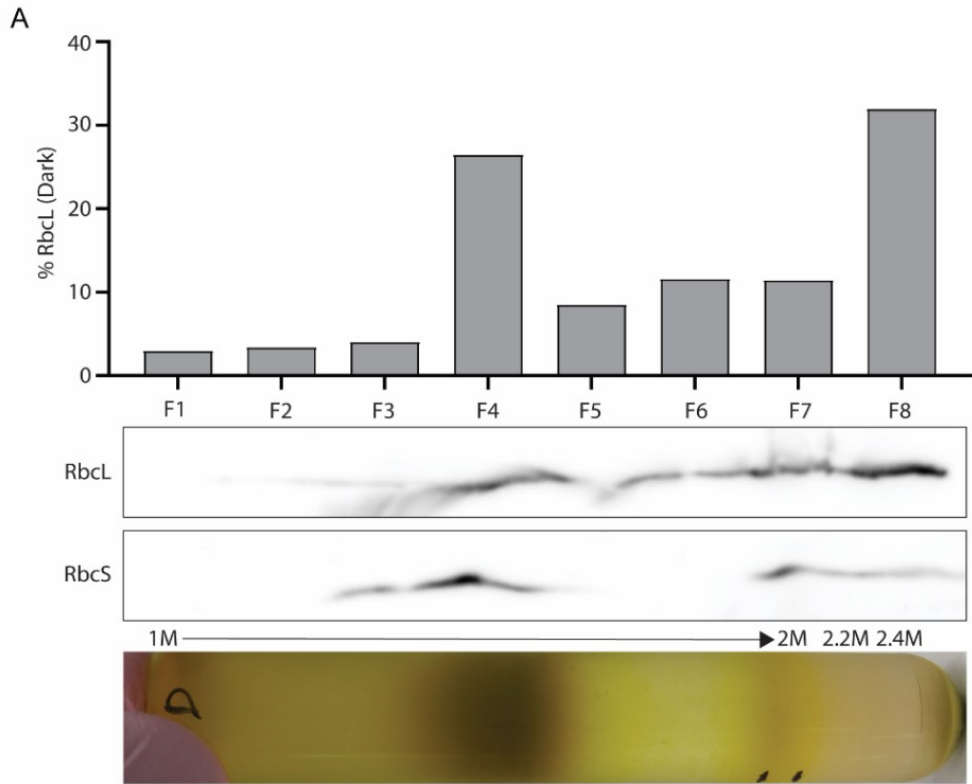


Figure 3.4. RbcL localizes to chloroplast translation membranes in the *y1* mutant.

Gradient fractions were examined from *y1* mutant cells grown in the dark (A) and following 4 hours of light exposure (B). 2.4M indicates the sucrose solution from which the membranes were floated, meaning the gradients were centrifuged at $10^5 \times g$ and membranes moved up into the gradient, banding according to their density. Each fraction was assayed by immunoblot, with antibodies against RbcL and RbcS. Bar heights indicate the percentage of total RbcL signal in each fraction.

3.3.3 RbcL localizes to chloroplast translation membranes during translation inhibition.

The quality control of oxidized RNA occurs by TQC pathways that require active translation. Given the evidence for a link between RbcL and translation, we next examined the effect of translation inhibition on RbcL localization to chloroplast translation membranes in wild-type cells. We prepared sucrose gradients from total membrane of cultures that were exposed to either 100 µg/ml of lincomycin or chloramphenicol, two inhibitors of chloroplast translation but not cytosolic translation (Figure 3.5). In the supernatant (S) fractions of the lysates, we observed both RbcL and RbcS, indicative of the Rubisco holoenzyme. As was found for untreated samples (Dhaliwal, 2013), RbcL was localized to chloroplast translation membranes (fractions F6-F7) in both chloramphenicol and lincomycin treated samples. This result suggests that the localization of RbcL to chloroplast translation membranes is independent of active translation.

3.3.4 The moonlighting functions of RbcL are not affected by selected cysteine mutations.

We previously demonstrated that a minor pool of RbcL, which is not in the Rubisco holoenzyme, has a moonlighting function which affects the level of oxidized RNA that accumulates in *Chlamydomonas*, and the tolerance to H₂O₂-induced oxidative stress (Zhan et al., 2015a). The inverse correlation of 8-oxoG RNA level and oxidative stress tolerance is consistent with a causal role of oxidized RNA quality control in stress tolerance. We next sought to determine whether specific features of the RbcL protein play a role in the non-Rubisco functions. Many of the characteristics of RbcL that we speculate to play a role in its non-Rubisco functions (holoenzyme disassembly, RNA binding activity, aggregation) are thought to be regulated by the reversible oxidation of specific cysteine residues during oxidizing conditions (Cohen et al., 2005; Marín-Navarro and Moreno, 2006; Moreno et al., 2008). Therefore, we tested three different cysteine mutants (*rbcL-C84S*, *rbcL-C172S*, and *rbcL-C449S/459S*) for three phenotypes: the accumulation

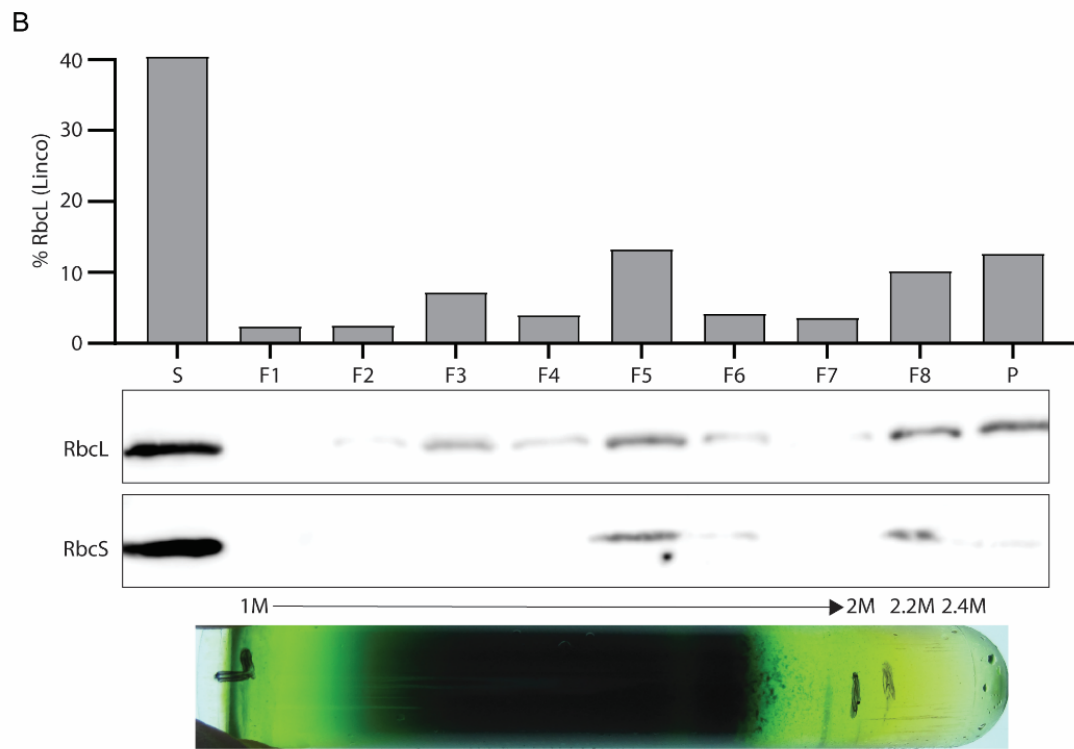
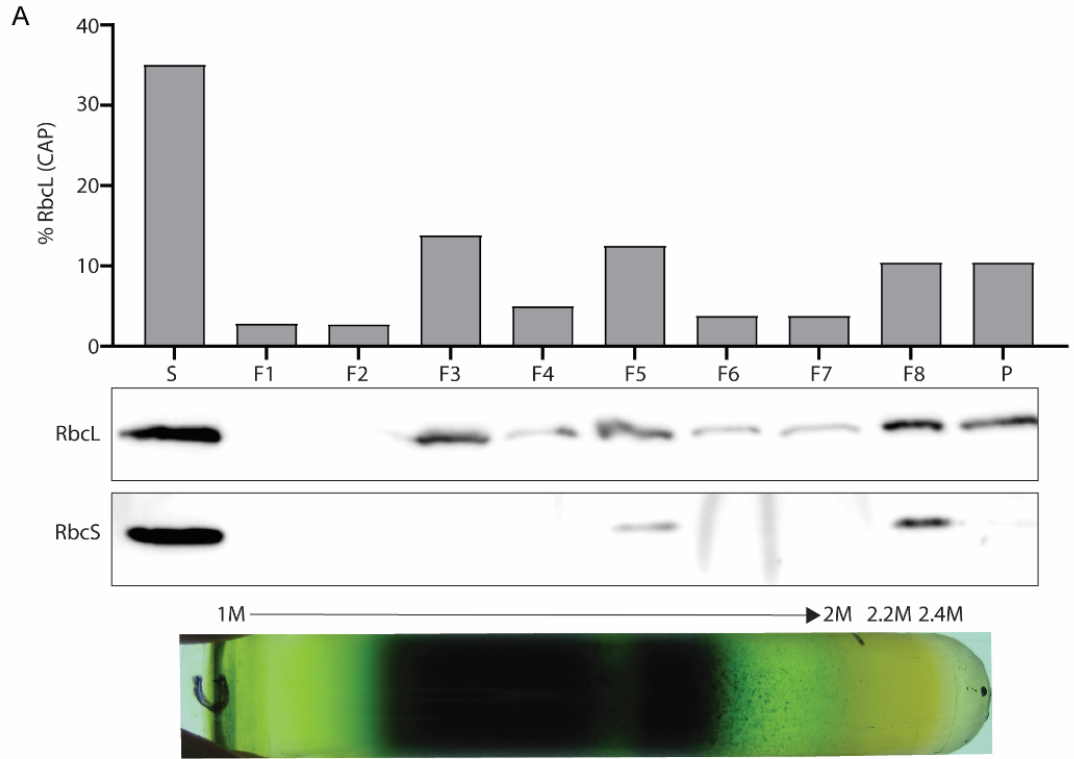


Figure 3.5. RbcL localizes to chloroplast translation membranes during translation inhibition.

Gradient fractions were examined from wild-type *C. reinhardtii* following 30 minutes of exposure to 100 µg/ml of chloramphenicol (A) and lincomycin (B). 2.4M indicates the sucrose solution from which the membranes were floated, meaning the gradients were centrifuged at $10^5 \times g$ and membranes moved up into the gradient, banding according to their density. Each fraction was assayed by immunoblot, with antibodies against RbcL and RbcS. S indicates the supernatant from the initial high-speed fractionation. P indicates the pellet of the sucrose gradient. Bar heights indicate the percentage of total RbcL signal in each fraction.

of the alternate form of RbcL, levels of oxidized (8-oxoG-containing) RNA, and tolerance to H₂O₂-induced oxidative stress.

To test for the presence of the altered form of RbcL in the *rbcL* cysteine mutants, we conducted subcellular fractionation to detect the relative levels of insoluble RbcL in the pellet fraction, as established previously (Zhan et al., 2015). As seen previously, under both non-stress and following exposure to 4 mM H₂O₂, the majority of wild-type RbcL was present in the supernatant fraction, with only a minor amount present in the pellet fraction (Figure 3.6A). The RbcL in the supernatant fraction likely corresponds to the holoenzyme form of the protein due to its soluble nature and co-fractionation with RbcS. Similar to wild-type cells, each of the cysteine mutants showed the vast majority of their RbcL protein present in the supernatant fraction, along with RbcS (Figure 3.6 B-D). Interestingly, despite the predicted roles of these cysteine residues in controlling the moonlighting of RbcL during oxidizing conditions, we saw no obvious difference in the fractionation pattern of RbcL in any of the mutants following exposure to H₂O₂. These data suggest that the absence of these cysteine residues does not affect the accumulation of RbcL in the Triton X-100-insoluble fraction (P16-TI). We next tested each mutant for cell survival during exposure to exogenous 4.0 mM H₂O₂. Survival was assessed by staining each culture with the dye, Trypan-Blue, and survival was measured as the percentage of cells that exclude the dye (Strober, 2001). Our prediction was that the lack of cysteine residues might negatively affect the ability of RbcL to carry out the moonlighting function(s) of RbcL in promoting survival during oxidative stress. Over a 4-hour time course, we observed that none of the cysteine point mutants exhibited a significant difference in survival relative to the wild-type strain (Figure 3.6F). These data suggest that the cysteine do not affect the function of RbcL in controlling survival during oxidative stress.

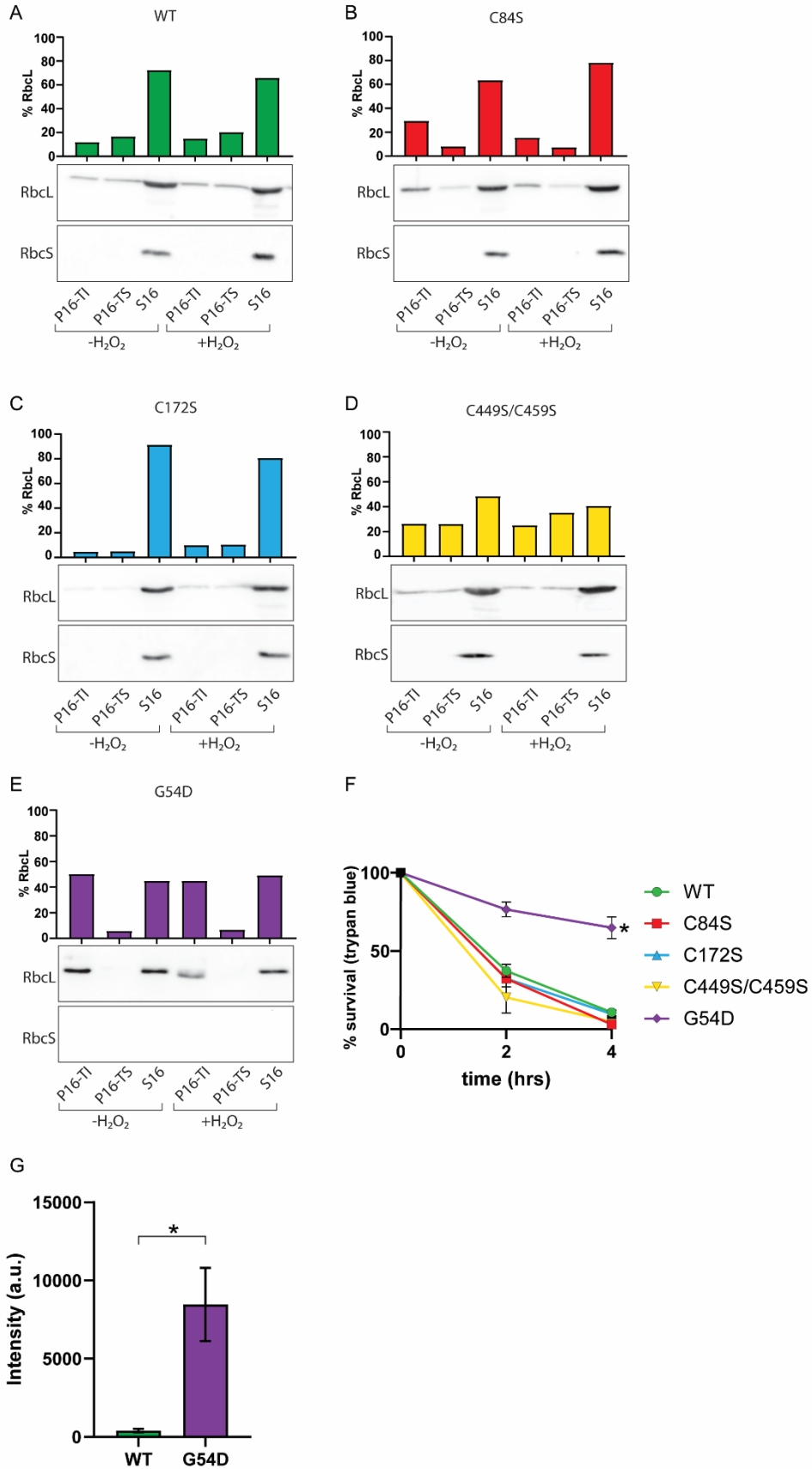


Figure 3.6. Analysis of RbcL moonlighting functions in site-directed mutants.

(A-E) RBCL fractionation during differential centrifugation and solubilisation with Triton X-100 was revealed by immunoblot analyses for (A) the wild-type strain, (B) *rbcL*-C84S, (C) *rbcL*-C172S, (D) *rbcL*-C449S/459S, and (E) *rbcL*-G54D. Proteins analysed were RbcL and RbcS. Where indicated, fractions were prepared from cells that had been exposed to 2.0 mM H₂O₂. Bar heights indicate the percentage of total RbcL signal in each fraction. S16 = supernatant fraction of a cell lysate; P16-TS = triton-soluble pellet fraction of a cell lysate; P16-TI = triton-insoluble fraction of a cell lysate. (F) Time course assays of cell survival, expressed as the mean percentage of initial survival as measured by Trypan Blue exclusion. (G) Levels of 8-oxoG in RNA from the wild-type strain and *rbcL*-G54D. The bar height represents the 8-oxoG ECL signal intensity from slot-blot experiments. (F-G) Asterisks indicate significance, as determined by two-sample t-tests (n = 3).

We then asked whether any of the cysteine mutants are altered in the levels of oxidized RNA that accumulates within them. We used a slot-blot approach to detect the levels of 8-oxoG in total RNA extracts from each mutant strain, as described previously (Zhan et al., 2015). None of the cysteine mutant strains showed a significantly different level of oxidized RNA relative to wild-type cells (data not shown). This was not surprising, given that none of the mutant strains were altered in their tolerance to H₂O₂, nor in the accumulation of the alternate form of RbcL. Therefore, it appears that the cysteine residues tested here have no role on any of the previously observed moonlighting functions of RbcL.

3.3.5 The moonlighting functions of RbcL are altered in an *rbcL-G54D* mutant.

We next tested another mutant form of RbcL for its ability to perform moonlighting functions. We selected an *rbcL-G54D* mutant because, while this strain possesses *rbcL* and both *RBCS* genes required for Rubisco, the *G54D* mutation renders RbcL unable to assemble into the Rubisco holoenzyme, and therefore, might have more readily available RbcL protein for the moonlighting role (Spreitzer, 1993).

In our first assay, we tested for the presence of the alternate, insoluble form of RbcL in this strain. The *rbcL-G54D* mutant had approximately half of its total RbcL amount in the Triton X-100 insoluble pellet fraction (P16-TI, Figure 3.6E). This is supportive of our model in which unassembled RbcL is biochemically altered relative to RbcL assembled in Rubisco. By contrast, each of the cysteine mutants were similar to the wild type in that the majority of their RbcL was present in Rubisco (i.e., with RbcS in fraction S16).

Next, we examined H₂O₂ tolerance in the *rbcL-G54D* mutant. As described for the cysteine mutants (above), cultures were exposed to 4.0 mM H₂O₂ and monitored for survival over a 4-hour time course using Trypan Blue (Figure 3.6F). In contrast to wild-type and the cysteine residue mutants, the *rbcL-G54D* mutant had significantly higher survival.

Finally, we examined the oxidized RNA levels in the *rbcL-G54D* mutant, using a slot-blot assay with an antibody against 8-oxoG. The *rbcL-G54D* mutant accumulated a significantly higher amount of oxidized RNA relative to wild-type (Figure 3.6G). This contrasts the phenotype of the *ΔRBCS* mutant (CC-4691), where unassembled RbcL resulted in increased tolerance to H₂O₂ and a *reduced* level of oxidized RNA. It is not clear to us why there is a positive correlation between 8-oxoG levels and H₂O₂ tolerance in the *rbcL-G54D* mutant. Nonetheless, the altered phenotypes for moonlighting functions of RbcL in this strain led us to investigate its other RbcL properties.

3.3.6 cpSGs are constitutively present in the *rbcL-G54D* mutant.

RbcL in wild-type cells localizes to cpSGs during oxidative stress (Uniacke and Zerges, 2008). In our model, this occurs following the stress-induced disassembly of the rubisco holoenzyme, which releases RbcL so that it can bind to mRNA and aggregate, forming microscopically visible foci. Because RbcL in the *rbcL-G54D* mutant does not assemble into the holoenzyme, we next examined the subcellular distribution of RbcL using immunofluorescence (IF) microscopy in this strain.

We observed several phenotypes in the *rbcL-G54D* mutant that differ from those of wild-type cells. First, RbcL was not present throughout the pyrenoid, but was found in multiple foci throughout the chloroplast, even in the absence of a stressor (Figure 3.7A). This is consistent with the absence of Rubisco in this mutant and the requirement for Rubisco in pyrenoid formation (Rawat et al., 1996). These foci appeared to be cpSGs, however, they were dispersed throughout the chloroplast and not confined to the perimeter of the pyrenoid as in wild-type cells, because this mutant most certainly lacks a pyrenoid. Second, we did not see a change in size or number of RbcL foci during exposure to 4.0 mM H₂O₂ (Figure 3.7A). We then asked whether the RbcL foci in the *rbcL-G54D* mutant have properties of cpSGs. Chloramphenicol treatment was previously found to

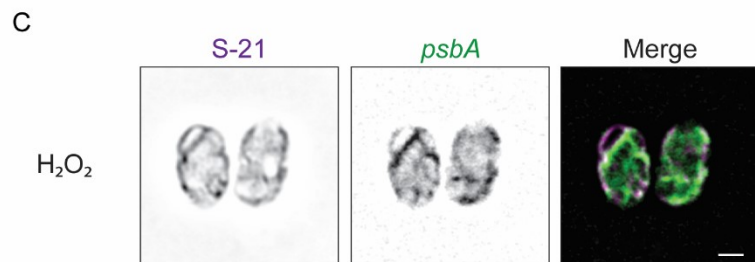
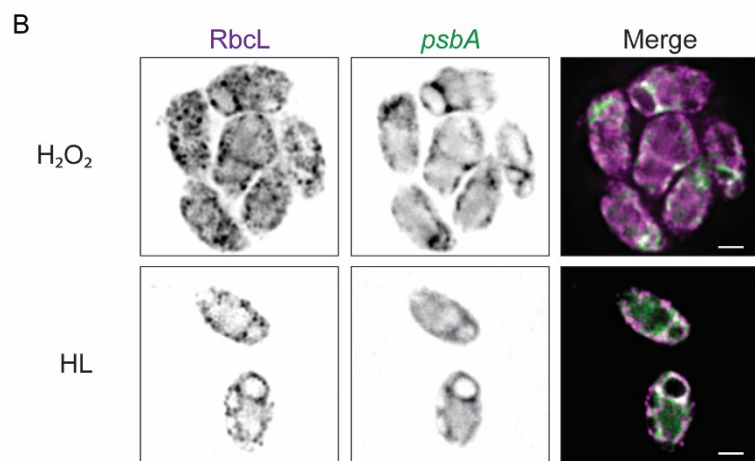
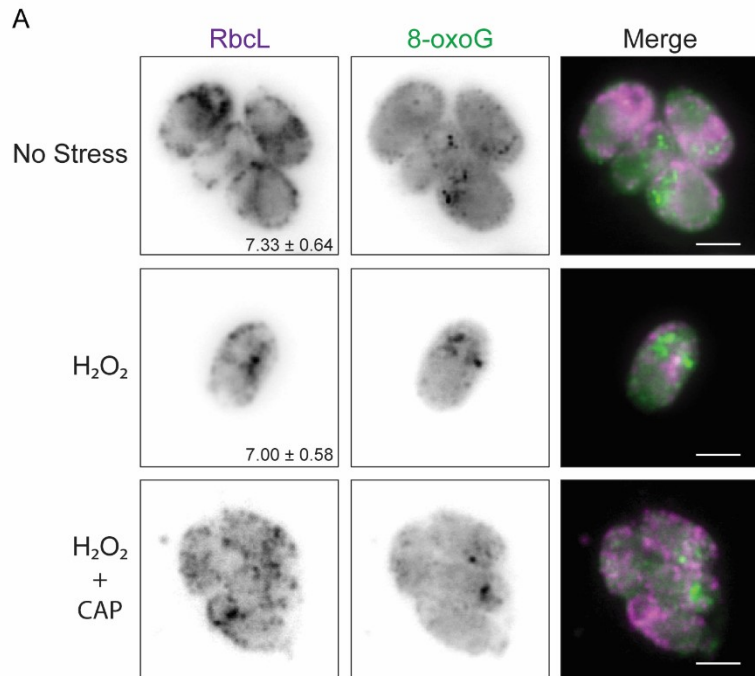


Figure 3.7. Localization of RbcL and 8-oxoG in the chloroplast in the *rbcL-G54D* mutant.

(A) Immunofluorescence signals of RbcL (left column) and 8-oxoG (middle column). Where indicated, cells were exposed to 4.0 mM H₂O₂ or both 100 µg/ml chloramphenicol (CAP) and 4.0 mM H₂O₂. Insets indicate the average number of RbcL foci per condition. (B)

Immunofluorescence signal of RbcL (left columns) and FISH signal of *psbA* (middle columns), in cells exposed to 4.0 mM H₂O₂ (top) or high light stress (2,000 µE m⁻¹ s⁻²) (bottom). (C)

Immunofluorescence signal of S-21 and FISH signal of *psbA*, in cells exposed to 4.0 mM H₂O₂

Scale bars indicate 2 µm.

prevent the formation of cpSGs (Uniacke and Zerges, 2008). Here, we found that chloramphenicol had no effect on the formation of RbcL foci in the *rbcL-G54D* mutant (Figure 3.7A). We also examined whether the RbcL foci in the *rbcL-G54D* mutant colocalized with two other markers for cpSGs: the chloroplast-encoded *psbA* mRNA and the small subunit of the chloroplast ribosome. We found that during exposure to H₂O₂, they did colocalize with the *psbA* FISH signal and with the IF signal of S-21, a protein of the chloroplast ribosome small subunit (Figure 3.7B and C). We also found colocalization between RbcL foci and *psbA* mRNA during high light stress, a condition that induces oxidative stress and cpSGs in *Chlamydomonas* (Uniacke and Zerges, 2008). These results suggest the RbcL-positive cpSGs are constitutively present in the *rbcL-G54D* mutant, but that they have altered properties relative to wild-type cells.

3.3.7 8-oxoG localization in the *rbcL-G54D* mutant.

We previously observed that oxidized RNA localizes to the pyrenoid in wild-type cells (Zhan et al., 2015). However, due to the lack of Rubisco in the *rbcL-G54D* mutant, it is highly unlikely that this strain has a pyrenoid, because Rubisco is an essential structural component of the pyrenoid (Rawat et al., 1996). Using IF-microscopy with an antibody against 8-oxoG, we examined the distribution of oxidized RNA in the *rbcL-G54D* mutant (Figure 3.7A). Unlike in wild-type cells, we did not see any enrichment of oxidized RNA in the basal region of the chloroplast, where the pyrenoid is normally situated. Instead, the 8-oxoG IF signal was present as dispersed foci throughout the cell. These foci did not appear to be cpSGs because they do not co-localize with RbcL foci. Additionally, they do not appear to be affected by exposure of the cells to H₂O₂, which is known to induce cpSG formation. Moreover, these foci are insensitive to treatment of cells with chloramphenicol, which is known to abolish cpSGs (Uniacke and Zerges, 2008).

3.3.8 RbcL localizes to chloroplast translation membranes in the *rbcL-G54D* mutant.

We next examined whether the localization of RbcL to chloroplast translation membranes is altered in the *rbcL-G54D* mutant. We generated cell lysates from *rbcL-G54D* mutant cultures that were either untreated or exposed to 4.0 mM H₂O₂. Soluble (S) material was separated from insoluble material by ultracentrifugation. The insoluble pellets, which contain all membranes, were then fractionated by buoyant density by isopycnic sucrose gradient ultracentrifugation (Figure 3.8).

Chloroplast translation membranes are defined as membranes that are lower (denser) than thylakoid membranes (the darkest green fractions of the gradient), and enriched chloroplast translation markers (Schottkowski et al., 2012). To observe the presence of chloroplast translation membranes, we probed each gradient with marker proteins for chloroplast translation (Figure 3.7). These include RB40, a translation factor for a photosystem II protein, and marker proteins for both the large and small subunits of the chloroplast ribosome. In the gradient of membranes from the non-stressed *rbcL-G54D* mutant gradient, we observed an enrichment of RbcL in chloroplast translation membrane fractions (Figure 3.8A), along with chloroplast translation markers, similar to wild-type (Dhaliwal, 2013). Unlike the unstressed treatment, the gradient from H₂O₂-treated cells had a broader distribution of RbcL across the gradient, with less enrichment in the chloroplast translation membrane fractions (Figure 3.8B). In both cases, we did not observe the presence of RbcS in any gradient fractions, consistent with our earlier observation that RbcS does not accumulate in this mutant, and that any RbcL activity in this context is independent of the Rubisco holoenzyme (Figure 3.6E).

3.3.9 RbcL functions during nutrient deprivation

During the recovery of yeast cells from stress, stress granules can be cleared by autophagy (Buchan et al., 2013). In *Chlamydomonas*, autophagy can be induced through nitrogen starvation (Goodenough et al., 2014; Pérez-Pérez et al., 2010). Therefore, we asked whether the *in situ*

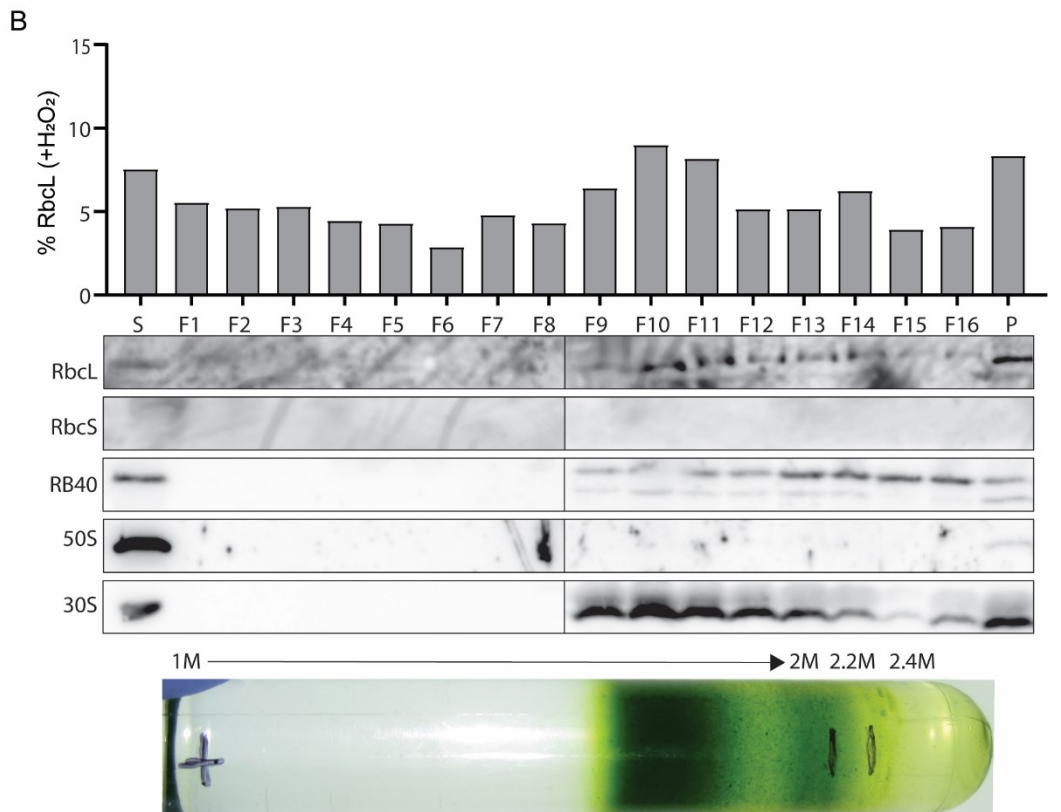
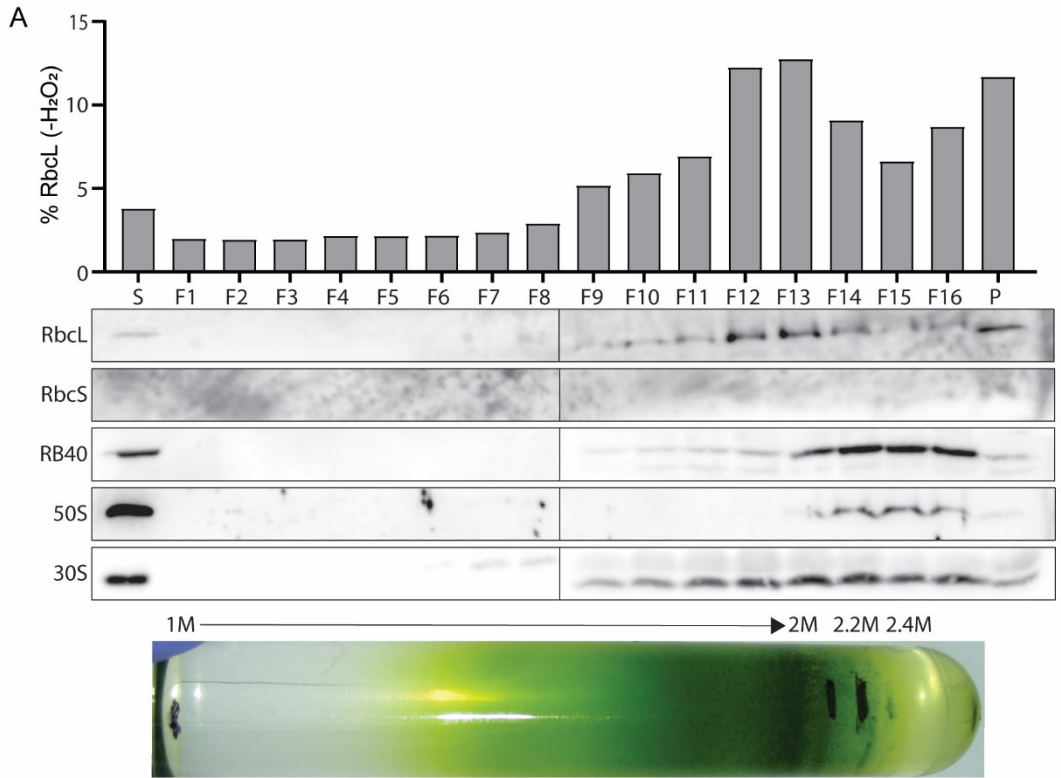


Figure 3.8. RbcL localizes to chloroplast translation membranes in the *rbcL*-G54D mutant.

Gradient fractions were examined from non-stressed *rbcL*-G54D cells (A) or cells exposed to 4.0 mM H₂O₂ (B). 2.4M indicates the sucrose solution from which the membranes were floated, meaning the gradients were centrifuged at 10⁵ x g and membranes moved up into the gradient, banding according to their density. Each fraction was assayed by immunoblot, with antibodies against RbcL, RbcS, and markers for chloroplast translation (RB40 and r-proteins from the chloroplast 50S and 30S ribosomal subunits). S indicates the supernatant from the initial high-speed fractionation. P indicates the pellet of the sucrose gradient. Bar heights indicate the percentage of total RbcL signal in each fraction.

distribution of RbcL is affected by nitrogen starvation. Using an antibody against RbcL, we observed that RbcL localizes to the pyrenoid under normal growth conditions (TAP), as expected (Figure 3.9). When cultures were starved for nitrogen, however, we observed cells with a second focus of RbcL. We observed an average of 1.57 RbcL foci per cell, with approximately 43% of cells having a second focus. This effect was specific to nitrogen starvation, as we did not observe multiple foci when cells were starved for phosphate or sulfur (Figure 3.9).

We then asked whether the loss of pyrenoid-localization and appearance of multiple RbcL foci during nitrogen starvation was a property specific to RbcL or to the presence of a pyrenoid. The *rbcS1-SSAT*, *rbcS1-SSHA*, and *rbcS1-SSSO* mutants are *Chlamydomonas* strains whose RbcS genes have been swapped for those of *Arabidopsis thaliana*, *Helianthus annuus*, or *Spinacia oleracea*, respectively (Genkov et al., 2010). While each strain assembles the Rubisco holoenzyme and is photosynthetic, none form a pyrenoid. We also asked whether the *rbcL-G54D* mutant had altered RbcL foci during nitrogen starvation because this strain lacks an apparent pyrenoid as well. In response to nitrogen starvation, none of the three “RBCS swap strains” formed a second RbcL focus, and nor did the *rbcL-G54D* mutant (Figure 3.10). This result suggests that the formation of a second focus of RbcL during nitrogen starvation depends on the presence of a normal pyrenoid.

3.4 DISCUSSION

Our previous work demonstrated that RbcL has non-Rubisco moonlighting functions in chloroplasts. This alternate function of RbcL is required for tolerance to oxidative stress and to determine the accumulation of oxidized RNA (Zhan et al., 2015). Here, using immunofluorescence microscopy, biochemical fractionation, and genetic analyses, we began to explore the possibility that the moonlighting functions of RbcL are related to chloroplast translation, and that RbcL may act as an RNA quality control factor. We examined the RbcL and 8-oxoG localization pattern in several contexts related to chloroplast translation: thylakoid membrane biogenesis during the early

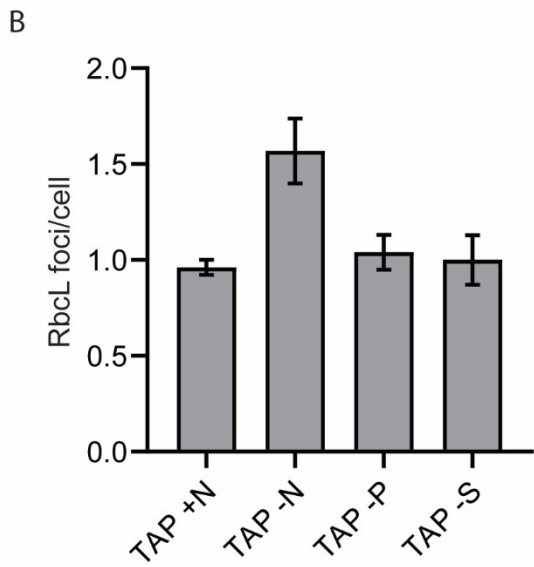
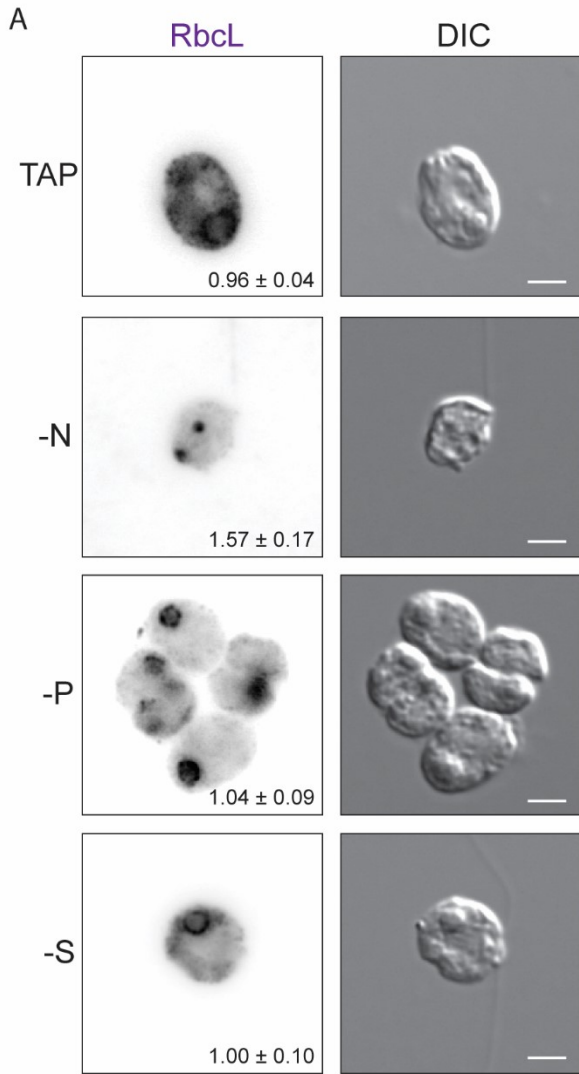


Figure 3.9. Localization of RbcL during nutrient starvation

(A) Immunofluorescence staining of RbcL in wild-type cells grown in TAP or starved for nitrogen (-N), phosphate (-P), or sulfur (-S) starvation. (B) Quantification of major RbcL foci during the indicated treatments. Error bars indicate S.E.M. Scale bars indicate 2 μ m.

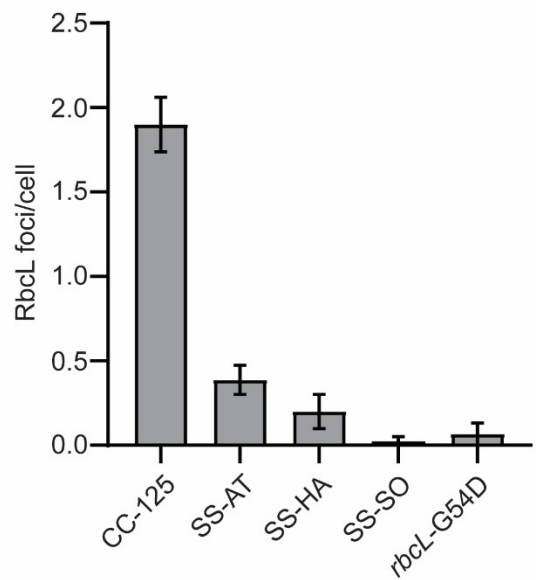
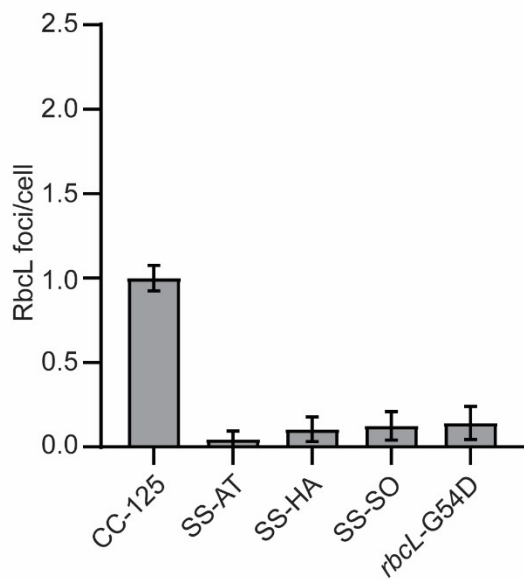
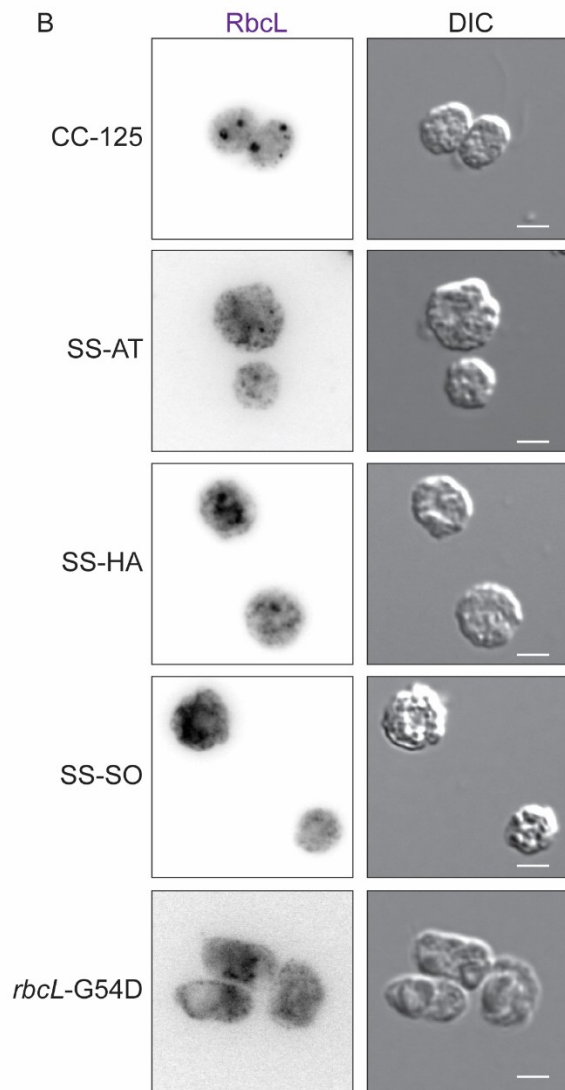
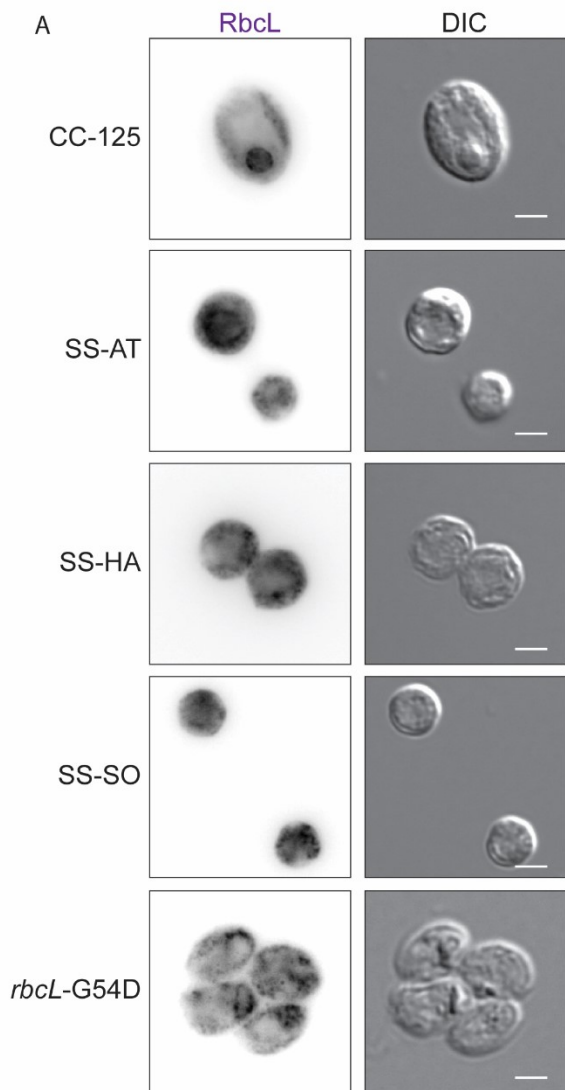


Figure 3.10. Localization of RbcL during nutrient starvation in pyrenoid-less mutants

(A) Immunofluorescence staining of RbcL in wild-type (CC-125), SS-AT, SS-HA, SS-SO, and *rbcL*-G54D cells grown in TAP (A) or starved for nitrogen (B). Graphs indicate the number of major RbcL foci during the indicated treatments. Error bars indicate S.E.M. Scale bars indicate 2 μm .

light phase of the diel cycle, thylakoid membrane biogenesis during greening in the *y1* mutant, and when chloroplast translation is inhibited using antibiotics (Figures 3.2-3.5). While we observed changes in the distribution of fluorescent signals across timepoints of the diel cycle, neither RbcL nor 8-oxoG localized to the translation zone. This result differs from what was seen for other markers of chloroplast translation, such as chloroplast r-proteins and RNA-binding proteins (Sun et al., 2019).

We noticed, however, that the RbcL signal around the pyrenoid becomes increasingly punctate during greening of the *y1* mutant. This pattern is reminiscent of the formation of cpSGs, which form during oxidative stress. This is interesting because the initial exposure to light that is required for greening in *y1* could cause oxidative stress, since the precursors to chlorophyll synthesis that accumulate in the dark can act as photosensitizers, which produce ROS in the light (op den Camp et al., 2003). Future work could address whether the appearance of these cpSGs is related to a potential function of RbcL as a translation quality control factor.

We previously found that RbcL fractionates to chloroplast translation membranes, membranes that are associated with translation and thylakoid membrane biogenesis (Dhaliwal, 2013; Schottkowski et al., 2012). Here, we also found that RbcL is present in chloroplast translation membrane fractions during two conditions: greening in *y1*, and when chloroplast translation is inhibited by antibiotic treatment (Figure 3.4 and 3.5). Surprisingly, there did not appear to be any major redistribution of RbcL when the *y1* cells were exposed to light, except for the loss of RbcL in the pellet fraction (Figure 3.4). We were also surprised to find that the fractionation of RbcL to chloroplast translation membranes did not change when chloroplast translation was inhibited (Figure 3.5). Based on these and the above results, one possible conclusion is that the presence of RbcL in compartments related to thylakoid membrane biogenesis is independent of active translation.

We next tested several mutants of RbcL to determine whether certain residues are required for the moonlighting functions of RbcL (i.e., promoting survival during oxidative stress and controlling the levels of oxidized RNAs). Other groups have reported on the disassembly of Rubisco during oxidizing conditions, and have explored whether the reversible oxidation of certain cysteine residues are involved in holoenzyme disassembly (Cohen et al., 2005; Moreno et al., 2008; Yosef et al., 2004). Because disassembled RbcL is required for its moonlighting functions, we tested whether the *rbcL-C84S*, *rbcL-C172S*, and *rbcL-C449S/C459S* mutants are affected in oxidative stress tolerance and oxidized RNA levels. In each case, we did not find a significant difference in stress tolerance, relative to wild-type (Figure 3.6) or in oxidized RNA levels (data not shown). Consistent with those findings, none of the cysteine residue mutants differed from wild-type in their levels of the alternate form of RbcL (Figure 3.6).

We also tested an *rbcL-G54D* mutant of RbcL. This mutant had an increased level of the alternate form of RbcL and had constitutively present RbcL foci (Figure 3.6 and 3.7). These results are consistent with the mutant's inability to form the Rubisco holoenzyme, despite the presence of both *RBCS* genes (Spreitzer, 1993). Interestingly, while this strain had elevated survival during oxidative stress, relative to wild-type, it also had elevated levels of oxidized RNA (Figure 3.6). This might suggest that the alternate function(s) of unassembled RbcL which promote survival during oxidative stress are independent of functions that control oxidized RNA levels.

The nature of the RbcL foci that form in the *rbcL-G54D* mutant also requires further study. Unlike in cpSGs in wild-type cells, these foci are constitutively present in non-stress conditions, do not increase in number when the cells are exposed to H₂O₂, and were not eliminated by treatment with chloramphenicol (Figure 3.6; (Uniacke and Zerges, 2008). Nonetheless, RbcL foci in the *rbcL-G54D* mutant did co-localize with other cpSG markers during stress (*psbA* mRNA and S-21). Therefore, while it appears that stress-induced recruitment of mRNAs to cpSGs occurs in these

mutant cells, the results raise some questions about the nature of the RbcL foci that are present in the *rbcL-G54D* mutant under non-stress conditions.

Lastly, we also examined the subcellular distribution of RbcL during nitrogen starvation, a condition that induces autophagy in *Chlamydomonas* (Goodenough et al., 2014; Pérez-Pérez et al., 2010). While dedicated pathways for Rubisco-specific autophagy have been described in wheat, tobacco, and *Arabidopsis*, none have been described for *Chlamydomonas* (Chiba et al., 2003; Ishida et al., 2008; Prins et al., 2008). We observed the loss of RbcL localization to the pyrenoid and the appearance of two distinct RbcL foci during nitrogen starvation (Figure 3.9). The loss of the pyrenoid localization and appearance of two distinct foci of RbcL is consistent with this protein being degraded by autophagy in response to nitrogen starvation. However, this possibility requires further exploration, as it remains unknown whether either RbcL focus is an autophagosome. Furthermore, it is unclear whether the appearance of the two RbcL foci is related in any way to the alternate functions of the protein. The observations that the SS-AT, SS-SO, SS-HA, and *rbcL-G54D* strains do not form dual foci during nitrogen starvation suggest that this phenomenon requires the presence of a pyrenoid.

CHAPTER 4: CONCLUSIONS AND FUTURE DIRECTIONS

4.1 Summary of Major Findings/Overview

This thesis aimed to elucidate cellular mechanisms for the quality control of defective RNA. Here, I provide the first evidence that the translation quality control pathways that handle defective mRNAs are compartmentalized to a novel organelle, ORBs, in *Saccharomyces cerevisiae*. I demonstrate that ORBs are a new member of a growing class of organelles called RNA granules, which are microscopically visible foci that form by phase separation of their constituent parts. I also provide evidence that the formation of ORBs depends on translation, as expected for a compartment that houses the surveillance mechanisms that detect stalled ribosomes via their collision. In addition to containing oxidized RNA, I show that the translation products of mRNAs lacking a stop codon are targeted to ORBs, along with ribosomal proteins and several NGD and RQC proteins (Dom34, Hbs1, Hel2, Rqc2). Using genetic analyses, I show that normal ORB formation is dependent on functional NGD and RQC pathways. Finally, I took advantage of the stability of ORBs *ex vivo* to characterize their proteome and provide, for future research, a list of candidate factors involved in translation quality control.

This thesis builds on our previous findings that RbcL in *Chlamydomonas* moonlights as an oxidized RNA quality control factor and is required for oxidative stress tolerance. I provide preliminary evidence that RbcL is associated with biochemical fractions and subcellular compartments that are locations of chloroplast translation and thylakoid membrane biogenesis. The nature of this association requires further study, as I found that inhibition of translation did not change the fractionation of RbcL to chloroplast translation membranes, and that the localization of RbcL to the translation zone did not change across various contexts associated with increased thylakoid membrane biogenesis. Here, I also characterized the moonlighting functions of an RbcL mutant that is unable to form the Rubisco holoenzyme (*rbcL-G54D*). While this strain has elevated

oxidative stress tolerance, it also has elevated levels of oxidized RNA. Our model speculates that unassembled RbcL should be more able to carry out its moonlighting functions, and it is therefore surprising that the oxidized RNA levels in the G54D mutant are higher than wild-type. It is unknown whether cpSGs are sites of defective mRNA degradation, and therefore the relationships between RbcL, cpSGs, and oxidized RNA remain to be determined. Nonetheless, the *rbcL-G54D* mutant form of RbcL was found in foci which appear to be cpSGs, and I detected increased levels of the alternate form of the protein in this mutant.

Finally, I also present preliminary findings that RbcL, and possibly the Rubisco holoenzyme, are degraded by autophagy during nitrogen starvation in *Chlamydomonas*. Whether the potential degradation of RbcL in autophagosomes is related to cpSG clearance or whether it involves a more general form of nutrient recovery during starvation bears further study. Specifically, one should determine whether marker proteins for autophagosomes localize to the second body with RbcL that forms during nitrogen starvation, and whether autophagy-deficient mutants form this putative autophagosome.

4.2 Outstanding Questions About ORBs

4.2.1 Identity and fate of the RNA in ORBs

Several questions arise from the results of this thesis that should be addressed with future experiments. Firstly, the specific nature of the defective RNAs that localize to ORBs should be characterized. This includes both the identity of the RNA species as well as the types of defects that result in compartmentalization. In addition, if ORBs are truly sites of TQC, I would predict that they are also sites of mRNA degradation.

To determine the profile of the RNAs that localizes to ORBs, I propose an RNA-seq analysis of the ORB transcriptome. Because ORBs are stable *ex vivo*, it would be relatively straightforward to prepare a cDNA library from an ORB preparation. This would entail the

enrichment of oxidized RNAs via immunoprecipitation, starting from a pellet fraction of yeast cell lysates, as was performed here for proteomics analyses. It would also be interesting to determine whether there is any enrichment of specific RNAs in ORBs, or whether any RNA can be oxidized and enriched in ORBs.

To determine the nature of the defects in RNA that localize to ORBs, several experiments are possible. First, the precise nature of all chemical modifications to RNAs in ORBs should be determined. While the focus of this thesis is on oxidized RNAs, ORBs may contain RNAs with other deleterious modifications. In particular, alkylation of mRNA has also been reported to interfere with translation (Wurtmann and Wolin, 2009; Yan et al., 2019). One could also continue to test reporter constructs with engineered defects in the coding sequence of an mRNA. Here I focused on an mRNA reporter that lacks a stop codon and is a substrate for NGD. mRNAs that contain a premature stop codon or repeated stretches encoding for basic amino acids should be tested, as these are known substrates for TQC (Simms et al., 2017a).

Finally, to study the fate of the RNAs that localize to ORBs, one could measure their stability. One of the initial steps during the TQC of ribosomes that stall during translation is the degradation of the defective mRNA. This occurs through an initial endonucleolytic cleavage event by Cue2, followed by the exonucleolytic degradation of the resulting 5'- and 3'- fragments by Xrn1 and the exosome, respectively (Doma and Parker, 2006; D'Orazio et al., 2019; Glover et al., 2020). A previous study of the fate of mRNAs that localize to P-bodies revealed that those RNA granules are not sites of mRNA degradation (Hubstenberger et al., 2017). A similar analysis should reveal whether ORBs are indeed sites of mRNA degradation.

4.2.2 Exploration of Novel TQC Factors

The ORB proteome provided here should be a valuable resource to identify novel TQC factors. Each of the 68 proteins included in the ORB proteome was validated by

immunofluorescence microscopy as localizing to ORBs. While it is possible that some localize as client proteins (i.e., newly synthesized proteins encoded by defective mRNAs), and that ORBs may have functions in addition to TQC, it is also highly likely that some act as novel TQC factors. The ORB proteome is enriched in RNA-binding proteins and ribosome-associated proteins. I note the presence of multiple factors that have known roles in ribosome biogenesis (e.g., Lsg1, Nob1, Nmd3, Tsr1 etc.). In particular, these proteins are known to associate with premature ribosomal subunits, keeping them from associating until their maturation is complete (Woolford and Baserga, 2013). Because the latter steps of the RQC pathway involve the splitting of the ribosome into 60S and 40S subunits for nascent chain extraction, it is possible that the above-mentioned ribosome biogenesis factors act at this stage (Brandman et al., 2012; Defenouillère et al., 2013; Shao et al., 2013; Shen et al., 2015). To address this, one could examine loss-of-function mutants for these ribosome biogenesis factors. Should they have TQC-related functions, I would expect to observe defects in ORB assembly and/or the accumulation of truncated nascent chains, as I showed for mutants of known TQC factors.

4.2.3 Context-Specific Studies of ORBs

Because this thesis is focused on the initial discovery and characterization of ORBs, I only examined them in non-stress and H₂O₂-induced oxidative stress. Cytosolic stress granules and P-bodies are known to form under several different stress conditions, and the composition of their protein and mRNA populations can change depending on the stress (Buchan et al., 2011). Therefore, I propose that future studies should characterize the formation of ORBs, as well as their composition during various stress conditions.

Relatedly, a natural extension of this work would be to test whether my findings in yeast are conserved in other organisms. We initially reported on the existence of ORBs in HeLa cells, therefore future experiments could include characterizing the proteome of human ORBs,

determining whether they too compartmentalize TQC factors, and whether they are affected by deletion of TQC proteins.

4.3 Outstanding questions about RbcL and TQC in chloroplasts

4.3.1 A Molecular Dissection of RbcL

This thesis examined only four site-directed mutants of RbcL. While I was able to identify one mutant with altered moonlighting properties of RbcL (*rbcL-G54D*), a much more detailed dissection of the protein should be carried out in the future. For example, RbcL has a known RNA-recognition motif and can bind non-specifically to RNA (Yosef et al., 2004). I propose that mutants of RbcL that lack RNA-binding activity should be tested for their oxidative stress tolerance, oxidized RNA levels, for the presence of the alternate form of the protein, and for the ability to form cpSGs.

4.3.2 The RbcL Interactome

Another avenue to further explore RbcL functions would be to characterize its interactome. TQC in the cytoplasm involves many factors that act at specific stages to detect collided ribosomes, split them, degrade defective mRNA, and target the aberrant nascent chains for degradation. Should RbcL have a role in a related process in chloroplasts, I would expect it to associate with other factors. To address this possibility, one could pull-out RbcL and subject it to mass spectrometry and proteomic analyses. Ideally this would be performed from biochemical fractions enriched in the alternate form of RbcL, or in mutants with elevated moonlighting functions.

4.4 On Possible TQC Systems in Chloroplasts

Finally, I would like to speculate on the nature of a TQC system in chloroplasts. To date, no conclusive evidence has been published on TQC in chloroplasts. Nonetheless, several findings suggest that one should exist.

A consequence of the electron transfer reactions housed in the thylakoid membranes of chloroplasts is the production of ROS (Asada, 2006). During oxygenic photosynthesis light energy is used to drive the oxidation of water, channelling its electrons through a photosynthetic electron transport chain. When light intensity is in excess of the ability of chloroplasts to utilize it, overreduction of the electron acceptors in the photosynthetic electron transport chain occurs (Takahashi and Murata, 2008). High light and other environmental stresses therefore compromise the ability of the photosynthetic machinery to harness light energy. These conditions lead to the potential for ROS production at several positions throughout the photosynthetic electron transport chain (Foyer and Shigeoka, 2011). Chloroplast translation often occurs in close proximity to the ROS producing photosynthetic electron transport chain (Asada, 2006; Uniacke and Zerges, 2007). Because mRNAs are susceptible to oxidation events that can induce ribosome stalling, it is reasonable to ask whether a quality control mechanism exists for translation in chloroplasts.

Because of their endosymbiotic origin, the possibility of TQC in chloroplasts is supported by the existence of systems that recognize stalled ribosomes in bacteria. Bacteria can resolve NGD and Non-Stop Decay (NSD) substrates using ribosome rescue systems such as: trans-translation, bacterial ribosome quality control, peptidyl-tRNA drop-off, and alternative ribosome rescue factors (Müller et al., 2021). Ribosome rescue systems can be presumed to also exist in mitochondria, another organelle of endosymbiotic origin. Like chloroplasts, mitochondria lack trans-translation, but do have alternative ribosome rescue factor homologues, called ICT1 and C12orf65 (Ayyub et al., 2020). While ribosome rescue activity of mammalian ICT1 has only been demonstrated in a heterologous system *in vitro* (Feaga et al., 2016), the yeast homologue of C12orf65 (Pth3/Rho55) is required for stalled ribosome rescue in a NGD-like manner *in vivo* (Hoshino et al., 2021). A homologue of the bacterial ribosome rescue factor, ArfB, was recently identified in *Arabidopsis*

thaliana (Nagao et al., 2020). This nuclear-encoded factor, called AtArfB, localized to chloroplasts in *Arabidopsis* and displayed ribosome rescue activity both *in vitro* and *in vivo*.

REFERENCES

- Aguzzi, A., and Altmeyer, M. (2016). Phase Separation: Linking Cellular Compartmentalization to Disease. *Trends Cell Biol.* 26, 547–558.
- Alberti, S., Gladfelter, A., and Mittag, T. (2019). Considerations and challenges in studying liquid-liquid phase separation and biomolecular condensates. *Cell* 176, 419–434.
- Allen, J.F., and Raven, J.A. (1996). Free-radical-induced mutation vs redox regulation: costs and benefits of genes in organelles. *J Mol Evol* 42, 482–492.
- Anderson, P., and Kedersha, N. (2006). RNA granules. *J Cell Biol* 172, 803–808.
- Anderson, P., and Kedersha, N. (2008). Stress granules: the Tao of RNA triage. *Trends Biochem. Sci.* 33, 141–150.
- Apel, K., and Hirt, H. (2004). Reactive oxygen species: metabolism, oxidative stress, and signal transduction. *Annu Rev Plant Biol* 55, 373–399.
- Asada, K. (2006). Production and Scavenging of Reactive Oxygen Species in Chloroplasts and Their Functions. *Plant Physiology* 141, 391–396.
- Ayyub, S.A., Gao, F., Lightowers, R.N., and Chrzanowska-Lightowers, Z.M. (2020). Rescuing stalled mammalian mitoribosomes – what can we learn from bacteria? *Journal of Cell Science* 133.
- Beckmann, B.M., Horos, R., Fischer, B., Castello, A., Eichelbaum, K., Alleaume, A.-M., Schwarzl, T., Curk, T., Foehr, S., Huber, W., et al. (2015). The RNA-binding proteomes from yeast to man harbour conserved enigmRBPs. *Nat Commun* 6, 10127.

Bengtson, M.H., and Joazeiro, C.A.P. (2010). Role of a ribosome-associated E3 ubiquitin ligase in protein quality control. *Nature* *467*, 470–473.

Brandman, O., and Hegde, R.S. (2016). Ribosome-associated protein quality control. *Nat Struct Mol Biol* *23*, 7–15.

Brandman, O., Stewart-Ornstein, J., Wong, D., Larson, A., Williams, C.C., Li, G.-W., Zhou, S., King, D., Shen, P.S., Weibezahn, J., et al. (2012). A Ribosome-Bound Quality Control Complex Triggers Degradation of Nascent Peptides and Signals Translation Stress. *Cell* *151*, 1042–1054.

Buchan, J.R. (2014). mRNP granules: Assembly, function, and connections with disease. *RNA Biology* e29034.

Buchan, J.R., Muhlrad, D., and Parker, R. (2008). P bodies promote stress granule assembly in *Saccharomyces cerevisiae*. *J Cell Biol* *183*, 441–455.

Buchan, J.R., Yoon, J.-H., and Parker, R. (2011). Stress-specific composition, assembly and kinetics of stress granules in *Saccharomyces cerevisiae*. *J Cell Sci* *124*, 228–239.

Buchan, J.R., Kolaitis, R.-M., Taylor, J.P., and Parker, R. (2013). Eukaryotic stress granules are cleared by autophagy and Cdc48/VCP function. *Cell* *153*, 1461–1474.

Cahoon, A.B., and Timko, M.P. (2000). yellow-in-the-dark mutants of *Chlamydomonas* lack the CHLL subunit of light-independent protochlorophyllide reductase. *Plant Cell* *12*, 559–568.

Calabretta, S., and Richard, S. (2015). Emerging Roles of Disordered Sequences in RNA-Binding Proteins. *Trends Biochem. Sci.* *40*, 662–672.

op den Camp, R.G.L., Przybyla, D., Ochsenein, C., Laloi, C., Kim, C., Danon, A., Wagner, D., Hideg, E., Göbel, C., Feussner, I., et al. (2003). Rapid induction of distinct stress responses after the release of singlet oxygen in Arabidopsis. *Plant Cell* *15*, 2320–2332.

Chiba, A., Ishida, H., Nishizawa, N.K., Makino, A., and Mae, T. (2003). Exclusion of ribulose-1,5-bisphosphate carboxylase/oxygenase from chloroplasts by specific bodies in naturally senescing leaves of wheat. *Plant Cell Physiol* *44*, 914–921.

Cohen, I., Knopf, J.A., Irihimovitch, V., and Shapira, M. (2005). A proposed mechanism for the inhibitory effects of oxidative stress on Rubisco assembly and its subunit expression. *Plant Physiol.* *137*, 738–746.

Cohen, I., Sapir, Y., and Shapira, M. (2006). A conserved mechanism controls translation of Rubisco large subunit in different photosynthetic organisms. *Plant Physiol.* *141*, 1089–1097.

Cole, S.E., LaRiviere, F.J., Merrikh, C.N., and Moore, M.J. (2009). A Convergence of rRNA and mRNA Quality Control Pathways Revealed by Mechanistic Analysis of Nonfunctional rRNA Decay. *Molecular Cell* *34*, 440–450.

Collart, M.A. (2016). The Ccr4-Not complex is a key regulator of eukaryotic gene expression. *WIREs RNA* *7*, 438–454.

Decker, C.J., and Parker, R. (2012). P-bodies and stress granules: possible roles in the control of translation and mRNA degradation. *Cold Spring Harb Perspect Biol* *4*, a012286.

Defenouillère, Q., Yao, Y., Mouaikel, J., Namane, A., Galopier, A., Decourty, L., Doyen, A., Malabat, C., Saveanu, C., Jacquier, A., et al. (2013). Cdc48-associated complex bound to 60S particles is required for the clearance of aberrant translation products. *PNAS* *110*, 5046–5051.

Defenouillère, Q., Zhang, E., Namane, A., Mouaikel, J., Jacquier, A., and Fromont-Racine, M. (2016). Rqc1 and Ltn1 Prevent C-terminal Alanine-Threonine Tail (CAT-tail)-induced Protein Aggregation by Efficient Recruitment of Cdc48 on Stalled 60S Subunits. *J. Biol. Chem.* *291*, 12245–12253.

Dhaliwal, J. (2013). A subpool of the large subunit of ribulose biphosphate carboxylase-oxygenase has a dual function in oxidative stress tolerance in *Chlamydomonas reinhardtii*.

Dimitrova, L.N., Kuroha, K., Tatematsu, T., and Inada, T. (2009). Nascent Peptide-dependent Translation Arrest Leads to Not4p-mediated Protein Degradation by the Proteasome. *J Biol Chem* *284*, 10343–10352.

Doma, M.K., and Parker, R. (2006). Endonucleolytic cleavage of eukaryotic mRNAs with stalls in translation elongation. *Nature* *440*, 561–564.

D’Orazio, K.N., Wu, C.C.-C., Sinha, N., Loll-Kripplber, R., Brown, G.W., and Green, R. (2019). The endonuclease Cue2 cleaves mRNAs at stalled ribosomes during No Go Decay. *ELife* *8*, e49117.

Ellis, R. (1979). The Most Abundant Protein in the World. *TIBS* *4*, 241–244.

Eulalio, A., Behm-Ansmant, I., Schweizer, D., and Izaurralde, E. (2007a). P-body formation is a consequence, not the cause, of RNA-mediated gene silencing. *Mol. Cell. Biol.* *27*, 3970–3981.

Feaga, H.A., Quickel, M.D., Hankey-Giblin, P.A., and Keiler, K.C. (2016). Human Cells Require Non-stop Ribosome Rescue Activity in Mitochondria. *PLOS Genetics* *12*, e1005964.

Foyer, C.H., and Shigeoka, S. (2011). Understanding oxidative stress and antioxidant functions to enhance photosynthesis. *Plant Physiol.* *155*, 93–100.

Fujii, K., Kitabatake, M., Sakata, T., Miyata, A., and Ohno, M. (2009). A role for ubiquitin in the clearance of nonfunctional rRNAs. *Genes Dev* *23*, 963–974.

Fujimura, K., Katahira, J., Kano, F., Yoneda, Y., and Murata, M. (2009). Microscopic dissection of the process of stress granule assembly. *Biochimica et Biophysica Acta (BBA) - Molecular Cell Research* *1793*, 1728–1737.

Garg, N., and Manchanda, G. (2009). ROS generation in plants: Boon or bane? *Plant Biosystems - An International Journal Dealing with All Aspects of Plant Biology* *143*, 81–96.

Genkov, T., Meyer, M., Griffiths, H., and Spreitzer, R.J. (2010). Functional hybrid rubisco enzymes with plant small subunits and algal large subunits: engineered rbcS cDNA for expression in chlamydomonas. *J Biol Chem* *285*, 19833–19841.

Ghezzi, P., and Bonetto, V. (2003). Redox proteomics: identification of oxidatively modified proteins. *Proteomics* *3*, 1145–1153.

Gill, S.S., and Tuteja, N. (2010). Reactive oxygen species and antioxidant machinery in abiotic stress tolerance in crop plants. *Plant Physiol. Biochem.* *48*, 909–930.

Glover, M.L., Burroughs, A.Max., Monem, P.C., Egelhofer, T.A., Pule, M.N., Aravind, L., and Arribere, J.A. (2020). NONU-1 Encodes a Conserved Endonuclease Required for mRNA Translation Surveillance. *Cell Rep* *30*, 4321-4331.e4.

Goodenough, U., Blaby, I., Casero, D., Gallaher, S.D., Goodson, C., Johnson, S., Lee, J.-H., Merchant, S.S., Pellegrini, M., Roth, R., et al. (2014). The Path to Triacylglyceride Obesity in the sta6 Strain of *Chlamydomonas reinhardtii*. *Eukaryot Cell* *13*, 591–613.

Harris, E.H. (1989). *The Chlamydomonas Sourcebook. A Comprehensive Guide to Biology and Laboratory Use*. Elizabeth H. Harris. Academic Press, San Diego, CA, 1989. xiv, 780 pp., illus. \$145. *Science* *246*, 1503–1504.

Hayakawa, H., Kuwano, M., and Sekiguchi, M. (2001). Specific binding of 8-oxoguanine-containing RNA to polynucleotide phosphorylase protein. *Biochemistry* *40*, 9977–9982.

Hayakawa, H., Uchiumi, T., Fukuda, T., Ashizuka, M., Kohno, K., Kuwano, M., and Sekiguchi, M. (2002). Binding capacity of human YB-1 protein for RNA containing 8-oxoguanine. *Biochemistry* *41*, 12739–12744.

Hayakawa, H., Fujikane, A., Ito, R., Matsumoto, M., Nakayama, K.I., and Sekiguchi, M. (2010). Human proteins that specifically bind to 8-oxoguanine-containing RNA and their responses to oxidative stress. *Biochem. Biophys. Res. Commun.* *403*, 220–224.

Hentges, P., Driessche, B.V., Tafforeau, L., Vandenhaute, J., and Carr, A.M. (2005). Three novel antibiotic marker cassettes for gene disruption and marker switching in *Schizosaccharomyces pombe*. *Yeast* *22*, 1013–1019.

Hofer, T., Badouard, C., Bajak, E., Ravanat, J.-L., Mattsson, A., and Cotgreave, I.A. (2005). Hydrogen peroxide causes greater oxidation in cellular RNA than in DNA. *Biol Chem* *386*, 333–337.

Honda, K., Smith, M.A., Zhu, X., Baus, D., Merrick, W.C., Tartakoff, A.M., Hattier, T., Harris, P.L., Siedlak, S.L., Fujioka, H., et al. (2005). Ribosomal RNA in Alzheimer disease is oxidized by bound redox-active iron. *J. Biol. Chem.* *280*, 20978–20986.

Hoshino, S., Kanemura, R., Kurita, D., Soutome, Y., Himeno, H., Takaine, M., Watanabe, M., and Nameki, N. (2021). A stalled-ribosome rescue factor Pth3 is required for mitochondrial translation against antibiotics in *Saccharomyces cerevisiae*. *Commun Biol* *4*, 1–11.

Hoyle, N.P., Castelli, L.M., Campbell, S.G., Holmes, L.E.A., and Ashe, M.P. (2007). Stress-dependent relocalization of translationally primed mRNPs to cytoplasmic granules that are kinetically and spatially distinct from P-bodies. *J Cell Biol* *179*, 65–74.

Hubstenberger, A., Courel, M., Bénard, M., Souquere, S., Ernoult-Lange, M., Chouaib, R., Yi, Z., Morlot, J.-B., Munier, A., Fradet, M., et al. (2017). P-Body Purification Reveals the Condensation of Repressed mRNA Regulons. *Molecular Cell* *68*, 144-157.e5.

Huh, W.-K., Falvo, J.V., Gerke, L.C., Carroll, A.S., Howson, R.W., Weissman, J.S., and O'Shea, E.K. (2003). Global analysis of protein localization in budding yeast. *Nature* *425*, 686–691.

Hyman, A.A., Weber, C.A., and Jülicher, F. (2014). Liquid-liquid phase separation in biology. *Annu. Rev. Cell Dev. Biol.* *30*, 39–58.

Ikeuchi, K., Tesina, P., Matsuo, Y., Sugiyama, T., Cheng, J., Saeki, Y., Tanaka, K., Becker, T., Beckmann, R., and Inada, T. (2019). Collided ribosomes form a unique structural interface to induce Hel2-driven quality control pathways. *The EMBO Journal* *38*, e100276.

Inada, T. (2020). Quality controls induced by aberrant translation. *Nucleic Acids Res* *48*, 1084–1096.

Ishida, H., Yoshimoto, K., Izumi, M., Reisen, D., Yano, Y., Makino, A., Ohsumi, Y., Hanson, M.R., and Mae, T. (2008). Mobilization of Rubisco and Stroma-Localized Fluorescent Proteins of Chloroplasts to the Vacuole by an ATG Gene-Dependent Autophagic Process. *Plant Physiology* *148*, 142–155.

Ivanov, P., Kedersha, N., and Anderson, P. (2018). Stress Granules and Processing Bodies in Translational Control. *Cold Spring Harb Perspect Biol* a032813.

Jain, S., Wheeler, J.R., Walters, R.W., Agrawal, A., Barsic, A., and Parker, R. (2016). ATPase-Modulated Stress Granules Contain a Diverse Proteome and Substructure. *Cell* *164*, 487–498.

Jamar, N.H., Kritsiligkou, P., and Grant, C.M. (2017). The non-stop decay mRNA surveillance pathway is required for oxidative stress tolerance. *Nucleic Acids Res* *45*, 6881–6893.

Jamar, N.H., Kritsiligkou, P., and Grant, C.M. (2018). Loss of mRNA surveillance pathways results in widespread protein aggregation. *Scientific Reports* *8*, 3894.

Juzkiewicz, S., Chandrasekaran, V., Lin, Z., Kraatz, S., Ramakrishnan, V., and Hegde, R.S. (2018). ZNF598 Is a Quality Control Sensor of Collided Ribosomes. *Molecular Cell*.

Kaganovich, D., Kopito, R., and Frydman, J. (2008). Misfolded proteins partition between two distinct quality control compartments. *Nature* *454*, 1088–1095.

Kedersha, N., and Anderson, P. (2009). Regulation of translation by stress granules and processing bodies. *Prog Mol Biol Transl Sci* *90*, 155–185.

Kedersha, N., Cho, M.R., Li, W., Yacono, P.W., Chen, S., Gilks, N., Golan, D.E., and Anderson, P. (2000). Dynamic shuttling of TIA-1 accompanies the recruitment of mRNA to mammalian stress granules. *J. Cell Biol.* *151*, 1257–1268.

Knight, S., Andersson, I., and Brändén, C.-I. (1990). Crystallographic analysis of ribulose 1,5-bisphosphate carboxylase from spinach at 2.4 Å resolution: Subunit interactions and active site. *Journal of Molecular Biology* *215*, 113–160.

Knopf, J.A., and Shapira, M. (2005). Degradation of Rubisco SSU during oxidative stress triggers aggregation of Rubisco particles in *Chlamydomonas reinhardtii*. *Planta* *222*, 787–793.

Kroschwald, S., Maharana, S., and Simon, A. (2017). Hexanediol: a chemical probe to investigate the material properties of membrane-less compartments. *Matters* *3*, e201702000010.

Lancaster, A.K., Nutter-Upham, A., Lindquist, S., and King, O.D. (2014). PLAAC: a web and command-line application to identify proteins with prion-like amino acid composition. *Bioinformatics* *30*, 2501–2502.

Li, Z., Wu, J., and Deleo, C.J. (2006). RNA damage and surveillance under oxidative stress. *IUBMB Life* *58*, 581–588.

Lui, J., Castelli, L.M., Pizzinga, M., Simpson, C.E., Hoyle, N.P., Bailey, K.L., Campbell, S.G., and Ashe, M.P. (2014). Granules Harboring Translationally Active mRNAs Provide a Platform for P-Body Formation following Stress. *Cell Rep* *9*, 944–954.

Lyumkis, D., Passos, D.O. dos, Tahara, E.B., Webb, K., Bennett, E.J., Vinterbo, S., Potter, C.S., Carragher, B., and Joazeiro, C.A.P. (2014). Structural basis for translational surveillance by the large ribosomal subunit-associated protein quality control complex. *PNAS* *111*, 15981–15986.

- Marín-Navarro, J., and Moreno, J. (2006). Cysteines 449 and 459 modulate the reduction-oxidation conformational changes of ribulose 1.5-bisphosphate carboxylase/oxygenase and the translocation of the enzyme to membranes during stress. *Plant Cell Environ.* 29, 898–908.
- McKay, R.M.L., and Gibbs, S.P. (1991). Composition and function of pyrenoids: cytochemical and immunocytochemical approaches. *Canadian Journal of Botany* 69, 1040–1052.
- Mehta, R.A., Fawcett, T.W., Porath, D., and Mattoo, A.K. (1992). Oxidative stress causes rapid membrane translocation and in vivo degradation of ribulose-1,5-bisphosphate carboxylase/oxygenase. *J. Biol. Chem.* 267, 2810–2816.
- Meyer, M.T., Whittaker, C., and Griffiths, H. (2017). The algal pyrenoid: key unanswered questions. *J Exp Bot* 68, 3739–3749.
- Mitchell, S.F., Jain, S., She, M., and Parker, R. (2013). Global analysis of yeast mRNPs. *Nature Structural & Molecular Biology* 20, 127–133.
- Miziorko, H.M., and Lorimer, G.H. (1983). Ribulose-1,5-bisphosphate carboxylase-oxygenase. *Annu. Rev. Biochem.* 52, 507–535.
- Moon, S.L., Morisaki, T., Stasevich, T.J., and Parker, R. (2020). Coupling of translation quality control and mRNA targeting to stress granules. *J Cell Biol* 219.
- Moreno, J., García-Murria, M.J., and Marín-Navarro, J. (2008). Redox modulation of Rubisco conformation and activity through its cysteine residues. *J. Exp. Bot.* 59, 1605–1614.
- Müller, C., Crowe-McAuliffe, C., and Wilson, D.N. (2021). Ribosome Rescue Pathways in Bacteria. *Front Microbiol* 12, 652980.

Mumberg, D., Müller, R., and Funk, M. (1995). Yeast vectors for the controlled expression of heterologous proteins in different genetic backgrounds. *Gene* 156, 119–122.

Nagao, M., Tsuchiya, F., Motohashi, R., and Abo, T. (2020). Ribosome rescue activity of an *Arabidopsis thaliana* ArfB homolog. *Genes Genet Syst* 95, 119–131.

Navickas, A., Chamois, S., Saint-Fort, R., Henri, J., Torchet, C., and Benard, L. (2020). No-Go Decay mRNA cleavage in the ribosome exit tunnel produces 5'-OH ends phosphorylated by Trl1. *Nat Commun* 11, 1–11.

Nunomura, A., Perry, G., Pappolla, M.A., Wade, R., Hirai, K., Chiba, S., and Smith, M.A. (1999). RNA oxidation is a prominent feature of vulnerable neurons in Alzheimer's disease. *J. Neurosci.* 19, 1959–1964.

Panasenko, O.O., Somasekharan, S.P., Villanyi, Z., Zagatti, M., Bezrukov, F., Rashpa, R., Cornut, J., Iqbal, J., Longis, M., Carl, S.H., et al. (2019). Co-translational assembly of proteasome subunits in NOT1-containing assemblyosomes. *Nat Struct Mol Biol* 26, 110–120.

Park, E.M., Shigenaga, M.K., Degan, P., Korn, T.S., Kitzler, J.W., Wehr, C.M., Kolachana, P., and Ames, B.N. (1992). Assay of excised oxidative DNA lesions: isolation of 8-oxoguanine and its nucleoside derivatives from biological fluids with a monoclonal antibody column. *Proc. Natl. Acad. Sci. U.S.A.* 89, 3375–3379.

Paull, T.T., Rogakou, E.P., Yamazaki, V., Kirchgessner, C.U., Gellert, M., and Bonner, W.M. (2000). A critical role for histone H2AX in recruitment of repair factors to nuclear foci after DNA damage. *Current Biology* 10, 886–895.

Peng, Z., Mizianty, M.J., and Kurgan, L. (2014). Genome-scale prediction of proteins with long intrinsically disordered regions. *Proteins: Structure, Function, and Bioinformatics* 82, 145–158.

Pérez-Pérez, M.E., Florencio, F.J., and Crespo, J.L. (2010). Inhibition of target of rapamycin signaling and stress activate autophagy in *Chlamydomonas reinhardtii*. *Plant Physiol.* 152, 1874–1888.

Poulsen, H.E., Specht, E., Broedbaek, K., Henriksen, T., Ellervik, C., Mandrup-Poulsen, T., Tonnesen, M., Nielsen, P.E., Andersen, H.U., and Weimann, A. (2012). RNA modifications by oxidation: a novel disease mechanism? *Free Radic. Biol. Med.* 52, 1353–1361.

Prins, A., van Heerden, P.D.R., Olmos, E., Kunert, K.J., and Foyer, C.H. (2008). Cysteine proteinases regulate chloroplast protein content and composition in tobacco leaves: a model for dynamic interactions with ribulose-1,5-bisphosphate carboxylase/oxygenase (Rubisco) vesicular bodies. *J Exp Bot* 59, 1935–1950.

Rawat, M., Henk, M.C., Lavigne, L.L., and Moroney, J.V. (1996). *Chlamydomonas reinhardtii* mutants without ribulose-1,5-bisphosphate carboxylase-oxygenase lack a detectable pyrenoid. *Planta* 198, 263–270.

Recuenco-Muñoz, L., Offre, P., Valledor, L., Lyon, D., Weckwerth, W., and Wienkoop, S. (2015). Targeted quantitative analysis of a diurnal RuBisCO subunit expression and translation profile in *Chlamydomonas reinhardtii* introducing a novel Mass Western approach. *J Proteomics* 113, 143–153.

Rogakou, E.P., Boon, C., Redon, C., and Bonner, W.M. (1999). Megabase Chromatin Domains Involved in DNA Double-Strand Breaks in Vivo. *J Cell Biol* 146, 905–916.

Satagopan, S., and Spreitzer, R.J. (2004). Substitutions at the Asp-473 latch residue of chlamydomonas ribulosebiphosphate carboxylase/oxygenase cause decreases in carboxylation efficiency and CO(2)/O(2) specificity. *J. Biol. Chem.* *279*, 14240–14244.

Schindelin, J., Arganda-Carreras, I., Frise, E., Kaynig, V., Longair, M., Pietzsch, T., Preibisch, S., Rueden, C., Saalfeld, S., Schmid, B., et al. (2012). Fiji: an open-source platform for biological-image analysis. *Nat Methods* *9*, 676–682.

Schottkowski, M., Peters, M., Zhan, Y., Rifai, O., Zhang, Y., and Zerges, W. (2012). Biogenic membranes of the chloroplast in *Chlamydomonas reinhardtii*. *Proc. Natl. Acad. Sci. U.S.A.* *109*, 19286–19291.

Shan, X., Tashiro, H., and Lin, C.G. (2003). The identification and characterization of oxidized RNAs in Alzheimer's disease. *J. Neurosci.* *23*, 4913–4921.

Shannon, P., Markiel, A., Ozier, O., Baliga, N.S., Wang, J.T., Ramage, D., Amin, N., Schwikowski, B., and Ideker, T. (2003). Cytoscape: A Software Environment for Integrated Models of Biomolecular Interaction Networks. *Genome Res.* *13*, 2498–2504.

Shao, S., von der Malsburg, K., and Hegde, R.S. (2013). Listerin-Dependent Nascent Protein Ubiquitination Relies on Ribosome Subunit Dissociation. *Molecular Cell* *50*, 637–648.

Shao, S., Brown, A., Santhanam, B., and Hegde, R.S. (2015). Structure and Assembly Pathway of the Ribosome Quality Control Complex. *Mol Cell* *57*, 433–444.

Shelkovnikova, T.A., Robinson, H.K., Southcombe, J.A., Ninkina, N., and Buchman, V.L. (2014). Multistep process of FUS aggregation in the cell cytoplasm involves RNA-dependent and RNA-independent mechanisms. *Human Molecular Genetics* *23*, 5211–5226.

Shen, P.S., Park, J., Qin, Y., Li, X., Parsawar, K., Larson, M.H., Cox, J., Cheng, Y., Lambowitz, A.M., Weissman, J.S., et al. (2015). Rqc2p and 60S ribosomal subunits mediate mRNA-independent elongation of nascent chains. *Science* 347, 75–78.

Shin, Y., and Brangwynne, C.P. (2017). Liquid phase condensation in cell physiology and disease. *Science* 357.

Shoemaker, C.J., Eyler, D.E., and Green, R. (2010). Dom34:Hbs1 Promotes Subunit Dissociation and Peptidyl-tRNA Drop-Off to Initiate No-Go Decay. *Science* 330, 369–372.

Simms, C.L., Hudson, B.H., Mosior, J.W., Rangwala, A.S., and Zaher, H.S. (2014). An active role for the ribosome in determining the fate of oxidized mRNA. *Cell Rep* 9, 1256–1264.

Simms, C.L., Thomas, E.N., and Zaher, H.S. (2017a). Ribosome-based quality control of mRNA and nascent peptides. *WIREs RNA* 8, e1366.

Simms, C.L., Yan, L.L., and Zaher, H.S. (2017b). Ribosome Collision Is Critical for Quality Control during No-Go Decay. *Mol. Cell* 68, 361-373.e5.

Sitron, C.S., and Brandman, O. (2019). CAT tails drive degradation of stalled polypeptides on and off the ribosome. *Nat. Struct. Mol. Biol.* 26, 450–459.

Spreitzer, R.J. (1993). Genetic Dissection of Rubisco Structure and Function. *Annu. Rev. Plant. Physiol. Plant. Mol. Biol.* 44, 411–434.

Spreitzer, R.J., and Salvucci, M.E. (2002). Rubisco: structure, regulatory interactions, and possibilities for a better enzyme. *Annu Rev Plant Biol* 53, 449–475.

- Stoecklin, G., and Bukau, B. (2013). Telling right from wrong in life - cellular quality control. *Nat. Rev. Mol. Cell Biol.* *14*, 613–615.
- Strober, W. (2001). Trypan blue exclusion test of cell viability. *Curr Protoc Immunol Appendix 3*, Appendix 3B.
- Sun, Y., Valente-Paterno, M., Bakhtiari, S., Law, C., Zhan, Y., and Zerges, W. (2019). Photosystem Biogenesis Is Localized to the Translation Zone in the Chloroplast of *Chlamydomonas*. *Plant Cell* *31*, 3057–3072.
- Takahashi, S., and Murata, N. (2008). How do environmental stresses accelerate photoinhibition? *Trends Plant Sci.* *13*, 178–182.
- Tanaka, M., Chock, P.B., and Stadtman, E.R. (2007). Oxidized messenger RNA induces translation errors. *Proc. Natl. Acad. Sci. U.S.A.* *104*, 66–71.
- Teixeira, D., and Parker, R. (2007). Analysis of P-body assembly in *Saccharomyces cerevisiae*. *Mol. Biol. Cell* *18*, 2274–2287.
- Tsuboi, T., Kuroha, K., Kudo, K., Makino, S., Inoue, E., Kashima, I., and Inada, T. (2012). Dom34:Hbs1 Plays a General Role in Quality-Control Systems by Dissociation of a Stalled Ribosome at the 3' End of Aberrant mRNA. *Molecular Cell* *46*, 518–529.
- Tuteja, N., Ahmad, P., Panda, B.B., and Tuteja, R. (2009). Genotoxic stress in plants: shedding light on DNA damage, repair and DNA repair helicases. *Mutat. Res.* *681*, 134–149.
- Uniacke, J., and Zerges, W. (2007). Photosystem II assembly and repair are differentially localized in *Chlamydomonas*. *Plant Cell* *19*, 3640–3654.

- Uniacke, J., and Zerges, W. (2008). Stress induces the assembly of RNA granules in the chloroplast of *Chlamydomonas reinhardtii*. *J. Cell Biol.* *182*, 641–646.
- Uniacke, J., Colón-Ramos, D., and Zerges, W. (2011). FISH and immunofluorescence staining in *Chlamydomonas*. *Methods Mol. Biol.* *714*, 15–29.
- Warde-Farley, D., Donaldson, S.L., Comes, O., Zuberi, K., Badrawi, R., Chao, P., Franz, M., Grouios, C., Kazi, F., Lopes, C.T., et al. (2010). The GeneMANIA prediction server: biological network integration for gene prioritization and predicting gene function. *Nucleic Acids Res* *38*, W214–W220.
- Weber, S.C., and Brangwynne, C.P. (2012). Getting RNA and protein in phase. *Cell* *149*, 1188–1191.
- Wheeler, J.R., Jain, S., Khong, A., and Parker, R. (2017). Isolation of yeast and mammalian stress granule cores. *Methods* *126*, 12–17.
- Wietrzynski, W., Traverso, E., Wollman, F.-A., and Wostrikoff, K. (2021). The state of oligomerization of Rubisco controls the rate of synthesis of the Rubisco large subunit in *Chlamydomonas reinhardtii*. *The Plant Cell* *33*, 1706–1727.
- Winzeler, E.A., Shoemaker, D.D., Astromoff, A., Liang, H., Anderson, K., Andre, B., Bangham, R., Benito, R., Boeke, J.D., Bussey, H., et al. (1999). Functional Characterization of the *S. cerevisiae* Genome by Gene Deletion and Parallel Analysis. *Science* *285*, 901–906.
- Woolford, J.L., and Baserga, S.J. (2013). Ribosome Biogenesis in the Yeast *Saccharomyces cerevisiae*. *Genetics* *195*, 643–681.

Wostrikoff, K., and Stern, D. (2007). Rubisco large-subunit translation is autoregulated in response to its assembly state in tobacco chloroplasts. *PNAS* *104*, 6466–6471.

Wu, J., and Li, Z. (2008). Human polynucleotide phosphorylase reduces oxidative RNA damage and protects HeLa cell against oxidative stress. *Biochem. Biophys. Res. Commun.* *372*, 288–292.

Wu, J., Jiang, Z., Liu, M., Gong, X., Wu, S., Burns, C.M., and Li, Z. (2009). Polynucleotide phosphorylase protects *Escherichia coli* against oxidative stress. *Biochemistry* *48*, 2012–2020.

Wurtmann, E.J., and Wolin, S.L. (2009). RNA under attack: Cellular handling of RNA damage. *Crit Rev Biochem Mol Biol* *44*, 34–49.

Yan, L.L., and Zaher, H.S. (2019). How do cells cope with RNA damage and its consequences? *J Biol Chem* *294*, 15158–15171.

Yan, L.L., Simms, C.L., McLoughlin, F., Vierstra, R.D., and Zaher, H.S. (2019). Oxidation and alkylation stresses activate ribosome-quality control. *Nat Commun* *10*, 5611.

Yonashiro, R., Tahara, E.B., Bengtson, M.H., Khokhrina, M., Lorenz, H., Chen, K.-C., Kigoshitansho, Y., Savas, J.N., Yates, J.R., Kay, S.A., et al. (2016). The Rqc2/Tae2 subunit of the ribosome-associated quality control (RQC) complex marks ribosome-stalled nascent polypeptide chains for aggregation. *ELife* *5*, e11794.

Yosef, I., Irihimovitch, V., Knopf, J.A., Cohen, I., Orr-Dahan, I., Nahum, E., Keasar, C., and Shapira, M. (2004). RNA binding activity of the ribulose-1,5-bisphosphate carboxylase/oxygenase large subunit from *Chlamydomonas reinhardtii*. *J. Biol. Chem.* *279*, 10148–10156.

Zhan, Y., Dhaliwal, J.S., Adjibade, P., Uniacke, J., Mazroui, R., and Zerges, W. (2015).

Localized control of oxidized RNA. *J. Cell. Sci.* *128*, 4210–4219.

Zheng, D., Ezzeddine, N., Chen, C.-Y.A., Zhu, W., He, X., and Shyu, A.-B. (2008).

Deadenylation is prerequisite for P-body formation and mRNA decay in mammalian cells. *J Cell Biol* *182*, 89–101.

Zheng, G., Fu, Y., and He, C. (2014). Nucleic Acid Oxidation in DNA Damage Repair and Epigenetics. *Chem. Rev.* *114*, 4602–4620.

SUPPLEMENTARY INFORMATION

Table S2.1: .xlsx file containing the list of validated ORB proteins

Table S2.2: .xlsx file containing the list of candidate ORB proteins

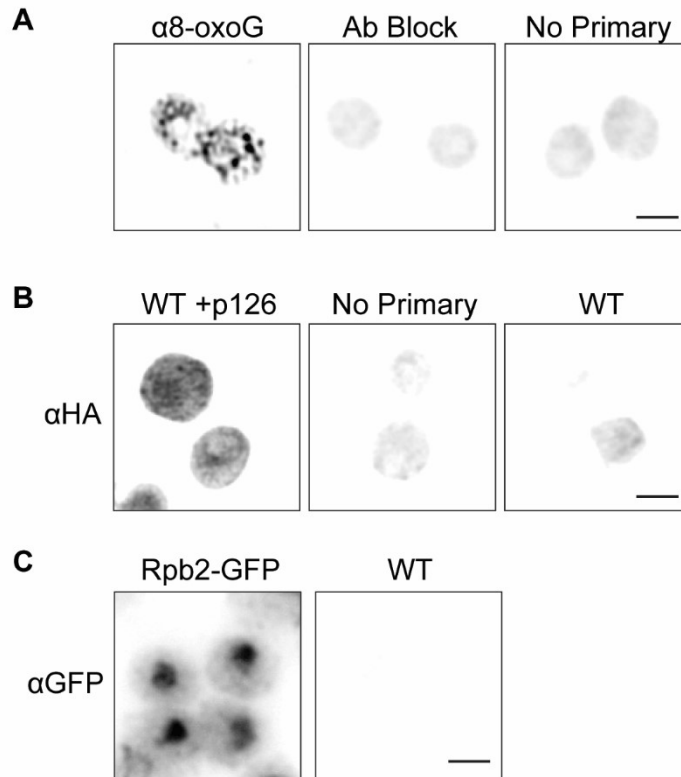


Figure S2.1. Controls for immunofluorescence (IF) staining.

(A) The $\alpha 8\text{-oxoG}$ antibody does not detect ORBs following block with 8-oxoG (10 $\mu\text{g}/\mu\text{g}$ of antibody) (**Ab Block**) or when the primary antibody against 8-oxoG was excluded (**No Primary**). (B) The αHA antibody detects the HA-tagged Ura3 nascent polypeptide in a transformant expressing it (**WT+p126**) because signal was not detected when the antibody was excluded (**No Primary**) or when the antibody was used to stain untransformed wild type cells (**WT**). (C) IF staining of GFP in untransformed cells (**WT**) or cells transformed with Rpb2-GFP, demonstrating that the GFP signal seen *in situ* is specific. Scale bars = 2.0 μm .

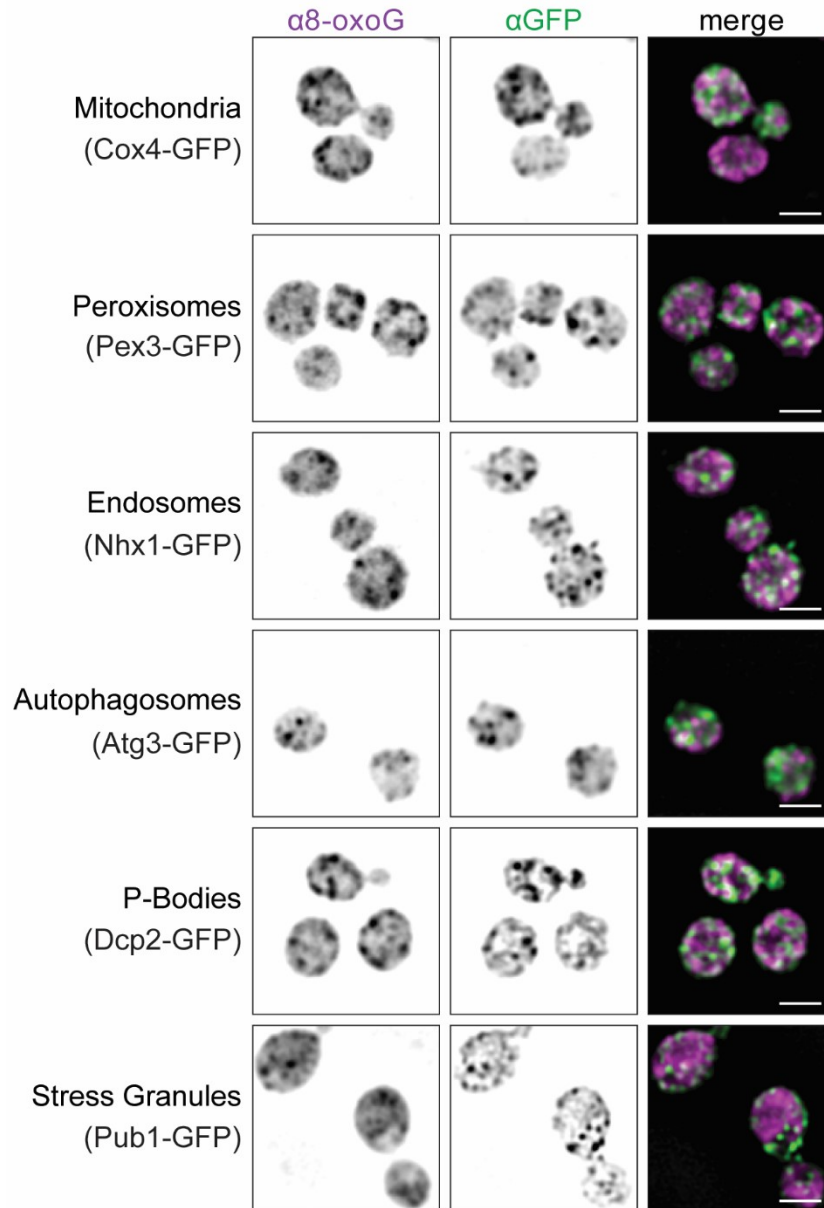


Figure S2.2. ORBs are none of the known RNA-containing organelles.

Co-IF staining of ORBs ($\alpha 8\text{-oxoG}$) and the indicated GFP-tagged marker proteins for membranous organelles and RNA granules *in situ*. Scale bars = 2.0 μm .

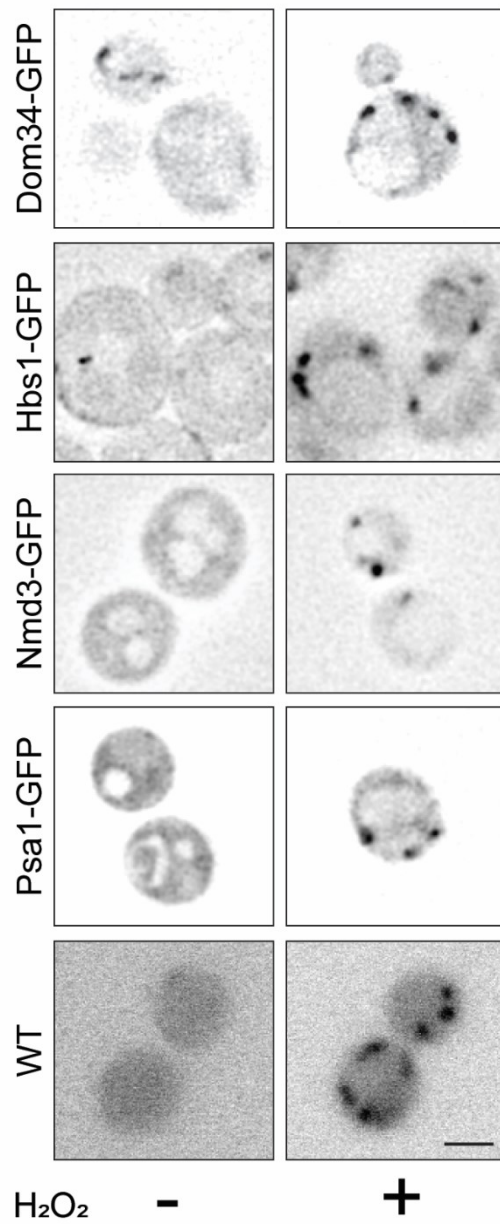


Figure S2.3. Foci form in response to hydrogen peroxide in live cells.

Fluorescence from Dom34-GFP, Hbs1-GFP, Nmd3-GFP, Psa1-GFP, or wild-type (WT) is shown in cells that were untreated or exposed to 5.0 mM hydrogen peroxide (H_2O_2) for 30 min. Scale bar = 2.0 μm .

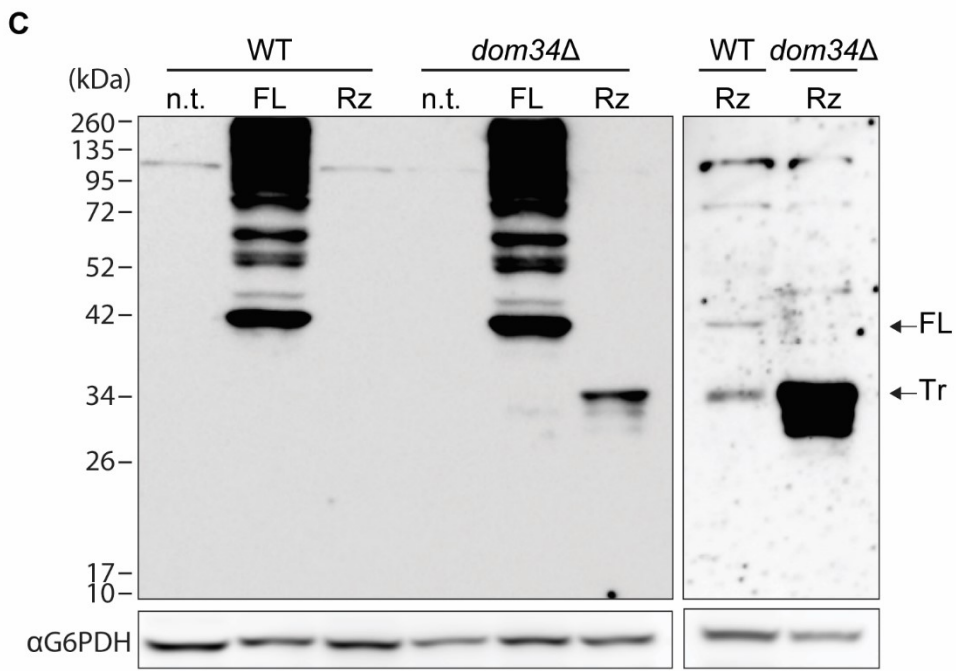
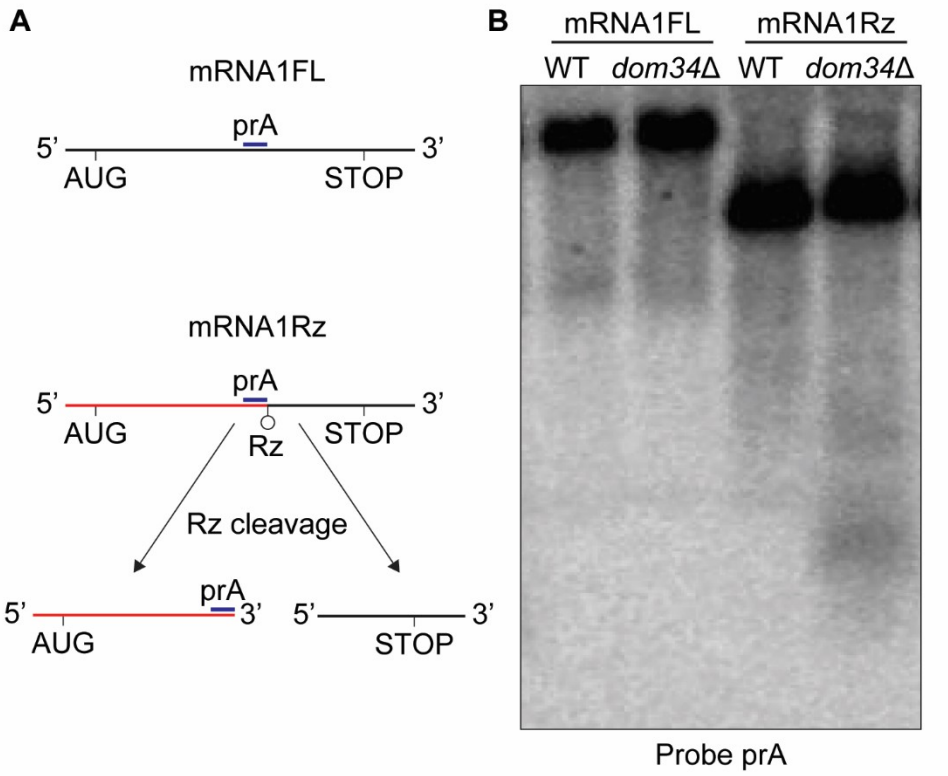


Figure S2.4. The truncated HA-Ura3 nascent polypeptide accumulates in *dom34Δ* background to serve as a marker for the stalled mRNA-ribosome-nascent polypeptide complex.

(A) The schematic shows the URA3-mRNA1FL (top) and URA3-mRNA1Rz (bottom). The locations of start (AUG) and stop codons, the probe used for northern blot analysis (prA), and the ribozyme (Rz) cleavage site are indicated. (B) Northern blot analysis of the levels of mRNA1FL and mRNA1Rz in *wild type* (WT) and *dom34Δ*. (C) Immunoblot analysis of HA-Ura3 in total protein from *wild-type* (WT) or *dom34Δ*, in strains that were transformed with either expression construct (mRNA1-FL (FL), mRNA1-Rz (Rz)) or non-transformed strains (n.t.).

Chlamydomonas strain	Genotype	Notes
CC-4051	wild-type 4A ⁺	used for CAP/Linc gradients
CC-125	wild-type 137c	used as WT for microscopy
CC-1168	<i>y1</i>	yellow-in-the-dark mutant
CC-4887	wild-type 2137	parental strain to SDMs
CC-4791	<i>rbcL-G54D</i>	
CC-4719	<i>rbcL-C84S</i>	
CC-4712	<i>rbcL-C172S</i>	
CC-4713	<i>rbcL-C449S/C459S</i>	
CC-4763	rbcS1-SSAT	
CC-4765	rbcS1-SSHA	
CC-4761	rbcS1-SSSO	

Table S3.1. Strains used in Chapter 3. Abbreviations: SDM refers to the site-directed mutants of RbcL listed in the table; CAP = chloramphenicol; Linc = lincomycin; N = nitrogen